Thesis for the Degree of Doctor of Philosophy

A Study on the Rheological Parameters of Silk Fibroin Solutions for Electrohydrodynamic Fabrication

전기수력학적 제조에서 실크 피브로인 용액의 유변학적 변수에 관한 고찰

February 2015

by

Moo Kon Kim

Department of Biosystems & Biomaterials Science and Engineering

Seoul National University

Abstract

Silk fibroin (SF) was fabricated using the electrohydrodynamic (EHD) process in order to prepare nanoscale fibers. Despite the high potential of SF nanofibers in biomedical applications, the EHD fabrication of SF has yet to be thoroughly studied. Most SF studies have focused on stable fiber formation, even though particles can be formed using the same process. Thus, the aim of this study is to provide a comprehensive understanding of EHD in the fabrication of SF from particles to fibers in the context of certain rheological properties of SF solution. In addition, a rheological parameter is proposed in order to predict the mode of EHD fabrications as well as product size, regardless of the concentration and molecular weight of SF. Samples of SF with different molecular weight were prepared by controlling the dissolution time of SF in $CaCl_2$/EtOH/H_2O solution. The average molecular weight of SF particles was reduced with increased dissolution time. Four different SF samples were prepared with dissolution times of 5, 30, 60 and 180 min, which were designated as SFC005, SFC030, SFC060 and SFC180, respectively. Initially, SF microparticles were prepared using a 1 M LiCl/DMSO solvent. Microparticles of about 200 μm were prepared; their shape was determined by the shear viscosity of the SF solution, regardless of the concentration and molecular weight of SF.

Since formic acid (FA) and hexafluoroisopropanol (HFIP) are the most common solvents used in the EHD fabrication of SF, both the shear and dynamic viscosity of SF in these solvents was investigated. With both FA and HFIP solvents, the mode of the EHD fabrication was determined by the solution plateau modulus,

regardless of the concentration and molecular weight of SF. The size of EHD products can be predicted using a rheological parameter. The size of particles can be predicted using the zero shear viscosity, whereas the size of fibers can be predicted using the solution plateau modulus. In conclusion, the proposed rheological parameters for SF solutions may be used in the future for the precise control of EHD fabrications.

Keyword : Silk fibroin, electrohydrodynamic fabrication, viscosity, microparticle, chain entanglement, plateau modulus

Student number : 2010-30307

TABLE OF CONTENTS

List of Tables

List of Figures

I. Introduction

The electrohydrodynamic (EHD) process is a fabrication method for nano- or microscale products involving the application of an electric field to a polymer solution [1-3]. In EHD fabrication, a polymer dope solution receives a controlled flow by a syringe pump and, at the same time, is exposed to a strong electric field. At a proper flow rate, a meniscus is formed at the end of the spinneret tip and maintains a constant form. With the increase of applied voltage, the meniscus starts to deform, and finally, a cone jet is formed, namely the Taylor cone. A droplet or jet is formed when the charge density at the surface of the meniscus overcomes the surface tension of polymer solution, and the stability limit of meniscus is known as the Rayleigh limit [4].

Although the EHD fabrication was initially proposed by Formhals in 1934 [5-6], in recent years it has garnered renewed interest as a simple method for the preparation of fine tuned nano- or microscale particles or fibers. This process has been used in the fabrication of a variety of materials such as patterned materials [7-8], films [9], coatings [10], membranes [11], scaffolds [12], drug carriers [13], or finely controlled structures [14]. In comparison with other fabrication methods for nano- or microscale particles or fibers, the EHD fabrication is cost effective, size controllable, reproducible, and fast.

The EHD fabrication is categorized by two modes, electrospraying and electrospinning. The former fabricates particles and the latter fabricates fibers. These modes can be controlled by several parameters such as applied voltage, flow rate, surface tension,

solution viscosity, needle size, and solvent volatility [2].

Among these parameters, the polymer viscosity arising from the chain entanglement of polymers is a crucial parameter in EHD fabrication. Doshi et al. suggested that the ideal viscosity for electrospinning is from 800 to 4000 cP [15, 16]. Below 800 cP, polymer chain entanglement is insufficient, resulting in beads or beaded fibers, owing to unstable jet formation. That is, if sufficient viscosity is attained, the jet is stabilized and cannot break into droplets.

Additionally, when droplets or fibers are formed from the tip, two competing effects occur during flight [17]. In the case of electrospraying, solvent starts to evaporate during flight; the surface tension of droplet thereby decreases and the charge density at the surface increases. This increases the internal repulsion force, resulting in droplet subdivision. This phenomenon is referred to as Coulomb fission. Since solvent evaporation occurs continuously, Coulomb fission continues and a greater number of smaller particles are formed. However, the chain entanglement of the polymers counteracts Coulomb fission, thus the subdivision of droplets is restricted. In the case of electrospinning, fibers are broken into thinner strands because of the stress caused by the electric attraction force between a fiber and a counter charged collector. With the increase of the electric attraction force, the increased stress stretches the fiber to a thinner diameter. However, the entanglement of polymers resists such stress, which limits the reduction of diameter.

Consequently, chain entanglement plays a critical role in EHD

fabrication. First, it affects the cone-jet stability, which determines the mode of the EHD fabrication (electrospraying or electrospinning). Second, it affects the stability of formed droplets or fibers, which limits the subdivision of droplets and the reduction of fiber diameter. Therefore, a comprehensive understanding of chain entanglement in polymer solutions is important for regulating EHD fabrications.

Silk fibroin (SF), which is produced by silkworms, is now a well-known biomaterial due to its biocompatibility, biodegradability, and low toxicity [18]. This natural polymer is thus considered a superior material in biomedical applications such as fibers [19], nanomats [20], sponges [21], films [22], hydrogels [23], and micro- or nanoparticles [24, 25].

Currently, many studies are focused on the application of SF nanofibers (or sub-micron fibers) that are prepared by electrospinning and are used as a scaffold [26] in tissue engineering. Although chain entanglement is significant in the EHD fabrication of SF, most researchers' primary aim is in the preparation of bead free nanofibers. The beads or beaded fibers are treated as failed products and no further studies have been performed on why such products are formed. Some researchers have focused on the effects of SF concentration on EHD fabrications, and concluded that is affected by the amount of chain entanglement in the solution [27-29]. Moreover, the effects of SF molecular weight on EHD fabrication were not studied because most researchers used a fixed SF extraction solution such as LiBr or $CaCl_2$/EtOH/H_2O. However, even under identical extraction conditions, the molecular weight of the resulting SF can be affected by various factors such as degumming conditions, silkworm

species, etc. Moreover, the fabrication of SF nano- or microparticles by EHD fabrication has not yet been comprehensively studied. Only SF nanopowder has been prepared, using formic acid as a solvent [30].

In this study, SF microparticles were prepared via electrospraying by dissolving SF in a 1 M LiCl/DMSO solvent, which had been used previously for the electrospraying of sericin. First, we investigated the dissolution behavior of SF in LiCl/DMSO solvent, since this solvent had not previously been used for SF dissolution. The effects of the molecular weight distribution (MWD) and the concentration of SF on EHD fabrication were also investigated to determine optimal conditions for the preparation of SF microparticles. In addition, the effects of the chain entanglement of SF on EHD fabrication were investigated thoroughly. The rheological behavior of SF in the two most common solvents, formic acid and HFIP, were studied in terms of the effects of chain entanglement on EHD fabrication. The relationship between the final products' shape and shear, or dynamic viscosity, was investigated and explained in terms of chain entanglement. Additionally, a new parameter was established for the degree of chain entanglement was used to predict the final products' shape and size.

II. Literature Survey

2.1 Relationship between chain entanglement and the EHD fabrication

2.1.1 Relationship between chain entanglement and concentration

When we plot the viscosity of polymer solution against polymer concentration, several regions can be distinguished such as dilute, semi-dilute unentangled, semi-dilute entangled, and concentrated, according to chain entanglement [31]. In the dilute region, polymer chains do not overlap and the viscosity increased proportionally to the polymer concentration ($\eta \propto c$). When the polymer concentration was increased further, polymer molecules began to overlap. This point is called the overlap concentration (c_{ov}). In the semi-dilute, unentangled region, the polymer chains begin to overlap but are not entangled significantly. In this region, the viscosity is proportional with concentration to the 1.25 power. When the concentration exceeds a critical entanglement concentration (c_e), chains are entangled significantly, and the viscosity becomes proportional with concentration to the 4.25-4.5 power, which is the semi-dilute entangled region:

$\eta \propto c^1$ dilute region

$\eta \propto c^{1.25}$ semi-dilute unentangled region

$\eta \propto c^{4.25-4.5}$ semi-dilute entangled region

Gupta et al. [32], Jun et al. [33], and Bock et al. [34] accounted for chain entanglement with c_{ov} and c_e. When c is less than c_{ov}, no chain entanglements are formed (dilute region). When $c_{ov} < c < c_e$, the chain will overlap but no significant entanglement occurs, which corresponds to the semi-dilute, unentangled region. When $c_e < c < 3c_{ov}$, the solution is now classified as semi-dilute, moderately entangled. Finally, at $c > 3c_{ov}$, the solution is referred to as concentrated or semi-dilute, highly entangled.

$c/c_{ov} < 1$ dilute region

$1 < c/c_{ov} < 3$ semi-dilute moderately entangled region

$3 < c/c_{ov}$ semi-dilute highly entangled region

Bock et al. [34] reviewed the effects of these concentration regions on the shape of product after EHD fabrication. Debris, beads, beaded fibers, or fibers were formed with polymer concentration falling in each of the different concentration ranges (Figure 1).

Furthermore, c_{ov} can be derived from the following equation:

$$c_{ov} = \frac{M_w}{4\pi(\quad)^3 N_{V}} \qquad (1)$$

where M_w is the molecular weight, R_g is the radius of gyration, and N_{av} is Avogadro's number. This means that the molecular weight of the polymer also plays an important role in determining c_{ov}.

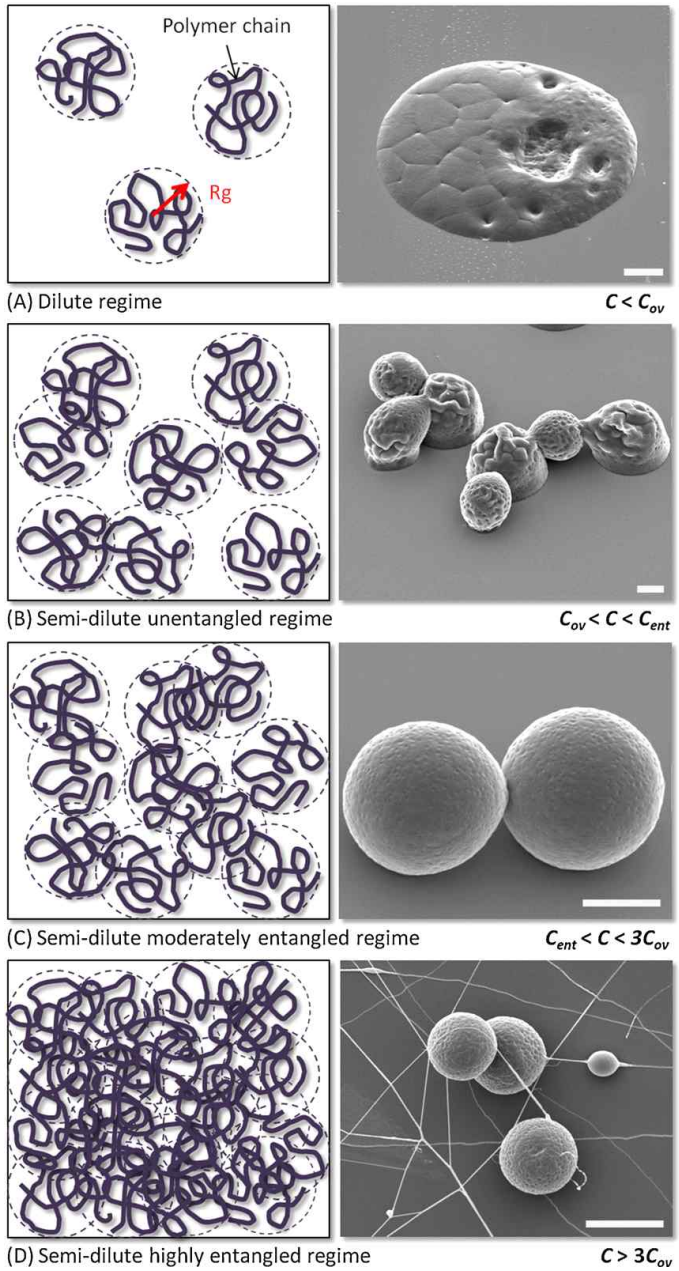

Figure 1. Physical representation at the molecular level of various entanglement regimes obtained for different polymer concentrations. [34]

Therefore, chain entanglements arise not only from the number of chains (polymer concentration) but also from the chain length (polymer molecular weight).

It can thus be concluded that the shape of product after EHD fabrication can be determined by the polymer concentration and the polymers' molecular weight.

2.1.2. Parameters of chain entanglement

There are several parameters that describe chain entanglement. The Berry number, also referred to as the Simha-Frisch parameter, is derived from the Huggins equation (Eq. 2), which describes the solution viscosity [35].

$$\eta_{sp}(c) = [\eta]c + k_H([\eta]c)^2 + \cdots \quad (2)$$

where $\eta_{sp}(c)$ is the specific viscosity, $[\eta]$ is the intrinsic viscosity, c is the polymer concentration and k_H is the Huggins coefficient. In this equation, $[\eta]c$ is the Berry number, B_e. This factor is used to predict the results of electrospinning. Koski et al. [36] used this parameter to predict the formation of bead or fiber structure of electrospun PVA, and Y. Yamashita et al. [37] used it to predict the diameter of electrospun polystyrene-polybutadiene alloy elastomer (SBS) nanofibers. In this theory, the dilute region is defined when $B_e < 1$ and the semi-dilute entangled region is represented by $B_e > 4$. To obtain fine structured nanofibers, B_e values should be between 5 and 12. This parameter assumes that each polymer chain has equivalent spherical hydrodynamics and does not interact with other chains.

However, at high concentrations, interactions between polymer chains are unavoidable. Therefore, the Berry number is only useful for solutions of relatively low polymer concentration.

On the other hand, the chain entanglement number in solution, $(n_e)_{soln}$, can also be used to describe chain entanglement. The entanglement molecular weight, M_e, denotes the average molecular weight between entanglement junctions of polymer in its melt state, and is derived from the following formula [38]:

$$M_e = \frac{4\rho RT}{G_N^0} \quad (3)$$

where ρ is polymer density, R is the ideal gas constant, T is temperature, and G_N^0 is the plateau modulus of the polymer. For reference, the M_e of polystyrene is 16 kDa, poly(ethylene oxide) (PEO) is 2 kDa, and poly(vinylpyrrolidone) (PVP) is 16 kDa [39]. In a polymer solution, the entanglement molecular weight is affected by the polymer volume fraction, ϕ_p, and thus, entanglement molecular weight in solution, $(M_e)_{soln}$ is defined as $(M_e)_{soln} = M_e/\phi_p$.

The variable $(n_e)_{soln}$ is derived from the relationship between M_e and molecular weight M_w (Eq. 4); $(n_e)_{soln}$ is the parameter that quantifies the number of entanglements per polymer chain [17].

$$n_{soln} = \frac{M_w}{(M_e)_{soln}} = \frac{(\Phi_p M_w)}{M_e} \quad (4)$$

Since two chains are needed to make an entanglement, the actual chain entanglement number per chain is $(n_e)_{soln} - 1$. For example, $(n_e)_{soln} = 2$ means one chain has one entanglement.

In the EHD fabrication, when $(n_e)_{soln}$ was less than 2, beads were formed, beaded fibers were then formed for values of 2-3.5. When $(n_e)_{soln}$ exceeded 3.5, fibers were formed. Actually, $(n_e)_{soln}$ has been used to predict the results of EHD fabrication for several polymers such as polystyrene (PS) [40], PEO [41], poly(D,L-lactic acid) (PDLA) [42], and poly(L-lactic acid) (PLA) [33]. These results show that regardless of polymer polarity, the mode of each EHD fabrication corresponded well to $(n_e)_{soln}$.

2.2. Nanostructure and self-assembly of SF solutions

In order to understand the bead- or fiber-formation mechanism in the EHD fabrication of SF, we have to first determine the molecular structure of SF.

Basically, SF is composed of heavy chains (350 kDa) and light chains (25 kDa), which are linked by a single disulfide bond [43, 44]. The heavy chains have large hydrophilic domains at their ends, with a large hydrophobic domain and small hydrophilic domains in the internal parts of chains (Figure 2). It has been established that SF molecules form a micelle in water or polar solvents by hydrophobic interaction. These micelles self-assemble by several factors such as concentration, applied shear force, secondary structure, or solvent properties.

Particularly, Jin et al. [45] and Lu et al. [46] studied the self-assembly mechanism of SF micelles during the silk spinning process of silkworms or spiders. In aqueous solution, SF molecules make micelles of 100-200 nm in size. With an increase of concentration by water elimination, micelles combine with one another to form larger structures.

However, the two works differed in opinion on the post mechanisms. Jin et al. [45] speculated that micelles compose globules, and these globules reassemble into a fibrillar structure (Figure 3). On the other hand, Lu et al. [46] concluded that micelles order into filaments, not globules, because of repulsive micelle charges caused

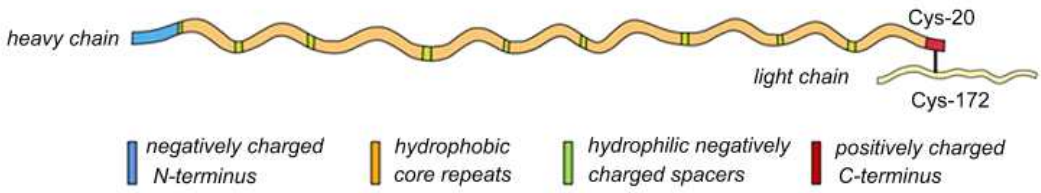

Figure 2. Structure of SF light chain and heavy chain. [24]

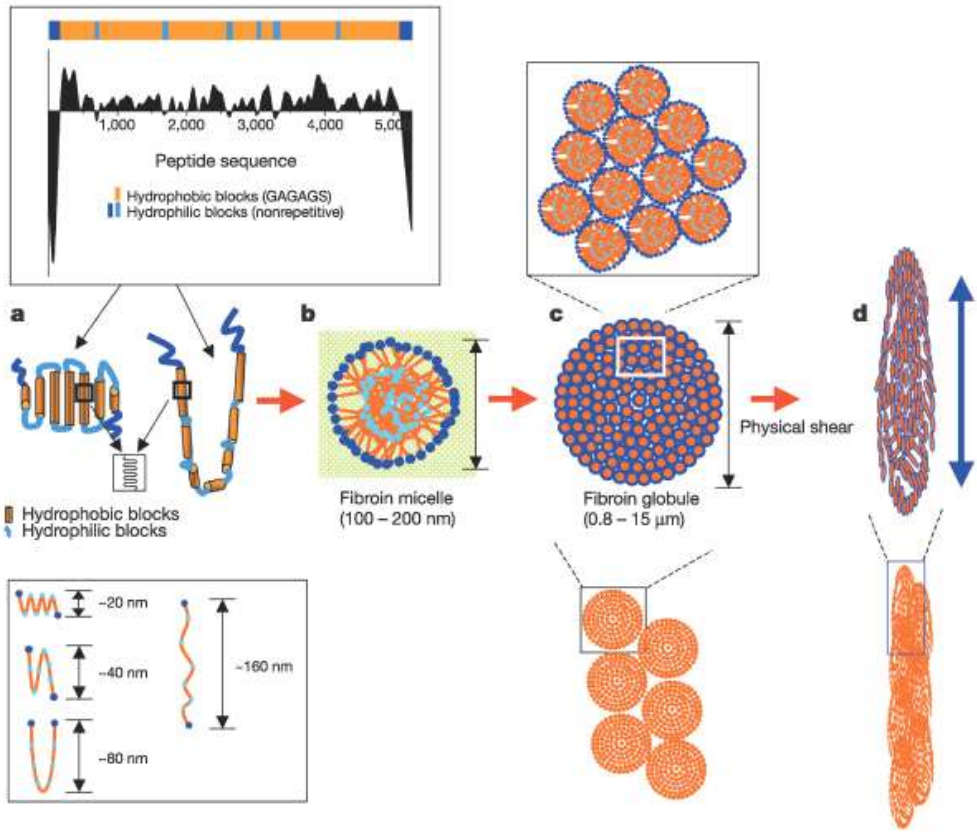

Figure 3. Micelle formation of SF molecules by hydrophobic interaction in aqueous solution. [45]

by the higher pH of aqueous solution (7-8) than the pI of SF (4-5), these filaments in turn form larger filaments. Zhang et al [47] explained the mechanism of SF electrospinning from formic acid as solvent with micelle interactions. In formic acid, SF molecules form micelles and each micelle weakly interacts with the others at low concentration. As concentration increases, interactions between micelles increase and nanofibers are formed. It is thought that this relationship between SF micelles and fiber formation can be applied to the EHD fabrication of SF.

2.3. Rheological behavior of SF solution

Generally, the rheological behavior of an SF solution depends on the solvent. In studies from Um et al. and Cho et al., high molecular weight SF showed a high shear viscosity in aqueous or formic acid [48-51]. In aqueous solution, shear thinning occurred at low shear rates (0.1-3 s^{-1}) because SF molecules aggregated by the shear force. On the other hand, in the formic acid, SF exhibited Newtonian behavior (negligible shear thinning) because SF molecules are stable and do not aggregate in formic acid.

Matsumoto et al. [52] observed reduced shear thinning at higher SF concentrations (13-17.5 wt%) albeit in aqueous solution. They reasoned that this was due to a reduction of the SF molecules' mobility. As concentration increases, intermolecular interactions are strengthened, which results in a reduced mobility of SF molecules. Shear viscosity above 17.5 wt% was not measurable due to the instability of the solutions. On the other hand, a drastic shear thickening behavior was observed by other researchers [53-55]. These phenomena were attributed to β-sheet crystallization. However, if the pH of aqueous solution was reduced to about 4, SF exhibited Newtonian behavior instead of shear thickening with increased shear viscosity. Such pH dependent shear viscosity is thought to be due to the hydrophilic domains at the ends of the heavy chains; these domains contain negatively charged amino acids such as Glu and Asp (pI = 4-5). At acidic pH, these portions are neutralized and induce additional intra- or intermolecular interactions such as hydrophobic

interaction and hydrogen bonding. As a result, a reduction of pH has an effect similar to that seen with increasing concentration [56]. From these works, we can see that the pH of a solvent has an important role in the rheological properties of a polymer solution because it can effect chain conformation or nanostructure.

Wang et al. [57] and Nisal et al. [58] reported on shear and dynamic viscosity using ionic liquid (1-allyl-3-methylimidazolium chloride, AmimCl) and aqueous solution, respectively. Rheological behavior of each solution at a high shear rate changed from Newtonian to shear thinning as SF concentration increased. Then, its slope of zero or specific viscosity against SF concentration dramatically increased at a specific concentration, called the critical concentration, C^*. This change means that a considerable chain entanglement has occurred. These changes may also be observed in dynamic viscosity measurements. The storage modulus showed a plateau at low frequency in the dilute region and gradually disappeared as the concentration increased. Above C^*, however, all of the storage and loss moduli increased with frequency increase, overlapping at high frequency.

2.4. Relationship of SF solution viscosity and the EHD fabrication

To produce an SF nanofibrous mat or scaffold by EHD fabrication, various conditions such as degummimg protocol [59, 60], dissolution protocol [61], and SF concentration [27] are considered, as these conditions have a decisive effect on product size and shape, i.e. fiber or bead. Of all these conditions, solution rheology arising from concentration, molecular weight, and molecular weight distribution (polydispersity index, PDI) has critical role in EHD fabrication. Generally, with an increasing viscosity of SF solution, uniform nanofibers are formed and their diameters increase. As the viscosity of the SF solution decreases, the diameters then decrease and beaded fibers or beads are formed. In cases where beads are produced, the fabrication method is called electrospraying.

2.4.1. In FA or HFIP solvent system

Many researchers fabricate nanofibrous SF mats or scaffolds by EHD fabrication with various solvents, such as formic acid [62], HFIP [63], water (aqueous solution) [64], or other solvents [65-68]. Among these solvents, formic acid and HFIP are the most frequently used.

In the formic acid case, Sukigara et al. [27, 69] researched the effects of solution concentration, applied voltage, and distance from tip to collector. They found that solution concentration is the most

dominant of these parameters in producing uniform and continuous fibers. At low SF concentrations, beads were formed, with continuous fibers formed only above a specific SF concentration. Additionally, fiber diameter increased with solution concentration. Min et al. [70] also demonstrated that continuous fibers can be obtained above a specific concentration, and concluded that chain entanglement plays an important role in electrospinning.

Zhang et al. [71] studied SF nanofiber mats fabricated with HFIP and FA. In their research, SF-HFIP solution viscosity was six times higher than that of SF FA solution, which resulted in differing diameters of SF fibermats. They argued that a greater solution viscosity may induce hard jet extension and disruption of electrospinning. Another study also addressed the relationship between solution concentration and electrospun products using solution rheology or chain entanglement. Min et al. [70] found that, at a SF-HFIP solution concentration of 7 wt%, solution viscosity increased significantly owing to entanglement of SF macromolecular chains and unimodal nanofibers were formed.

Despite the many studies on the effects of viscosity on EHD fabrications, only the SF concentration was observed to have changed. Other factors that could affect the solution viscosity, such as molecular weight or the PDI of SF have not been investigated in depth.

Cho et al. [61] observed the effects of the molecular weight of SF on EHD fabrication by altering the dissolution protocol and storage time. They dissolved SF in 9.3 M LiBr and $CaCl_2$/EtOH/H_2O

solution. With an increased dissolution time for $CaCl_2/EtOH/H_2O$, the molecular weight of SF decreased because of the decomposition of SF macromolecules by salt. Then, as the storage time of SF-FA dope solutions increased, the molecular weight of SF was decreased by hydrolysis. The authors of this study then confirmed that the shear viscosity of SF-FA solutions had increased with increasing molecular weight. Consequently, owing to the increase of shear viscosity, the SF with high molecular weight was favorable for fiber formation (without beads or beaded fibers). Ko et al. [60] obtained SF by various degumming methods such as high temperature high pressure (HTHP), citric acid, and sodium oleate/sodium carbonate solution (soap/soda). In their research, degumming with soap/soda led to greater degradation and that with HTHP caused less degradation. The molecular weight and viscosity increased in the following order: HTHP, acid, soap/soda. As with the work of Cho et al., a high molecular weight SF dope solution had high viscosity and was favorable for fiber formation. Ko et al. also argued that there is a critical solution viscosity to produce fibers. At values exceeding this critical solution viscosity, fibers were formed; beads or beaded fibers were formed for lower viscosities.

2.4.2. In other solvent systems

Similar behaviors were found in other solvent systems. In aqueous solution, droplets or beaded fibers were obtained at low concentrations, while fibers were obtained at high concentrations, owing to the increase of viscosity. In aqueous solution, SF

macromolecules had random coil conformations with few chain entanglements and exhibited shear thinning at low shear rates [29, 72]. However, with increased concentration, sufficient chain entanglements occurred and shear viscosity was independent of shear force. Hodgkinson et al. [73] also studied these behaviors. In their research, for high molecular weight polymer such as SF, shear thinning at intermediate concentrations (13-27 wt%) is caused by shear induced changes to chain entanglement, interaction, deformation, and orientation. Additionally, the loss modulus (G″) was higher than the storage modulus (G′) for all frequencies and the two values increased depending on concentration and frequency. Particularly, at high concentration, G′ and G″ increased in parallel and a crossover point was not observed, meaning that the solutions approached gelation.

However, when pH conditions were changed, different rheological behavior was observed [75]. For pH 6.9, Newtonian behavior was observed at 30 wt%, and shear thinning was observed at low shear rates when the concentration was higher than 30 wt%. If the pH decreased to the pI of SF (pH 4-5), shear thinning with low shear rates and shear thickening with a high shear rate were observed, even at lower concentrations. Additionally, lowering the pH made it possible to reduce the electrospinnable concentration while the average diameter of the nanofibers became smaller. It is thought that low pH reduces the repulsive force between SF molecules and improves hydrophobic interaction. These behaviors agreed with the previously mentioned work by Matsumoto et al.

SF-TFA solution also exhibited similar rheological behavior and

EHD fabricated products [68]. With increasing SF concentration, shear viscosities and shear thinning at low shear rates increased, and EHD fabricated products went through several steps from bead, beads on string, beads integrated into fiber, branched fiber, and finally to fiber. The fibers were more fine and their diameters increased with increasing concentration. The authors of Ref. [68] also explained these tendencies in terms of solution viscosity. With increasing concentration, more chain entanglements arise, and the solution has a higher elongational viscosity.

Although there are many studies on the relationship between EHD fabrications and SF concentration, studies on the effects of SF molecular weight and PDI on EHD fabrication are scarce. It is thought that because most researchers degum and dissolve SF with fixed chemicals and conditions, SF might have constant molecular weight and PDI.

Aznar-Cervantes et al. studied the effects of SF dissolution protocol on EHD fabrication [76]. SF was dissolved in 9.3 M LiBr, $CaCl_2/EtOH/H_2O$, and $CaCl_2/H_2O$ solution. In these protocols, the molecular weight and PDI of SF was varied with different dissolution solvents. The SF dissolved in 9.3 M LiBr had the highest molecular weight and the narrowest PDI. The SF dissolved in $CaCl_2/EtOH/H_2O$ was most polydispersed. Although the rheological properties of SF solutions were not mentioned in this study, nanofibers fabricated with SF dissolved in 9.3 M LiBr solution had the smallest diameters and the narrowest size distribution. In the case of the nanofibers fabricated from SF dissolved in the $CaCl_2/EtOH/H_2O$, the greatest polydispersed size distributions were observed. Based on this

research, we can assume that the molecular weight and PDI of SF plays an important role in EHD fabrication.

2.5. Fabrication of SF microparticles

2.5.1. Fabrication methods of SF microparticles

SF nano- and microparticles were previously prepared using several different methods. Although emulsion techniques are frequently used to prepare polymeric microparticles, only a few cases have been reported in which this technique was used to prepare SF microparticles. Baimark et al. prepared porous SF microparticles using a water-in-oil emulsion technique [77]. Here, the particles had a spherical shape and their sizes ranged from 50-150 nm. The most widely used method for SF nano- and microparticle preparation involves the self-assembly of SF molecules. Jin and Kaplan reported that SF forms a sphere like micelle via a self-assembly mechanism [45]. This mechanism can be induced either by adding a hydrophilic polymer to the mixture [78] or by adding water miscible organic solvents, such as acetone [79], ethanol [80], and dimethylsulfoxide [81]. When a hydrophilic polymer is mixed with the SF solution, a phase separation occurs between the two polymers and the SF assembles into nano- or microparticles [78]. In addition, some water miscible organic solvents can serve as non-solvents for SF and, therefore, the addition of SF solution into an organic solvent, or vice versa, can induce SF precipitation. A gradual addition of water miscible organic solvents induces a transition to the secondary structure of SF, which is followed by the precipitation of SF. The precipitation will not proceed into forming large aggregates because of electrostatic repulsion; thus, nano- or microparticles are formed [79-81]. Another technique that has been used for SF microparticle

preparation is spray drying [82]. Although it is difficult to prepare nanoscale particles with this fabrication method, it is relatively simple when compared to other methods. Other miscellaneous methods for SF nano- or microparticle preparation include techniques such as the use of supercritical CO_2 [83], a template technique using liposomes [84], a salting out system [85], a capillary microdot technique [86], a milling process [87], and a laminar jet break up technique [88].

Electrospraying, sometimes referred to as EHD spraying, uses strong electrostatic forces to emit polymer particles from the meniscus of the polymer solution. Particles ranging in size from nano- to micrometers can be prepared in this way, and the size distribution of this technique is quite narrow under optimal conditions. In addition, if one uses two needle coaxial electrospraying, then capsules and bubbles can also be prepared [89]. The basic principles of electrospraying are similar to electrospinning, with the exception that fibers are formed in the latter case. Therefore, using a single type of polymer and set of equipment, either particles or fibers can be formed, depending on the input parameters. For example, particles will be formed if the polymer solution has a low viscosity (or low concentration), but fibers will be formed when the viscosity (or concentration) of the solution increases [47]. In addition, there are several parameters that can affect particle size, including the viscosity and conductivity of the polymer solution, the applied voltage, and the feeding rate of the dope solution. An advantage of the electrospraying technique is that it only requires basic instrumentation and allows for monodispersed particle generation with high production efficiency. Electrospraying induces less shear stress compared to the emulsion technique, its microparticle size is easier to control compared to the

self-assembly method, and no heat is required (a requisite for spray drying) [1, 34]. Recent studies have suggested that various types of polymers can be produced by electrospraying and then used for drug delivery thanks to the small size of the electrosprayed particles [2, 25]. SF has also been produced by eletrospraying, wherein SF nanopowder was prepared using formic acid as a solvent. In this case, the size of the SF nanopowder particles were about 80 nm when using a 0.25% (w/w) solution [30].

III. Materials and Methods

3.1. Materials

Bombyx mori cocoons for SF extraction were purchased from Heungjin (Korea). Lithium chloride (LiCl), formic acid, sodium carbonate (Na_2CO_3), sodium oleate, calcium chloride ($CaCl_2$) and formic acid were purchased from Sigma Aldrich (USA). Methanol and ethanol (EtOH) were purchased from Samchun (Korea) and dimethyl sulfoxide (DMSO) was purchased from Acros (USA). 1,1,1,3,3,3-hexafluoro-2-propanol (HFIP) was purchased from Matrixscientific (USA). Other reagents were purchased from Sigma Aldrich (USA).

3.2. Preparation of regenerated SF

The cocoons were degummed twice with a 0.2 wt% (w/v) sodium carbonate and 0.3 wt% (w/v) Marseille soup solution at 100℃ for 30 min, then rinsed with distilled water to remove the sericin. The remaining SF fibers were dried in an oven overnight at 50℃. After this, the SF fibers were dissolved in two different solutions: a $CaCl_2$/EtOH/H_2O (SFC) and a LiBr (SFL) solution. For the first solution, the SF fibers (20 g) were dissolved in 500 ml of a $CaCl_2$/EtOH/H_2O (1/2/8 molar ratio) solution at 80℃, with dissolution

times ranging from 5 min to 180 min. The second solution was prepared in a similar manner; the same weight of SF was dissolved in 500 ml of a 9.3 M LiBr solution at room temperature for 15 h. Each of the SF solutions underwent dialysis in a dialysis tube (Spectra/Por®, MWCO 6-8,000, USA) against distilled water for 72 h. The dialysis water was changed every 2 hours during the day time. Finally, after dialysis, the SF solutions were lyophilized to obtain an SF powder. Table 1 shows a summary of the sample codes for each of the SF powders that were used in this study.

3.3. Physical measurements of SFCs

The molecular weights of the SFCs were measured by gel filtration chromatography (GFC) (ÄKTA purifier, GE Healthcare, USA) using a Superdex column (Superdex 200 10/300GL, GE Healthcare, Sweden) at a flow rate of 0.5 ml/min and a 6 M urea solution was used for elution. Gel filtration markers (Gel Filtration Markers Kit for Protein Molecular Weights 29,000-700,000 Da, Sigma Aldrich, USA) were used to create a calibration curve for molecular weight calculation.

Densities of SFCs were calculated using the following formula, (Eq.5)

$$\rho_s = m_s / (m_s - m_h) \times \rho_h \quad (5)$$

where ρ_s (g/cm^3) is the density of the SFC powder, ρ_h is density of hexane. m_s (g) is the mass of SFCs in air, and m_h is the mass of SFCs in hexane.

Table 1. SF samples used in this study

Sample	Solvent	Dissolution temperature	Dissolution time
SFL	LiBr	R.T	15 h
SFC005	$CaCl_2/EtOH/H_2O$	80℃	5 min
SFC030			30 min
SFC060			60 min
SFC180			180 min

3.4. Fabrication of SFC microparticles with 1M LiCl/DMSO solvent by EHD process

3.4.1 SFCs Solubility test in LiCl/DMSO solvent

To find an optimal concentration of LiCl in DMSO, SFC005 powders were dissolved in LiCl/DMSO solvents having different LiCl concentrations (0.5 M, 1 M, 1.5 M). Then, 100 mg of SF powder was added to 1 ml of LiCl/DMSO solvent, and stirred at 40 C for 60 min to allow the SF to dissolve. Any undissolved SF was then precipitated by centrifugation at 10,000 g, and the absorbance of the supernatant was measured using a UV spectrometer (Optizen UV2120, Duksan Mecasys, Korea) at 280 nm. A calibration curve was used to calculate the total amount of dissolved SF; this was obtained from the standard SF solution that had no observable precipitates after centrifugation. After finding the optimal concentration of LiCl in DMSO, the maximum solubility of the SFCs was measured in a similar manner, and a predetermined amount of SFCs were added to a 1 M LiCl/DMSO solvent. Finally, any undissolved portion of the solution was removed and the absorbance of the supernatant was measured at 280 nm.

3.4.2. EHD fabrication of SFCs with 1 M LiCl/DMSO solvent

Dope solution was prepared by dissolving SFCs in 1 M LiCl/DMSO

solvent at 40℃ for 60 min. Prepared dope solution was filtered with a nonwoven filter and loaded into a 1 ml syringe with a 21 gauge metal needle. Then, dope solution was EHD fabricated to a methanol coagulation bath using a syringe pump (KDS100, KD scientific, Korea). The distance from tip to collector was 10 cm. The applied voltage was 22 kV and the flow rate was 0.4 ml/hr. Fabricated SFCs were washed three times with methanol then collected. After drying, the shapes and sizes of the fabricated SFCs were measured using a field emission scanning electron microscope (FE-SEM).

3.5. EHD fabrication of SFCs with formic acid and HFIP

3.5.1. EHD fabrication of SFCs

SFCs were dissolved in formic acid at RT for 10 h and in HFIP at RT for 3 days. Each prepared dope solution was loaded into a 1 ml syringe with a 21 gauge metal needle and then EHD fabricated onto aluminum foil. The distance from tip to collector was 10 cm. The applied voltage was 13 kV and the flow rate was 0.3 ml/hr. The shapes and sizes of the fabricated SFCs were measured using an optical microscope (LV100D, Nikon, Japan) and an FE-SEM (JSM-7600F, JEOL, Japan).

3.5.2. Property analysis of SFCs dope solution

SFC particle size distribution in 0.5 wt% (w/v) solution was measured using an electrophoretic light scattering spectrophotometer (ELS-8000, Otsuka Electronics, Japan).

The rheological properties of SFC dope solutions were measured using a rheometer (Advanced Rheometric Expansion System (ARES), Rheometric Scientific, UK) with 50 mm and 0.04 rad cone and plate geometry. About 1.5 ml of each SFC dope solution was loaded onto the cone and plate. Shear viscosity was measured using a steady rate sweep test mode and shear rates ranged from 1.0 to 700 s^{-1} at 25℃. Dynamic moduli analysis of the SFC dope solutions was measured by a dynamic frequency sweep test (strain controlled) mode. The frequency range was 0.5-510 rad/s and strain was 200.

IV. Results and Discussion

4.1. Properties of SF

The molecular weight and PDI of SF samples were calculated from the calibration curve of molecular weight markers from FPLC. The calibration curve was drawn according to the molecular weight of the markers and their elution volume. From the calibration curve, each elution volume was converted to a molecular weight. Additionally, the intensities of the molecular weight distribution curve of the SFCs were converted to numbers of molecules. From these conversions, number average (M_N) (Eq. 6) and weight average (M_W) (Eq. 7) molecular weights were calculated.

$$\frac{\sum N_i \cdot M_i}{N} \qquad (6)$$

$$M_W = \frac{\sum N_i \cdot M_i}{\sum N_i \cdot M_i} \qquad (7)$$

Here, N_i was converted from intensity and M_i was converted from elution volume, and the polydispersity index = M_W/M_N.

When dissolution times with $CaCl_2/EtOH/H_2O$ solution were increased from 5 min to 180 min, molecular weight decreased and PDI increased (Figure 4, Table 2).

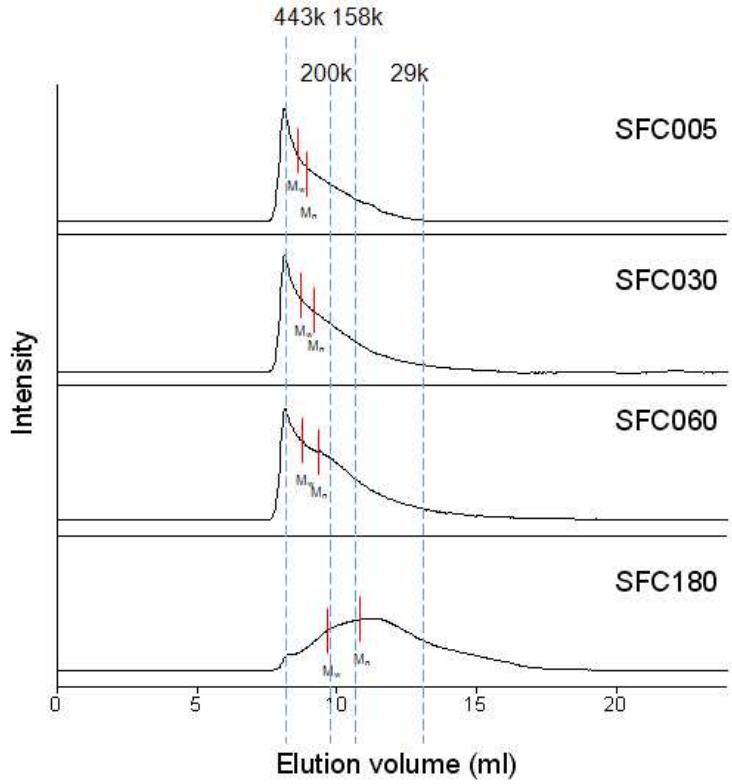

Figure 4. Molecular weight distribution of SFCs by dissolution times in $CaCl_2$/EtOH/H_2O solution.

Table 2. Molecular weight, molecular weight distribution and density of SFCs prepared by dissolution in $CaCl_2$/EtOH/H_2O solution

	M_N (kDa)	M_W (kDa)	PDI	Density (g/cm^3)
SFC005	324	398	1.23	1.25±0.07
SFC030	286	378	1.32	1.26±0.02
SFC060	257	359	1.40	1.30±0.02
SFC180	114	219	1.92	1.31±0.02

The weight averaged molecular weight of SFCs dissolved for 5 min, 30 min, 60 min, and 180 min were approximately 398 kDa, 378 kDa, 359 kDa, and 219 kDa, respectively, with PDI values increasing as 1.23, 1.32, 1.40 and 1.92, which indicates limited polydispersion. This increase is due to a reduced decomposition of specific sites of SF molecules by $CaCl_2$.

Densities were also calculated. Generally, an unknown polymer density is calculated from the polymer melt state or by the following formula:

$$\rho = M_{mon}/v_{mon}N_{AV} \quad (8)$$

M_{mon} is the monomer molar mass, v_{mon} is the volume occupied by a single monomer, and N_{AV} is Avogadro's number.

However, it is impossible to find SF in a melt state, so the former calculation method is useless. Furthermore, in solution state, SF molecules form micelles, making it virtually impossible to identify the occupied volume of a single monomer. Thus, it is also difficult to determine the SF density by the latter calculation method. For these reasons, most researchers studying SF do not attempt to measure density. However, some have made indirect calculations using the liquid-displacement method for finding the density of an SF scaffold. In this study, this method is also used and the calculated density value was about 1.2-1.3 g/cm^3. This value is similar to that of another report (1.3 g/cm^3) [91]. The densities subtly increased with concentration, which is thought to be due to smaller micelles being formed with decreasing molecular weight, allowing more macromolecules into the unit volume.

4.2. Fabrication of SFC microparticles with 1 M LiCl/DMSO by EHD fabrication

4.2.1. Determining optimal conditions for SF dope solution with 1 M LiCl/DMSO

The preparation of the polymer dope solution is critical because the solution can affect the entire downstream process of the polymer. Generally, the SF dope solution can be prepared in three steps. First, the sericin must be removed by a degumming process in order obtain a pure SF fiber. Second, the pure SF fiber can be dissolved using various methods to produce an aqueous SF solution. Currently, highly concentrated LiBr solution, or a tertiary solvent system of a $CaCl_2$/EtOH/H_2O solution, are commonly used at this stage and the salts are then removed by dialysis. Several studies have used aqueous SF solution as the dope solution. However, owing to the poor stability of SF in aqueous solution, this can induce irreversible aggregation, which can prove problematic further along in the procedure [49]. Therefore, in most cases, a third step is required to obtain a stable SF dope solution. Typically, the aqueous SF solution is lyophilized into a powder and then redissolved into another solvent such as HFIP or formic acid. In this study, LiCl/DMSO was used as solvent to prepare the SF dope solution instead of the HFIP and formic acid solvent. We had previously used this solvent to prepare sericin microparticles [92], and this solvent is optimal to work with because it is less expensive and less toxic when compared with HFIP. In addition, with this LiCl/DMSO solution, there is no

indication of degradation during dissolution when compared with the formic acid solvent. Figure 5 shows the solubility of SF powder in a LiCl/DMSO solvent system. Two types of SF powder were prepared for this experiment. SF fiber was dissolved either in a 9.3 M LiBr (SFL) solution or in a $CaCl_2$/EtOH/H_2O (SFC) solution. The results indicate that the addition of LiCl is necessary for dissolving the SFs in DMSO, regardless of the method of preparation. When 1 M LiCl was added to DMSO, the SFC005 completely dissolved within 60 min; however, in the 2 M LiCl/DMSO solvent, the solubility of the SFC005 decreased to 75 wt%, due to the salting out effect. Compared to SFC, SFL had limited solubility in LiCl/DMSO. When a 0.5 M LiCl solution was added to DMSO, nearly 40 wt% of the SFC005 dissolved, but the addition of this solvent did not dissolve the SFL at all. The maximum SFL solubility within the given time of one hour was approximately 80 wt% in 1 M LiCl/DMSO. Previous reports indicated that LiCl can cleave the hydrogen bonds in cellulose and protein [93, 94], thereby increasing the solubility of these polymers in the organic solvent. The different values for solubility may be attributable to the difference in the molecular weight distribution (PDI) of SFL and SFC. We previously reported on the differences between SFL and SFCs based on the PDI and hydrodynamic radius [49]. While the original molecular weight of SF remains intact with SFL, there is significant molecular weight degradation during the preparation of SFC. As a result, the hydrodynamic radius of SFL is smaller than that of the SFCs because the nondegraded SFL can maintain its original compact structure.

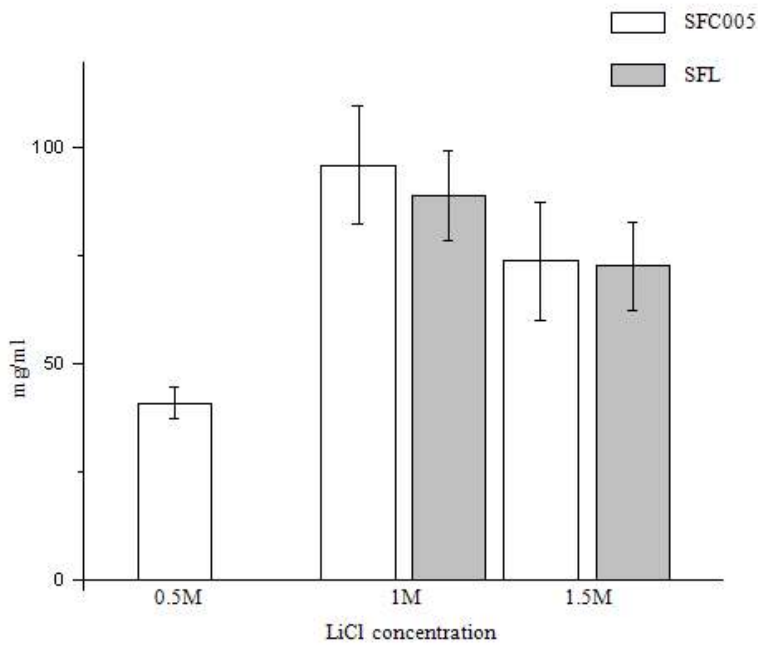

Figure 5. Solubility of SFC005 in LiCl/DMSO solvent by LiCl concentration.

Therefore, for a specified dissolution time, the solubility of SFL will be limited because of its compact structure, which hinders LiCl penetration. For these reasons, we used SFCs as raw material and 1 M LiCl/DMSO as a solvent for further experiments.

The molecular weight of SFC, which was discussed above, degrades significantly compared to the original SF. Therefore, we assumed that the solubility of SFCs would be different according to the degree of degradation. In this study, four different SFC samples were prepared according to their dissolution time in a $CaCl_2/EtOH/H_2O$ solution; Table 2 shows the PDI of each sample. As a result of degradation, the SFCs′ low molecular weight increases as dissolution time increases. In order to find the maximum solubility of different SFC samples, a predetermined amount of each SFC was dissolved in 1 M LiCl/DMSO. Figure 6 shows the absorbance of the supernatant of each solution according to the amount of SFCs initially added to the solvent. No further increase of absorbance indicates a maximum solubility. Thus, the maximum solubility of SFC005, SFC030, SFC060, and SFC180 were 10, 11, 13, and 14 wt%, respectively. It can be clearly observed that the SFCs with higher degradation can reach a higher maximum solubility in 1 M LiCl/DMSO. This result could be attributable to the relatively low molecular weight of the more degraded SFCs.

4.2.2. EHD fabrication of SFCs with 1 M LiCl/DMSO

A standard technique for electrospraying uses a volatile solvent that is volatilized before it reaches the collection plate. However, in this

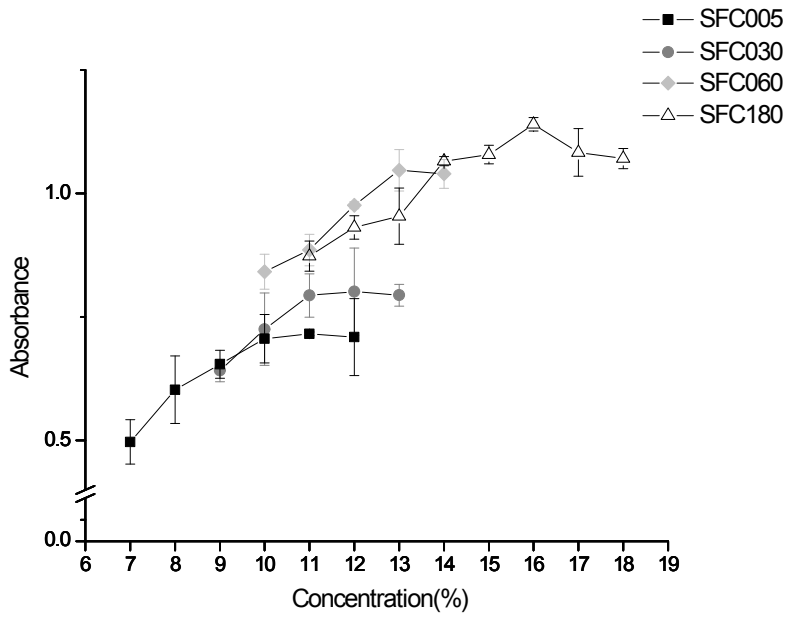

Figure 6. Solubility of SFCs in 1 M LiCl/DMSO prepared at various dissolution times in $CaCl_2/EtOH/H_2O$ solution.

study, DMSO was used, which has a boiling point that is much higher than room temperature. Therefore, the SF dope solution was electrosprayed toward a coagulant bath (instead of the collecting plate), which solidified the SF droplets emitted from the needle tip. Methanol was used as a coagulant because it is a well established standard and is the most common solvent that can make SF insoluble. Throughout the electrospraying of the polymer, the shape and size of the nano- or microparticles greatly depends on several parameters including the concentration of the polymer solution, the molecular weight of the polymer, the applied voltage, the flow rate, and the tip to collector distance. In this study, we focused on the concentration of dope solution and the PDI of the SF. Therefore, the applied voltage, flow rate, and tip to coagulant bath distance were fixed.

4.2.2.1. Concentration effects

Figure 7 shows the effects of SFC concentration on the shape of the microparticles. In the analysis of SFC005, the microparticle shape changed from irregular (6 wt%) to ovoidal (9 wt%) and finally became spherical (10 wt%) with increasing SFC concentration. Previous studies indicated that the concentration of the polymer has a high impact on the shape of the particles during electrospraying. Recently, Bock et al. [34] reviewed the electrospraying process of polymers and explained the effects of polymer concentration on the shape of the resulting polymer: The polymer concentration is important because it is correlated with polymer chain entanglement.

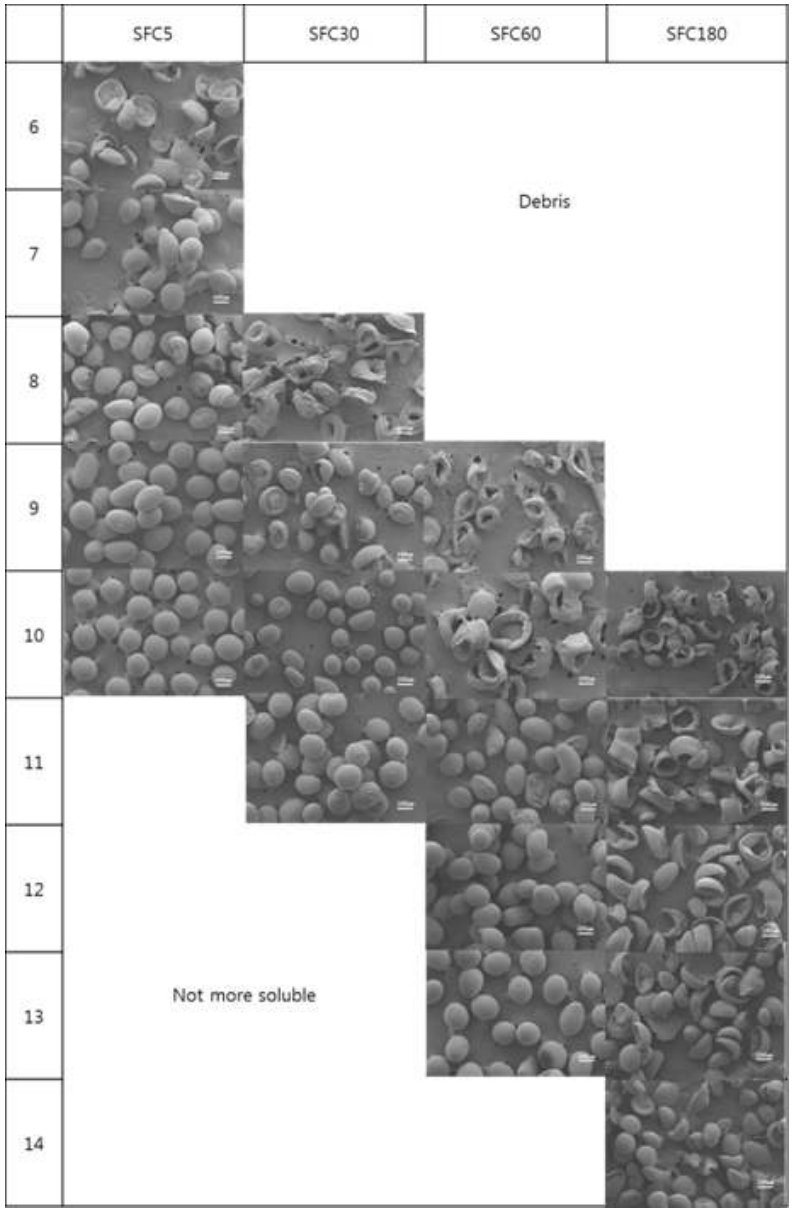

Figure 7. SEM images of EHD fabricated SFCs dissolved in 1 M LiCl/DMSO solution. Scale bar : 200 μm. Applied voltage is 22 kV, flow rate is 0.4 ml/hr, distance from tip to collector is 10 cm.

In a dilute polymer solution, there will be no chain entanglement between individual polymer chains.

However, when concentration increases, the polymer chains start to overlap; this specific concentration is referred to as the critical chain-overlap concentration (C_{ov}). Therefore, if the concentration of the polymer in the solution is lower than C_{ov}, no chain entanglement will occur (known as the dilute region). Under this condition, electrospraying is impossible or debris is formed. If the concentration is higher than C_{ov}, three different regions are possible: The first region is the semi-dilute, unentangled region where the concentration of the polymer is sufficient for polymer chain overlap but the chains will have limited entanglement. In this region, particles have an irregular, nonreproducible morphology. The second region is known as the semi-dilute, moderately entangled region and occurs when the polymer concentration further increases, causing the polymer chains to have moderate entanglement which creates dense particles. The semi-dilute, moderately entangled region is specified because this is the only region where the formation of spherical particles can be achieved by electrospraying. Finally, if there is an additional increase in concentration, then fibers or beaded fibers are formed, particularly if the polymer concentration greatly exceeds C_{ov}. This third region is called the semi-dilute, highly entangled region, and the process that occurs therein is referred to as electrospinning. Similar behaviors were also observed in our study. For each SFC sample, irregular shapes were formed when the SFC concentration was relatively low. Specifically, this can be observed at the following concentrations: SFC005 $\leq$ 8 wt%, SFC030 $\leq$ 9 wt%, and SFC060 $\leq$ 11 wt%. In the

case of SFC180, regular shaped particles were not obtained for any concentration. These irregular shapes indicate that stable SFC droplets cannot be formed during flight owing to limited entanglement between SFC chains; this could be referred to as the semi-dilute, unentangled region. In some samples, however, hemispherical shapes were observed (SFC005 at 7 and 8 wt% and SFC030 at 9 wt%), which indicates that the SFC droplets initially had a spherical shape during flight but were not dense enough to maintain that shape and thus deformed upon collision with the surface of the coagulant bath. Regardless, in these conditions, uniform particles cannot be prepared. However, when the concentration was increased further, more spherical particles were obtained. Sphere-like microparticles were found, along with some bean-like or oval microparticles. For the trials with SFC005 at 10 wt%, SFC030 at 11 wt%, and SFC060 at 12 wt%, the occurrence of sphere-like microparticles increased significantly. At these concentrations, chain entanglement was sufficient for creating a dense droplet, which overcame the surface tension of the coagulant. These concentrations would then represent the semi-dilute, moderately entangled region for SFC. The semi-dilute, highly entangled region was not observed in this study because of the inability to prepare a highly concentrated SFC solution (Figure 7). The diameters of the sphere-like SFC microparticles were around 200 nm. Interestingly, during the production of the SFC180 microparticles, sphere-like microparticles did not form, even at the maximum concentration. This result indicates that the molecular weight distribution of SF is also important. Thus, the effects of the molecular weight distribution of SF were also investigated in this study.

4.2.2.2. Effects of dissolution time in $CaCl_2/EtOH/H_2O$ solution

Examination of the 10 wt% concentration of all SFC samples indicates that a similar change from an irregular shape to a sphere-like shape can be observed from the SFC180 and SFC060 cases to the SFC030 and SFC005 cases. The PDI of each SFC may be responsible for this result, since the PDI values of SFCs are greatly affected by dissolution time in a $CaCl_2/EtOH/H_2O$ solution, as shown in Figure 4. A previous study reported that the shear viscosity of SFCs in water and formic acid is also greatly affected by dissolution time [28]. Because shear viscosity is an important factor in the electrospraying process, we investigated how the shear viscosity of SFCs in a 1 M LiCl/DMSO affects the final shape of the microparticles.

Figure 8 shows the rheological behavior of SFCs in 1 M LiCl/DMSO solvent. The original SF in the silkworm gland exhibits non-Newtonian behavior, typically a shear thinning [56]. In this study, SF in 1 M LiCl/DMSO solvent also exhibited shear thinning, though the extent of shear thinning was very small. A similar shear thinning of SF has been observed in other solvents such as formic acid [49]. SFCs that were prepared with greater dissolution time had a lower shear viscosity.

The increased portion of the low molecular weight SFCs should allow for less entanglement between the SFCs chains, which would result in a lower shear viscosity. Based on the notion that entanglement is the determining factor for the shape of microparticles, a decreased entanglement would have the same effect as a reduced

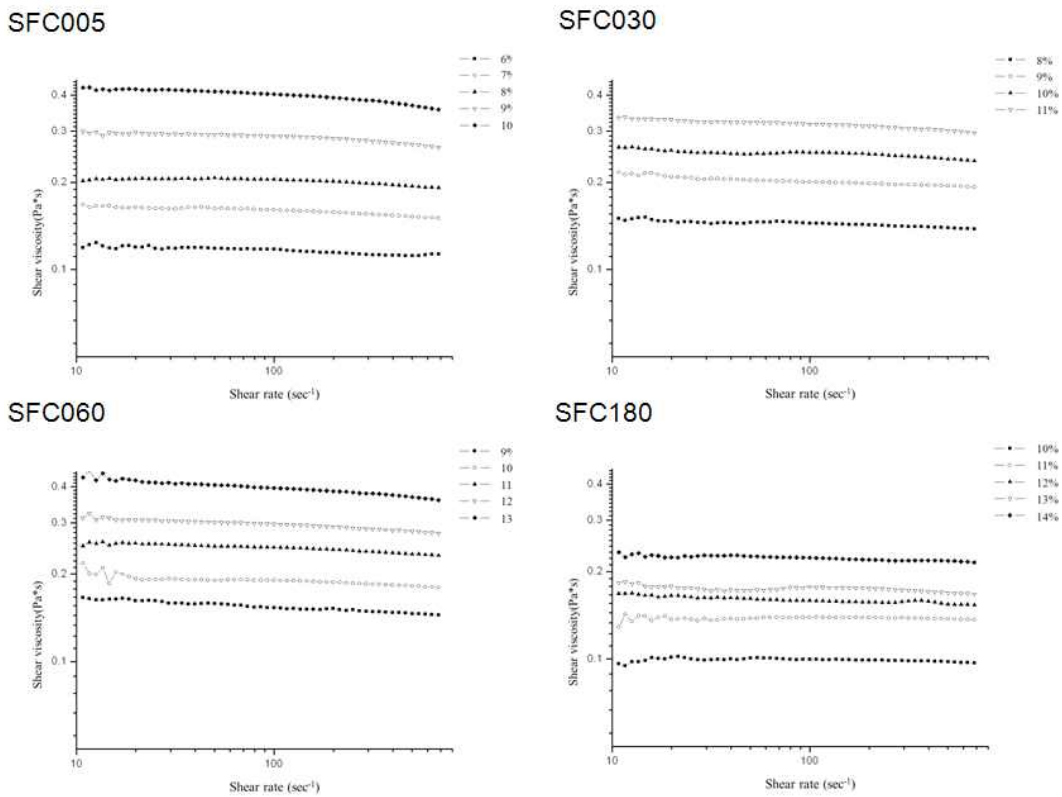

Figure 8. Effect of molecular weight and concentration of SFCs on shear viscosity of SFC solutions dissolved in 1M LiCl/DMSO.

concentration. Therefore, it can be concluded that both concentration and dissolution time in a $CaCl_2$/EtOH/H_2O solution can affect the final shape of SFC microparticles.

4.2.2.3. Spherical microparticle preparation

The study has demonstrated that both the concentration and dissolution time in a $CaCl_2$/EtOH/H_2O solution affect the shape of SF microparticles. To understand effects of these parameters, the shear viscosities of SF-DMSO solutions were measured by ARES (Figure 8).

All solutions showed Newtonian behavior or a slight shear thinning behavior over the whole shear rate which means that SF molecules are stable in 1 M LiCl/DMSO solvent. With lower concentration and molecular weight, lower shear viscosity was observed, owing to reduced chain entanglement.

Figure 9 presents a summary of the previously discussed results, with a plot of concentration versus shear viscosity. Based on the flow rate of the SF solution in the needle, the shear rate during the electrospraying was calculated to be 16 s^{-1} (Eq.9).

$$= \frac{32Q}{\pi} \qquad (9)$$

Here, r is shear rate at the tip of needle, Q is flow rate, and D is needle diameter.

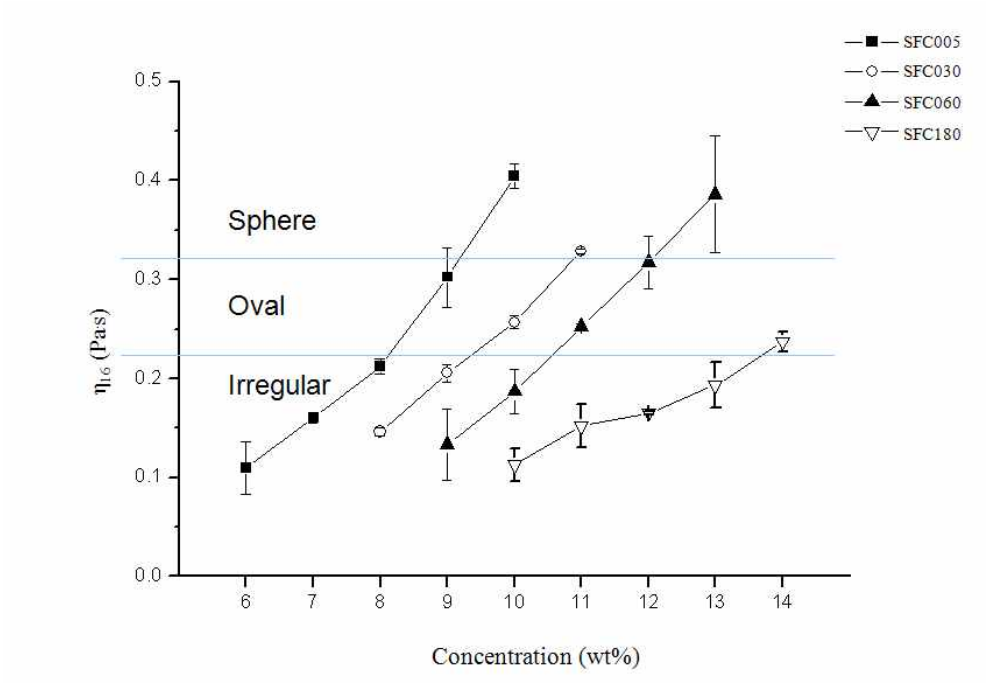

Figure 9. Effect of molecular weight and concentration of SFCs on shear viscosity at 16 s^{-1} of SFC solutions dissolved in 1M LiCl/DMSO.

We compared the shear viscosity at this shear rate with the concentration and the final shape of the SF microparticles in Figure 10. Based on the observed shapes of the SF microparticles, the graph can be divided in to three regions. First, where shear viscosity is low, SF molecules in droplets emitted from the tip have no significant entanglement weaker than the repulsion force between identical charged molecules. As a result, SF molecules cannot aggregate and debris are formed. As the shear viscosity increases, bean-like or oval microparticles were formed, but the degree of entanglement remained sufficient for creating sphere-like particles. Finally, when the shear viscosity exceeded about 0.33 Pa·s, sphere-like microparticles were formed because of the relatively high degree of entanglement, which overcomes the repulsion force between molecules, and which resulted in the formation of dense droplets. Figure 10 also illustrates that the shear viscosity is a critical factor in determining the shape of the SFC microparticles. Furthermore, any specific concentration and dissolution time that satisfies a particular shear viscosity range should create similar shapes.

4.3. Studies on the rheological parameters of SF solutions affecting the EHD fabrication

From the literature survey, we concluded that the viscosity of SF solution plays a critical role in EHD fabrication. The viscosity of an SF solution can affect the jet stabilization in electrospinning or Coulomb fission in electrospraying by chain entanglement. Since polymer concentration and molecular weight are the primary determining factors for the viscosity of polymer solution, their effect on the rheological properties of SF in two of the most common solvents, FA and HFIP, were investigated. Further, the effects of rheological properties of the SFs in each solvent on the EHD fabrication were also evaluated. Particularly, we studied how the rheological properties of SF in each solvent determined the mode of the EHD fabrication and the size of final product. The process parameters during EHD fabrication, such as applied voltage, tip to collector distance, and flow rate, were fixed in order to produce both particles and fibers under identical fabrication conditions.

4.3.1. EHD fabrication of SF with formic acid

4.3.1.1. Effects of concentration and molecular weight of SF

Figure 10 shows SEM images of SFC particles or fibers prepared by EHD fabrication using FA as solvent. Both dissolution time and SFC concentration affect the products' shape and size. Here, we

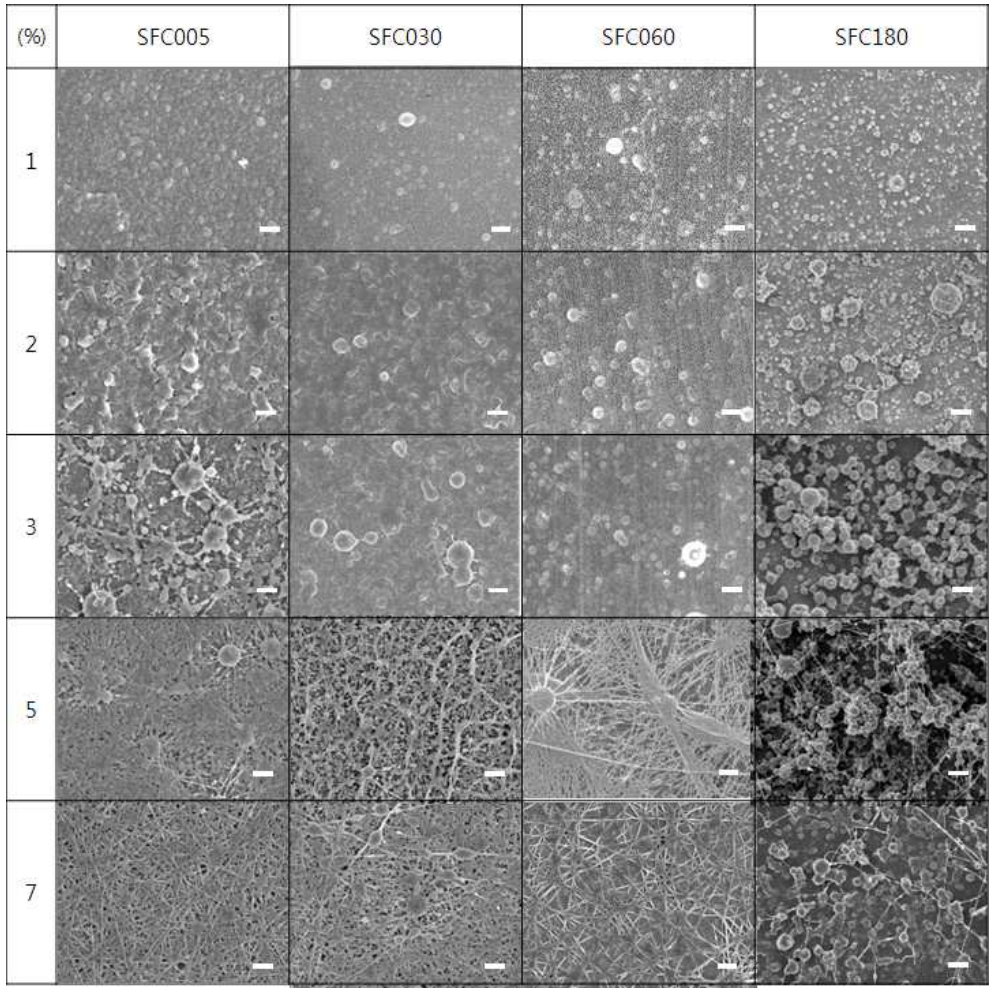

Figure 10. SEM images of EHD fabricated SFCs dissolved in formic acid. Scale bar : 1 μm. Applied voltage is 13 kV, flow rate is 0.3 ml/hr, distance from tip to collector is 10 cm.

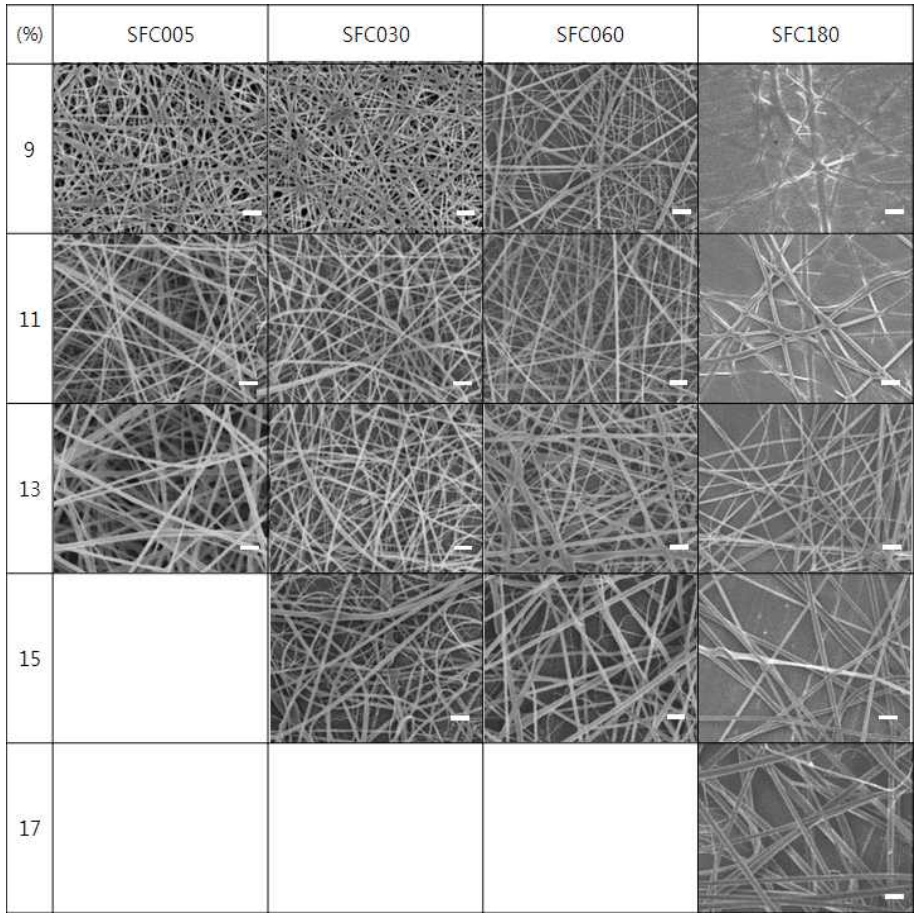

Figure 10. (Continued)

categorized the morphology of the particles or fibers into three categories: bead dominant forms, intermediate forms, and fine fiber forms. The intermediate forms included beaded fibers and fibers with junctions. The bead dominant forms were observed when SFC concentrations were low. For SFC005, SFC030, and SFC180, bead dominant forms were observed for concentrations of less than 5 wt%. In the case of SFC180, the bead dominant form was observed even at 7 wt%. The intermediate forms were not observed for moderate SFC concentrations. In the case of SFC005, these forms were observed between 5 and 9 wt%. The concentration range for intermediate-form formation with SFC030 and SFC060 was between 5 and 11 wt%. For SFC180, this concentration range was 7-13 wt%. Fine fiber forms were obtained with concentrations exceeding 11, 13, 13 and 15 wt% for SFC005, SFC030, SFC060 and SFC180, respectively. These results suggest that in order to obtain a fine fiber form, both concentration and molecular weight must be sufficiently high.

Apart from the SF morphologies, the size distributions of the fabricated particles and fibers were also affected by the concentration and molecular weight. Figure 11 shows the size distribution of beads prepared with different SFCs and at different concentrations. For SFC005, average particle sizes increased from 320 to 686 nm when the concentration was increased from 1 to 3 wt%. The average particle size for SFC030 and SFC060 increased from 245 to 600 nm and from 214 to 523 nm, respectively, when concentration increased from 1 to 3 wt%. Particles fabricated with SFC180 were in the range of 135-248 nm for respective concentrations of 1-4 wt%. Compared to

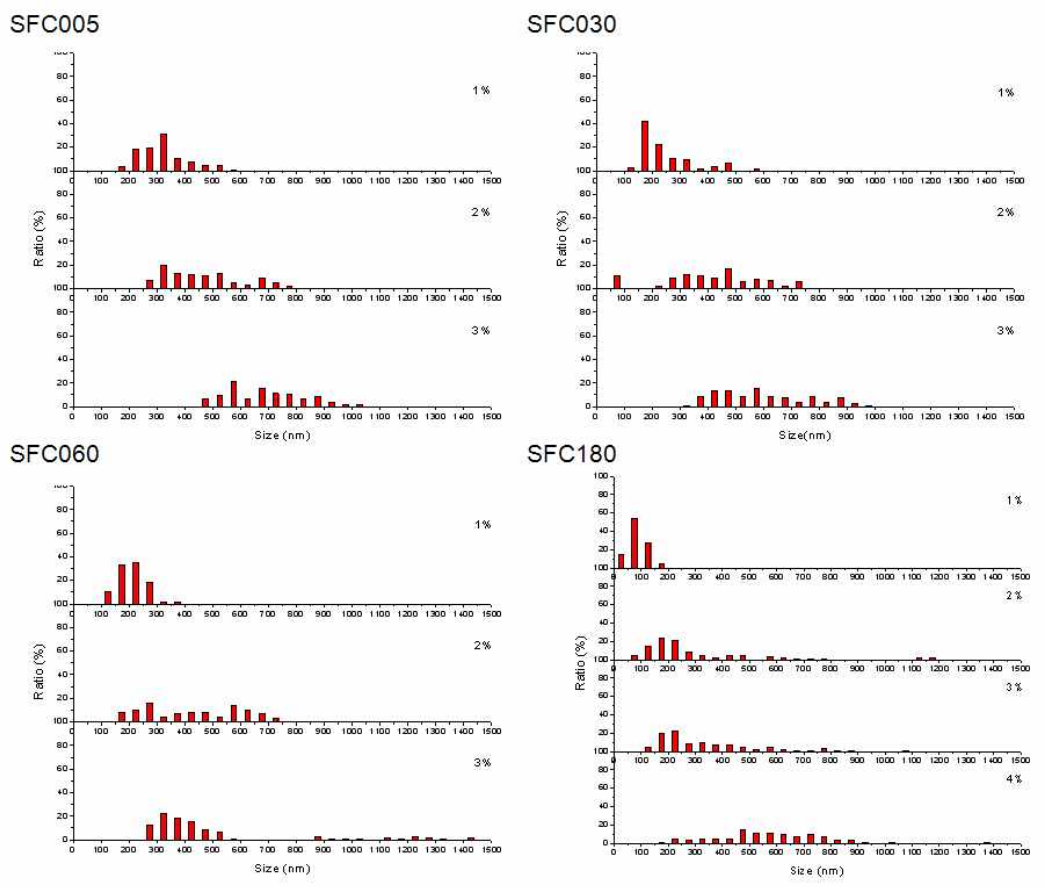

Figure 11. Particle size distributions of EHD fabricated SFCs dissolved in formic acid.

other SFCs, SFC180 had a much smaller particle size at equal concentrations. This indicates that the molecular weight of SFCs affects the particle size, whereas higher molecular weight resulted in larger particle size. The average particle sizes for SFC005, SFC060, SFC090, and SFC180 were 320, 245, 214 and 135 nm, respectively. It should be noted that the average molecular weight of the SFCs decreased in the following order: SFC005, SFC030, SFC060, and SFC180.

Not only the average particle size but also the average nanofiber size was affected by the concentration and molecular weight of the SFCs (Figure 12). The average size of the SFC005 nanofibers increased from 143 nm to 212 nm with a concentration increase from 10 to 13 wt%. Nanofibers obtained from SFC030 and SFC060 had an average fiber size of 180 nm to 242 nm and 134 nm to 184 nm, respectively, for a concentration range of 13-15 wt%. For SFC180, fibers were fabricated from 13 wt% and their average sizes ranged from 112 to 318 nm. Here, the average molecular weight of SFCs also affected the average fiber size. At a concentration of 13 wt%, the average fiber sizes were 212, 180, 134, and 112 nm for SFC005, SFC030, SFC060, and SFC180, respectively.

Thus far, it can be concluded that both the concentration and molecular weight of the SFCs affects the morphology and size of EHD fabricated products. At the same concentration, with an increase of molecular weight, the morphology of EHD fabricated products tends to change from bead dominant form to fine fiber form. Among the same morphologies, particle size increased for higher molecular weights. For identical molecular weight conditions, with an increasing

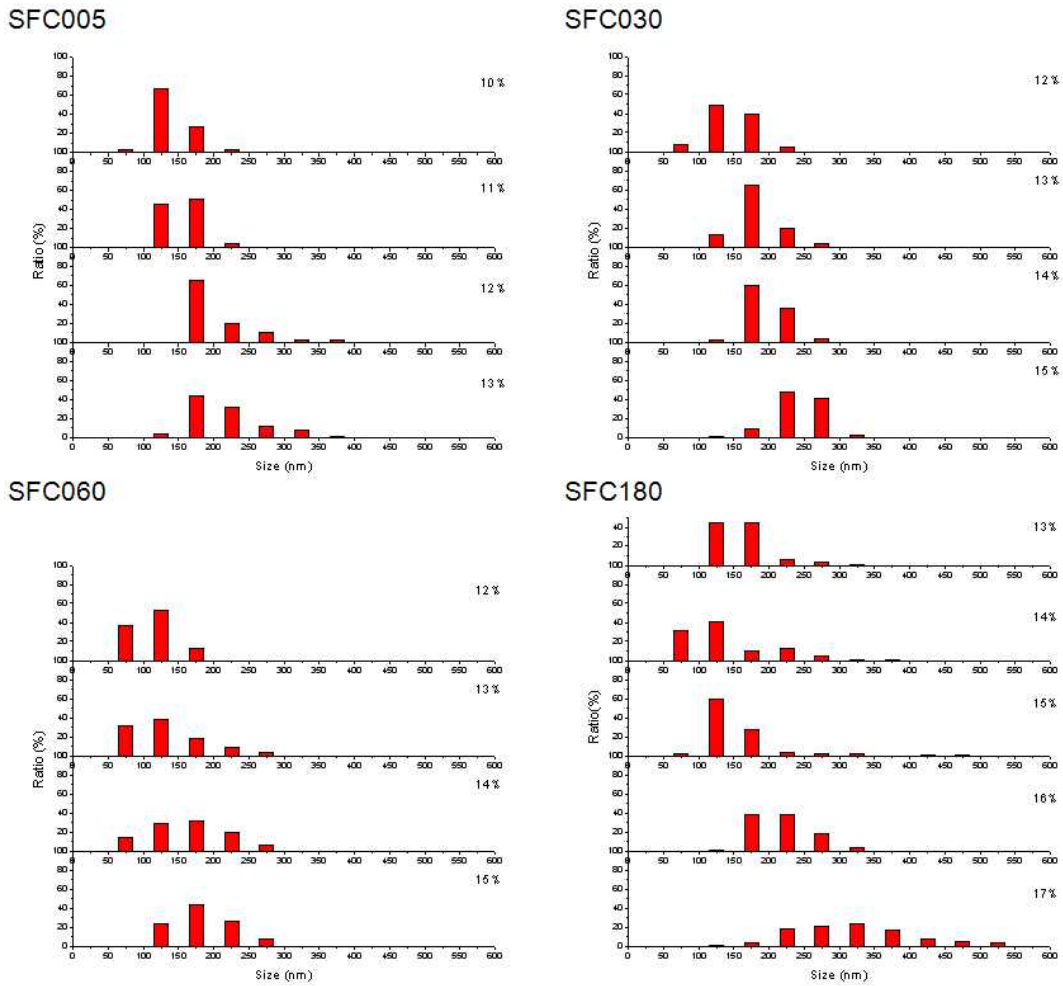

Figure 12. Fiber size distributions of EHD fabricated SFCs dissolved in formic acid.

concentration, the morphology of EHD fabricated product tended to change the from bead dominant form to the fine fiber form. Among the same morphologies, particle size increased as the concentration increased.

In order to elucidate this trend, SFC sizes were measured using DLS. As mentioned earlier, SF molecules are similar to amphiphilic polymer composed of hydrophilic-hydrophobic-hydrophilic domains, and these molecules assemble into micelles [43, 44]. This is a markedly different behavior compared to other linear polymers. For linear polymers, single chains with a defined radius of gyration will entangle each other, while in the case of SF, multiple chains of SF (i.e. micelles) will entangle each other. It has been reported that SF micelles tend to agglomerate into nanofibers through self-assembly [47]. Based on this theory, the micelle size of SFCs should affect the size and morphology of EHD fabricated products.

Figures 13 and 14 show the size distribution of SFCs in aqueous solution and formic acid solution, respectively. In aqueous solution (Figure 13), the sizes of SFC macromolecules were 189.5 nm for SFC005 and 91.7 nm for SFC180. Since the increased dissolution time reduced the molecular weight of SFC, it is obvious that the hydrodynamic size of SFCs will decrease in the following order: SFC005, SFC030, SFC060, and SFC180. In formic acid (Figure 14), the sizes of the SFCs were much smaller than in aqueous solution (21.6 nm for SFC005 and 2.5 nm for SFC180). This size reduction of SF in formic acid compared to aqueous solution is in agreement with previous results [48, 95]. Um et al. [95] found that the water has a lower dissolution capacity than formic acid and induces aggregation

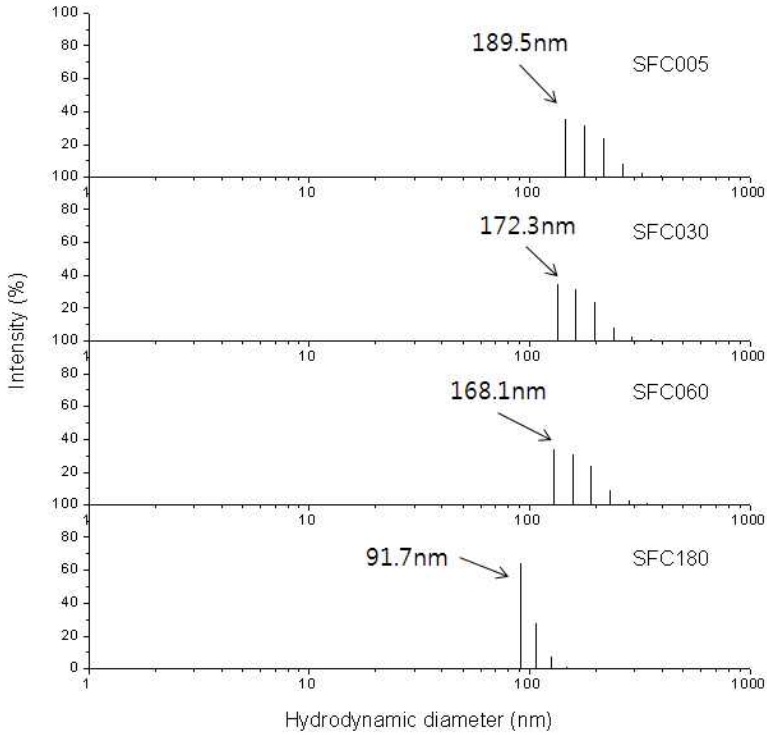

Figure 13. Hydrodynamic diameter of SFCs macromolecules in aqueous solution.

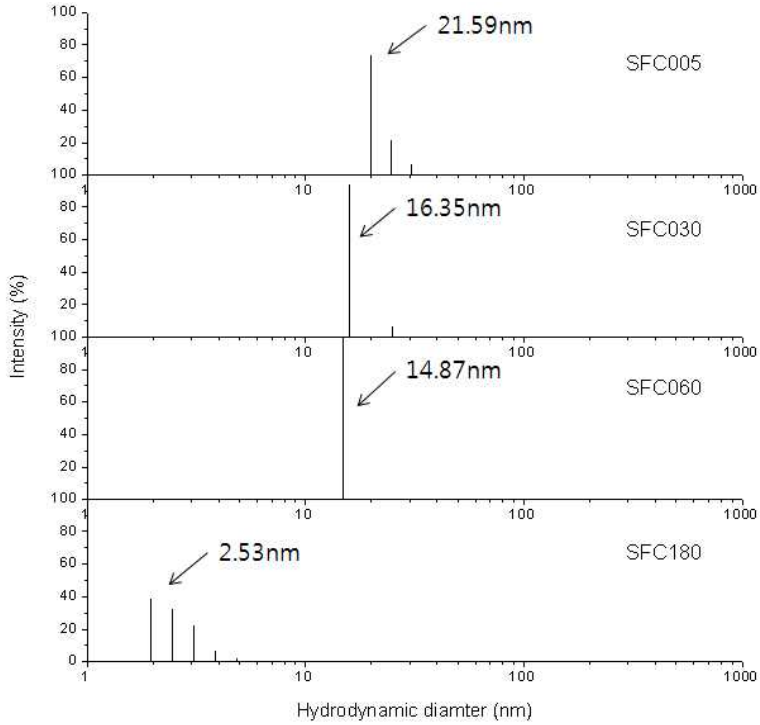

Figure 14. Hydrodynamic diameter of SFC macromolecules in formic acid.

of SF micelles by hydrophobic interaction. In aqueous solution, it is more appropriate to assume that aggregated SF molecules are dispersed rather than dissolved. In contrast, formic acid has a good dissolution capacity, owing to interactions between its polar groups and the hydrophilic domains (Arg, Lys, Asp or Glu) of SF. Additionally, among various kinds of carboxylic acids, formic acid has the smallest R groups. This small size is advantageous for entering and solvating SF molecules. For these reasons, SF in FA solution forms much smaller molecules and is more stable than in aqueous solution.

Regardless, it has been clearly shown that the increased dissolution time of SF in $CaCl_2$/EtOH/H_2O solution results in a smaller molecular size for SFCs. This difference in molecular size imparts a decrease of particle or fiber size because more, smaller SFC molecules are aggregated. However, the modes of an EHD fabrication cannot be fully determined by the molecular size of SFC. Therefore, a more direct parameter is required to predict both the modes and product size of EHD fabrications.

4.3.1.2. Relationship between shear viscosity of SF-FA solution and EHD fabrication

Previously, we concluded that both the concentration and molecular weight of SFCs greatly affect the EHD fabrication. The concentration and molecular weight of polymer are primary factors in determining the viscosity of a polymer solution. Based on the fact that the viscosity of a polymer solution is dependent on the entanglement of

polymer chains in solution, the rheological properties of a polymer solution might offer a more comprehensive tool for predicting the EHD fabrication. Therefore the zero shear viscosities of SF-FA solutions were measured using ARES (Figure 15).

Although the shear induced behaviors of SF dope solutions in a conventional cone and plate (or parallel plate) rheometer are obtained from a two dimensional flow field on the sample rather than a one dimensional field of extensional flow, these responses can provide valuable information since SF dope solutions experience a shear force from the attractive electrostatic forces at the end of the spinneret tip.

At low shear rates, in some samples, instrumental errors occurred, especially in those having low concentration. For clarity, these data were omitted. Shear viscosity of all SFCs was independent of the shear rate but increased with the concentration (Figure 15). Shear thinning or thickening, which respectively indicate an increased chain entanglement or disentanglement, were not observed. This is in agreement with previous reports, indicating that SF molecules are stable in FA [49, 50]. This Newtonian behavior of the SF-FA solution made it possible to find the zero viscosity for each SFC by linear fitting.

In Figure 16, the zero shear viscosity of SFCs is plotted against its corresponding concentration. Based on the morphology of EHD fabricated products, the zero shear viscosity is divided into two regions: bead dominant forms and intermediated and fine fiber forms.

In the bead dominant region, the zero shear viscosities increased depending on the exponent of concentration, with a slope of 0.74-0.92

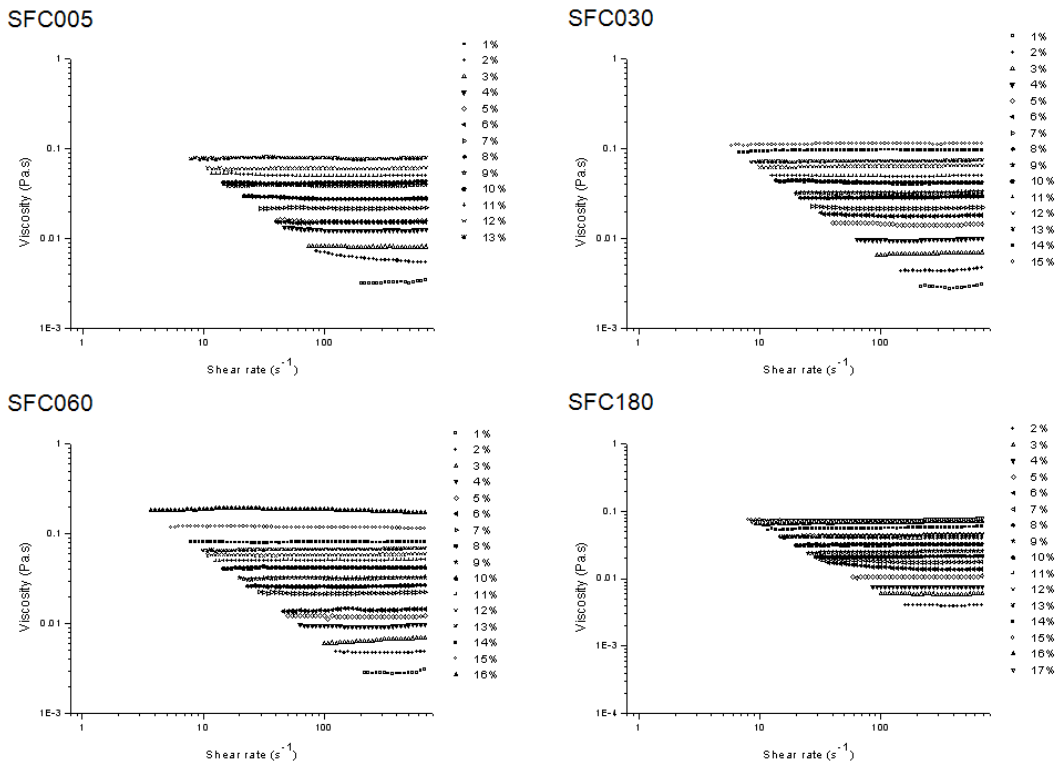

Figure 15. Effect of molecular weight and concentration of SFCs on shear viscosity of SFC solutions dissolved in formic acid.

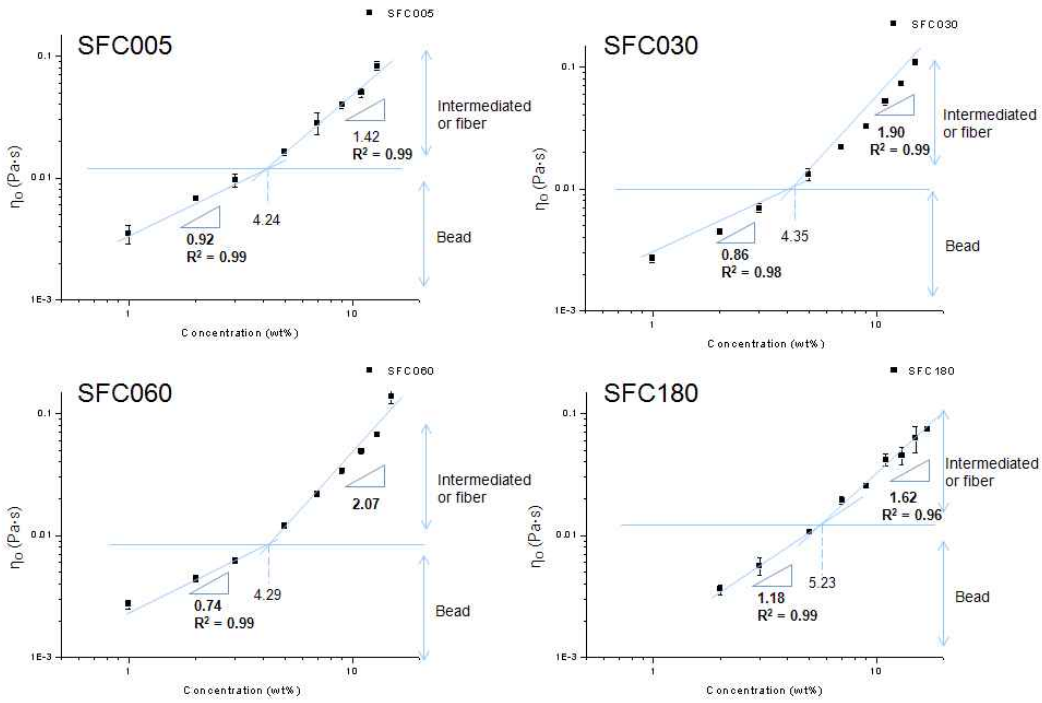

Figure 16. Effect of molecular weight and concentration of SFCs on zero shear viscosity of SFC solutions dissolved in formic acid.

($\eta \propto c^{0.74-0.92}$). In the intermediate and fine fiber regions, a slope of 1.42 ($\eta \propto c^{1.42}$) is obtained. These changes in slope are the result of chain entanglement. According to a previous report, these areas can be divided into two regions [31]. The region where the slope is less than one could be the semi-dilute, moderately entangled region (typically an SFC concentration less than 5 wt%). In this region, the SFC chains are significantly entangled and reproducible beads were formed. When the concentration was increased further, chains were highly entangled, and intermediate forms (5-9 wt%) and fine fiber forms (above 11 wt%) resulted. In this region, the slope is greater than 1.4 and could be designated as the semi-dilute, highly entangled region or concentrated region.

As mentioned in the literature survey, these regions were classified by zero shear viscosity. However, in this research, the zero shear viscosity region that produced beads was $\eta \propto c^{0.74-0.92}$ and the beaded fiber or fiber forming region was $\eta \propto c^{1.42}$. These values are quite different from other research based on linear synthetic polymers (beads for $c^{1.25}$, beaded fiber or fibers for $c^{4.25-4.5}$) [31].

On the other hand, c/c_{ov} can also be used to analyze the relationship of EHD fabrication and viscosity. Values for c_{ov} can be calculated from the following formula [32]:

$$c_{ov} = \frac{M_w}{4\Pi^3} \qquad (1)$$

From the DLS results (Figure 14), the R_h values for SFC005, SFC030, SFC060, and SFC180 were 10.8, 8.2, 7.4, and 1.3 nm, respectively. With these values, the calculated c_{ov} values of SFC005,

SFC030, SFC060, and SFC180 are 11.6, 25.4, 32.1, 1216 wt%. These values are unrealistic, especially for SFC180.

Generally, polymers used in these calculations are linear and have a random coil structure [96, 97]. Therefore, they exist as single chains in the solution state. However, SF differs greatly from linear polymers. As mentioned earlier, SF molecules form micelles in solution state with one or more chains, unlike other linear polymers. Therefore, SF macromolecules entangle each other on a larger scale than linear polymers. Consequently, conventional methods for linear polymers such as determining the relationship between shear viscosity and the exponent of concentration or the calculation of cov based on the volume of a single chain are inadequate for SF.

4.3.1.3 Relationship between dynamic viscosity of SF-FA solution and EHD fabrication

On the other hand, dynamic viscosity can be used to determine the rheological properties of SF solutions [98, 99]. Figure 17 shows the storage and loss moduli of SF-FA solutions of SFCs having different concentrations. The modulus magnitudes of all samples increased with concentration and molecular weight at all frequencies. This behavior is due to the increase of chain entanglement, and similar behaviors were demonstrated in crosslinked spider silk hydrogel [100], networking polymers [101], self-assembled proteins [102], and acidified SF dope solution from native silkworms [103]. This behavior generally represents an increase of molecular bonds by chemical or physical means. For low to moderate frequencies, both G′ and G″

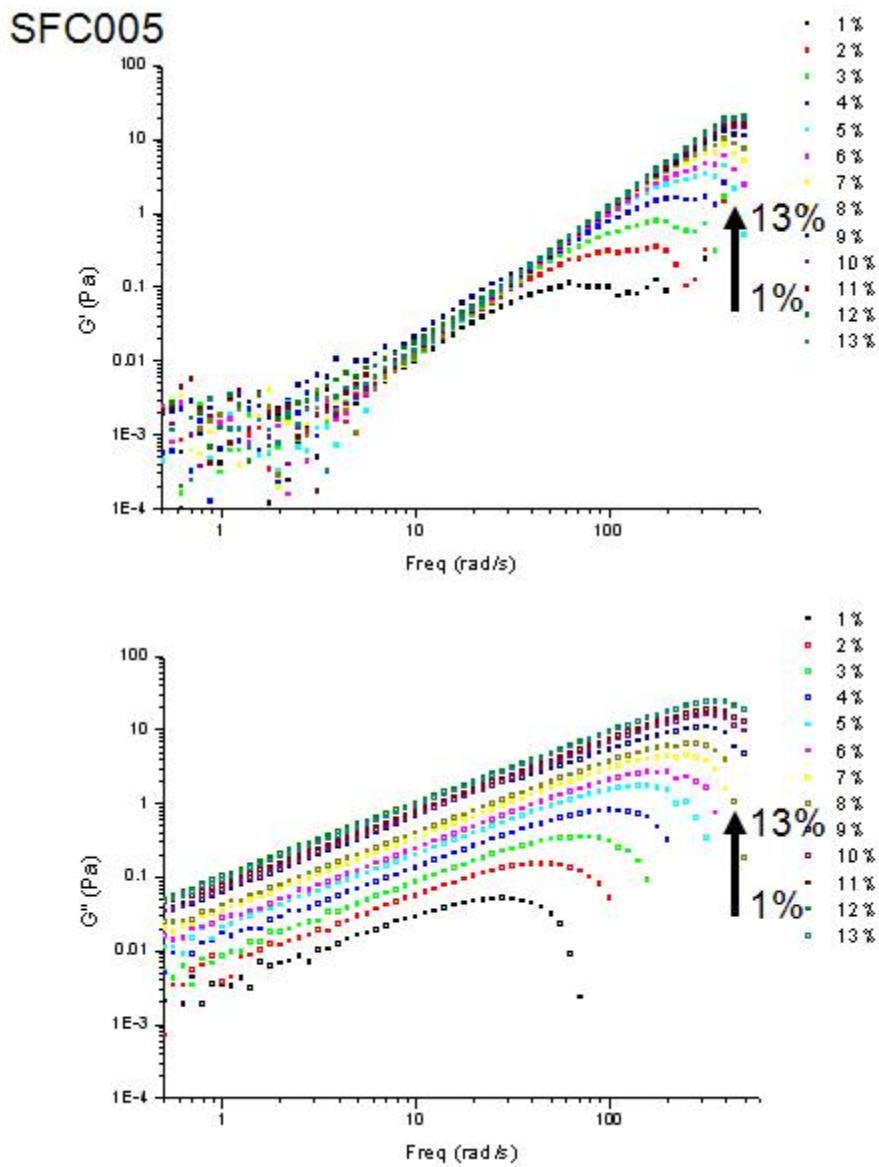

Figure 17. Effect of molecular weight and concentration of SFCs on dynamic viscosity of SFC solutions dissolved in formic acid.

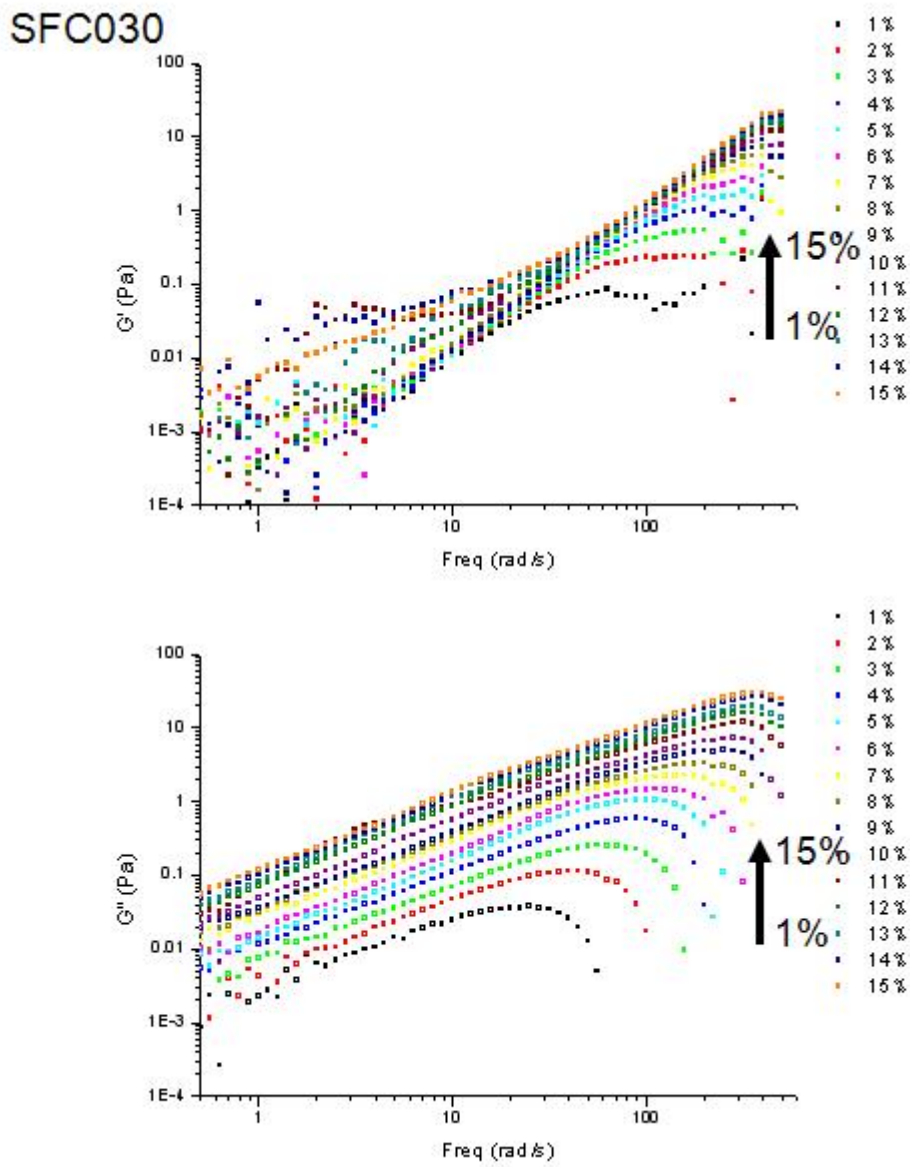

Figure 17. (Continued)

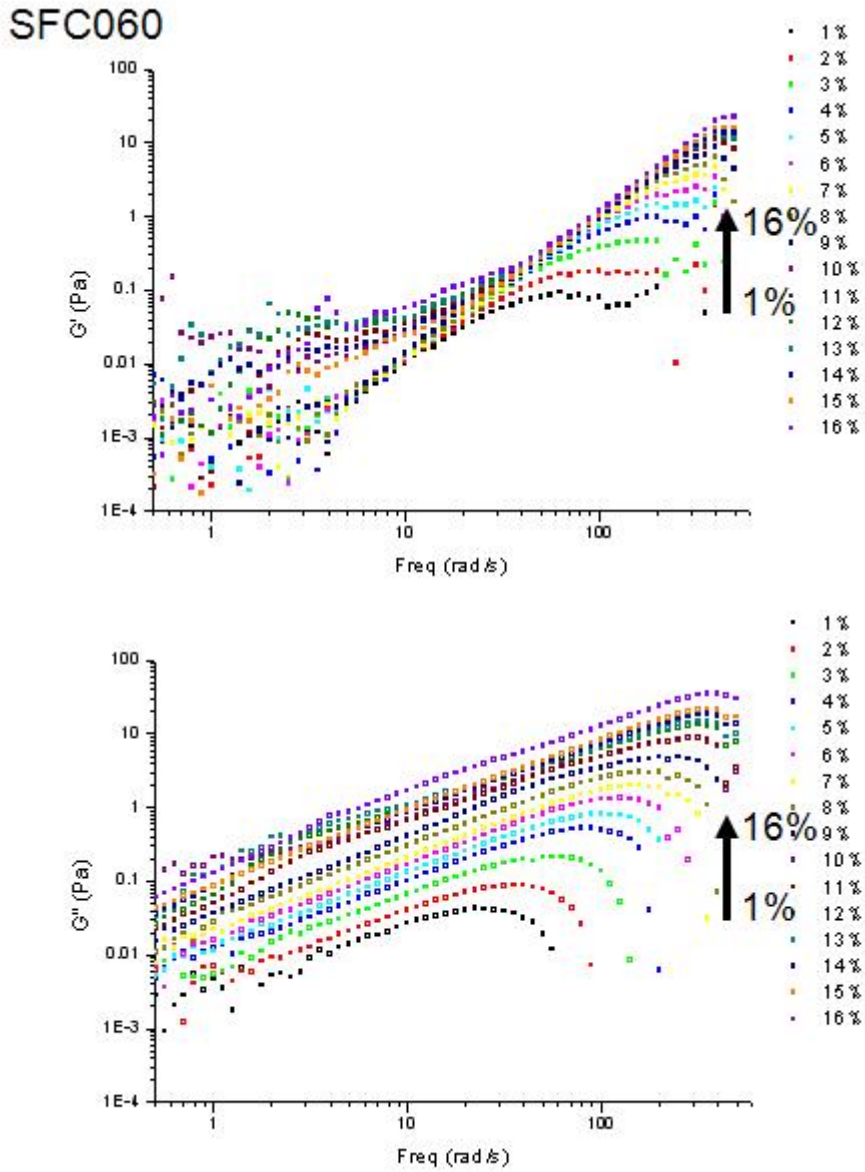

Figure 17. (Continued)

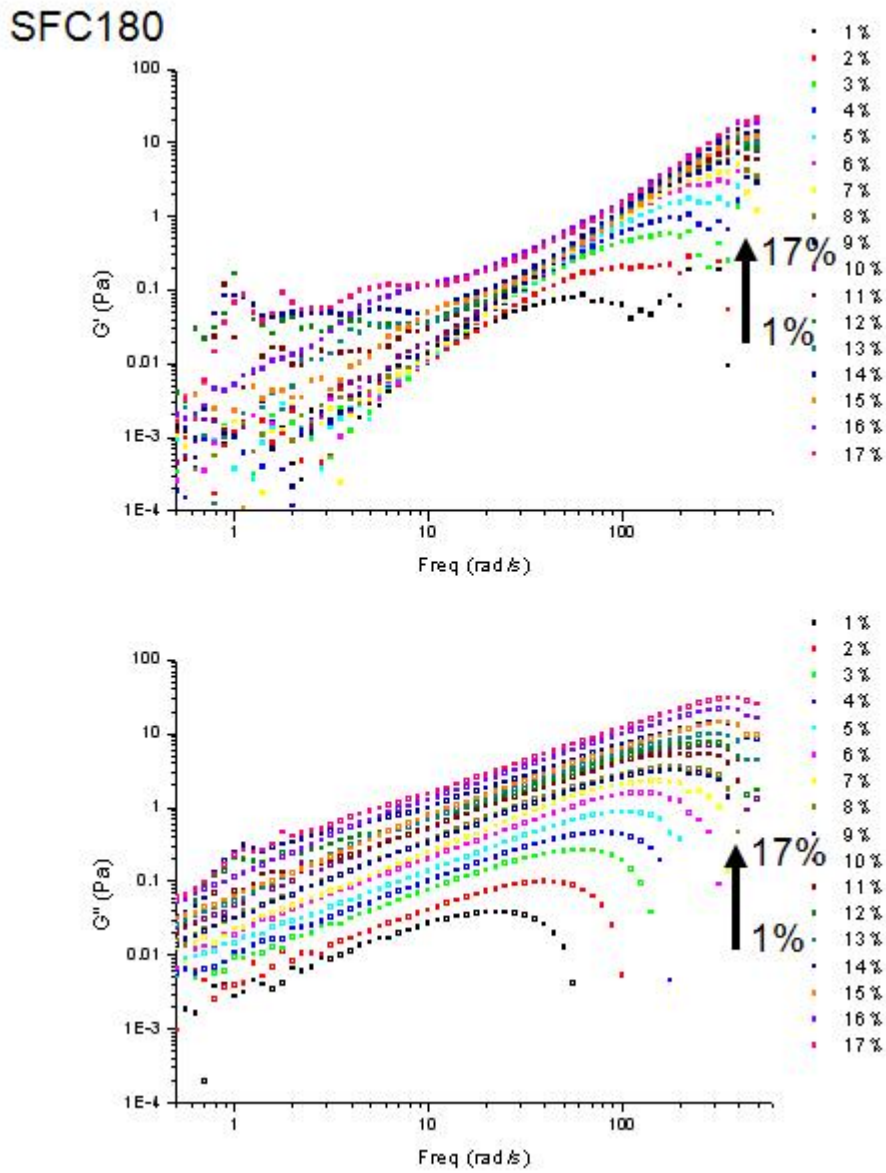

Figure 17. (Continued)

increase proportionally with frequency. If G″ is greater than G′, the dope solution behaves like a liquid. After the crossover point where G′ becomes greater than G″, the dope solution exhibits elastic behavior. If gelation occurs after the crossover point, G′ is independent of frequency and G″ decreases.

In Figure 18, the frequency at the crossover point is shown to increase proportionally with SFC solution concentration. At equal concentrations, SFCs having higher molecular weight showed slightly higher frequency at the crossover point. Below the crossover point, applied strain can disrupt the chain entanglement of SF. However, if the SF concentration or molecular weight increases, more chain entanglements occur, and in turn, more strain is required. Therefore, the crossover points increase proportionally with the concentration and molecular weight of SF. Particularly, liquid behavior for low frequency regions and elastic behavior in high frequency regions of SF having high molecular weight means that the system forms a viscoelastic fluid with a low crosslink density to prevent it from forming a network structure. This is in agreement with the Rouse-Zimm theory. Consequently, SF-FA solutions will act as a weak gels [104].

4.3.1.4. Establishment of the plateau modulus of SF-FA solution

There are a number of parameters for discretizing the degree of polymer chain entanglements such as entanglement molecular weight

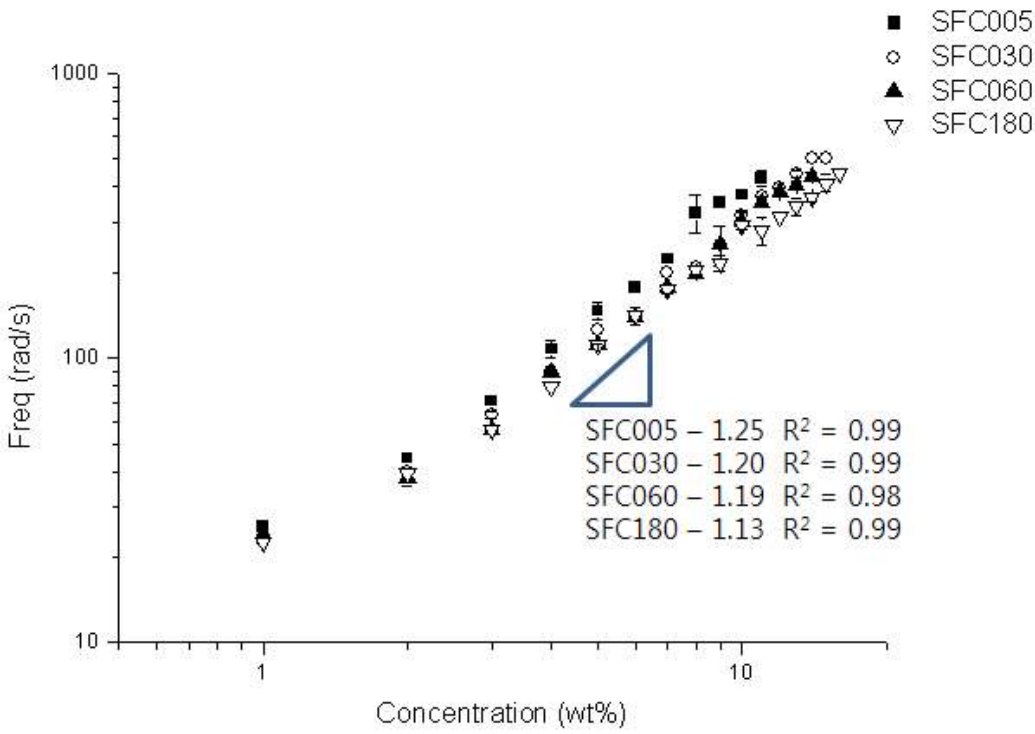

Figure 18. Crossover frequency where G'=G" (tanδ = 1) of SFC solutions dissolved in formic acid. Crossover frequencies of 12-13 wt% for SFC005, 14-15 wt% for SFC030, 15-16 wt% for SFC060 and 17 wt% for SFC180 were not measured due to instrumental limit.

and chain entanglement number. In this study, these parameters were used predict the EHD fabrication mode of SF.

Entanglement molecular weight, M_e, is defined as the mean molecular weight between entanglement junctions in the polymer melt, and can be calculated by the following equation [38]:

$$M_e = \frac{4\rho RT}{G_N^0} \quad (3)$$

where ρ is polymer density, R is the ideal gas constant, T is temperature and G_N^0 is the plateau modulus.

In a polymer solution, entanglement molecular weight is affected by the polymer volume fraction, ϕ_p; thus, the entanglement molecular weight in solution state, $(M_e)_{soln}$, is defined as $(M_e)_{soln} = M_e/\phi_p$.

Chain entanglement number, $(n_e)_{soln}$, can be derived from the relationship between $(M_e)_{soln}$ and M_w and is the parameter that quantifies number of entanglements per polymer chain [17].

$$n_{soln} = \frac{M_w}{(M_e)_{soln}} = \frac{(\Phi_p M_w)}{M_e} = \frac{4}{5}\frac{\Phi_p M_w G^0}{\rho RT} \quad (4)$$

Using $(n_e)_{soln}$, the morphology of EHD fabricated products is easily predicted [34]. However, during the calculation of $(n_e)_{soln}$, the critical parameters that affect the final value of $(n_e)_{soln}$ are G_N^0 and ϕ_p. That is, the plateau modulus of a 100 wt% polymer solution state without solvent (or polymer melt state) and its concentration in the solution. Since silk fibroin has a higher melting point than its thermal decomposition point, it is impossible to produce SF in a melt state. Therefore, another parameter should be established. In the present

study, the G_N^0 value of a solution by SF concentration, $(G_N^0)_{soln}$, called the solution plateau modulus, is used as a substitute parameter. Previously, $(G_N^0)_{soln}$ was used to measure the degree of entanglement [102] or crosslinking [106-108].

The commonly used G_N^0 of polymer melt or solution is defined by the G′ at the plateau region, and it is the recommended value for monodispersed and high molecular weight polymers. However, polymers are usually polydispersed, and several substitute methods were suggested, depending on polymer dispersity, molecular weight, or properties of the measuring instrument.

Commonly, the minimum (MIN) method, integral (INT) method, maximum (MAX) method, and crossover modulus based methods have been used for polydispersed polymer [109-111]. These methods are expressed as

MIN method, $G_N^0 = G'(w)_{\tan\delta \to \text{minimum}}$ where $\tan\delta = G''/G'$ (9)

INT method, $G_N^0 = \frac{4}{\pi} \int_{\infty}^{w_{max}} G''(w) d\ln w$ (10)

MAX method, $G_N^0 = 4.83\ G''_{max}$ (11)

Crossover modulus-based method,

$$\log\left(\frac{G_N^0}{G}\right) = 0.38 + \frac{2.63\log\frac{M_W}{M_N}}{1+2.45\log\frac{M_W}{M_N}} \quad (12)$$

where G_x occurs when G' = G".

Among these methods, the INT method is suitable for polydispersed polymer, especially when the experimental data at high frequency cannot obtained due to instrument limitations.

In the present study, the SFCs had PDI values of 1.2-1.9 and molecular weights were in the range of 200-400 kDa. The ARES instrument used in this study has limited frequency (0.5 to 510 rad/s). Because of this limitation, it was impossible to measure a plateau region of G′, especially for SFCs of high molecular weight, which were expected to occur at higher frequencies. Therefore, the INT method was adopted to calculate $(G_N^0)_{soln}$.

In Figure 19, the $(G_N^0)_{soln}$ values of SF-FA solutions, which were calculated by the INT method, are plotted against SFC concentration; the $(G_N^0)_{soln}$ values exponentially increased with SF concentration. If we consider the relationship between $(G_N^0)_{soln}$ and the EHD fabricated product's morphology, three regions can be defined. Below a $(G_N^0)_{soln}$ value of 1 Pa, all SFCs were of the bead dominant form, which corresponds to the semi-dilute, moderately entangled region. For $(G_N^0)_{soln}$ values between 1 and 35 Pa, an intermediate form occurred, which corresponds to the semi-dilute, highly entangled region. Above values of 35 Pa, fine fibers were formed, corresponding to the concentrated region.

These results suggest that the $(G_N^0)_{soln}$ can be used as a substitute parameter for $(n_e)_{soln}$, which defines regions of varying degrees of chain entanglement. In order to derive an exact $(n_e)_{soln}$ for SF, one should know the density of SF in melt state. However, as mentioned

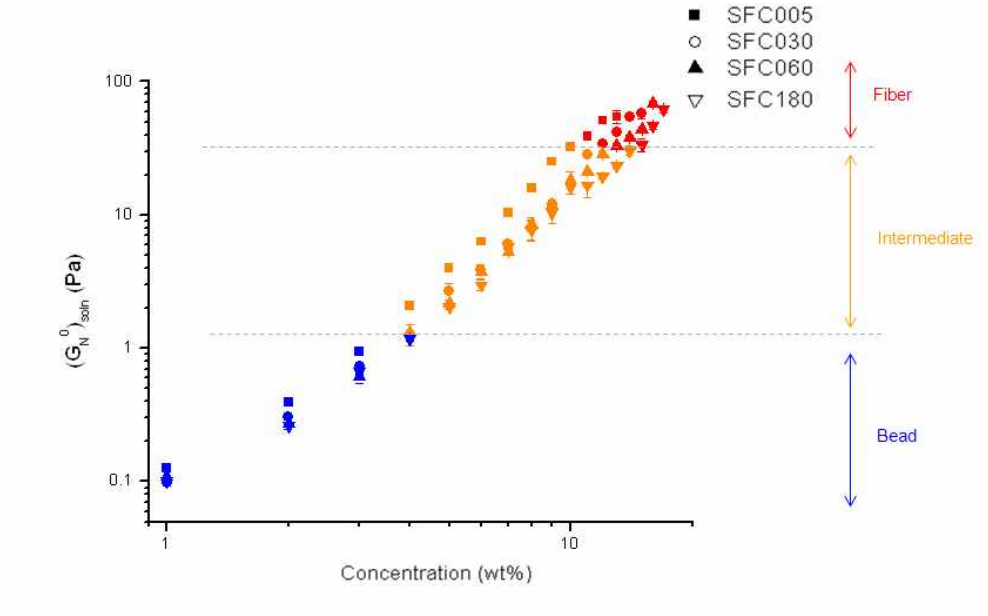

Figure 19. Effect of molecular weight and concentration of SFCs on solution plateau modulus ($(G_N^0)_{soln}$) of SFC solutions dissolved in formic acid.

before, it is impossible to find the actual density of SF in this state. Therefore, $(G_N^0)_{soln}$ is a more practical parameter for determining the degree of entanglement of SF. In addition, this parameter includes the interaction of polymer and solvent, because $(G_N^0)_{soln}$ is measured directly from the polymer solution itself.

4.3.1.5. Application of solution plateau modulus on the size variation of EHD fabricated products

Thus far, it can be concluded that the mode of an EHD fabrication for SF can be predicted by the solution plateau modulus. However, a method for predicting the size of an EHD fabricated product would be very useful.

Most researchers use solution concentration such as c (wt%) or c/c_{ov} for size predictions. In most cases, the relationship between concentration and product size is mathematical (either exponential or proportional).

In Figures 20 and 21, the size distributions of SF nanoparticles and fibers, respectively, prepared from different SFCs are plotted against SF concentration. If the same SFCs are used for EHD fabrication, the particle or fiber size is predictable. In the case of SFC particles, SFC005, SFC030, and SFC060 had similar slopes, while SFC180 had a far lower slope. A similar tendency can be observed for SFC fibers. However, the prediction is only applicable if only the same SFCs were used. This means if the molecular weight differs, size cannot be predicted by the concentration alone. Thus, in this

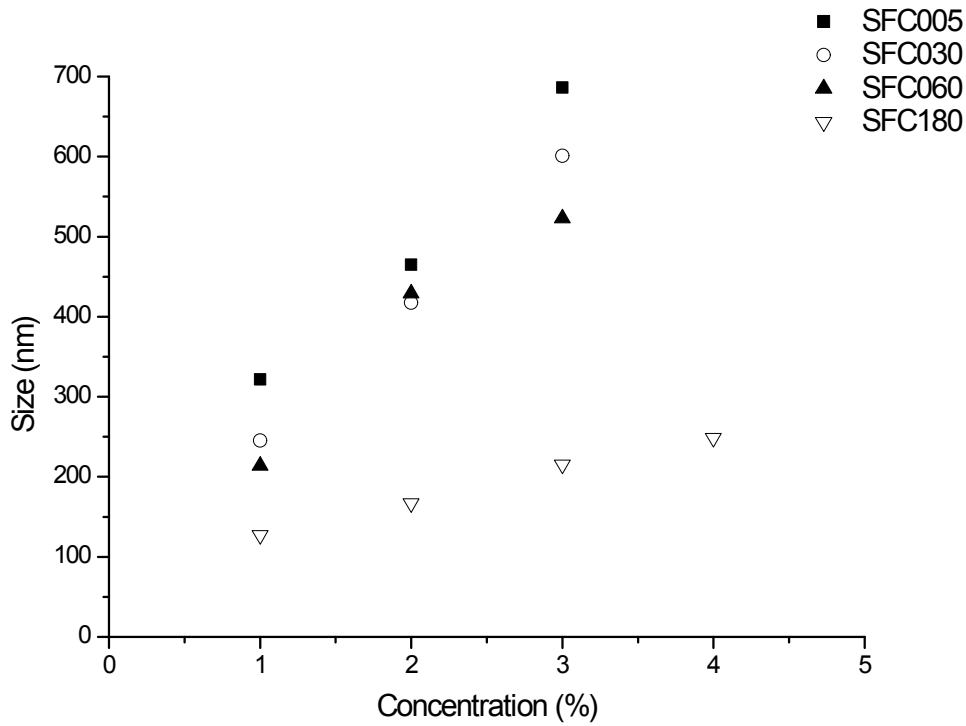

Figure 20. Particle sizes of EHD fabricated SFCs with formic acid prepared by various dissolution times in $CaCl_2$/EtOH/H_2O solution and concentration.

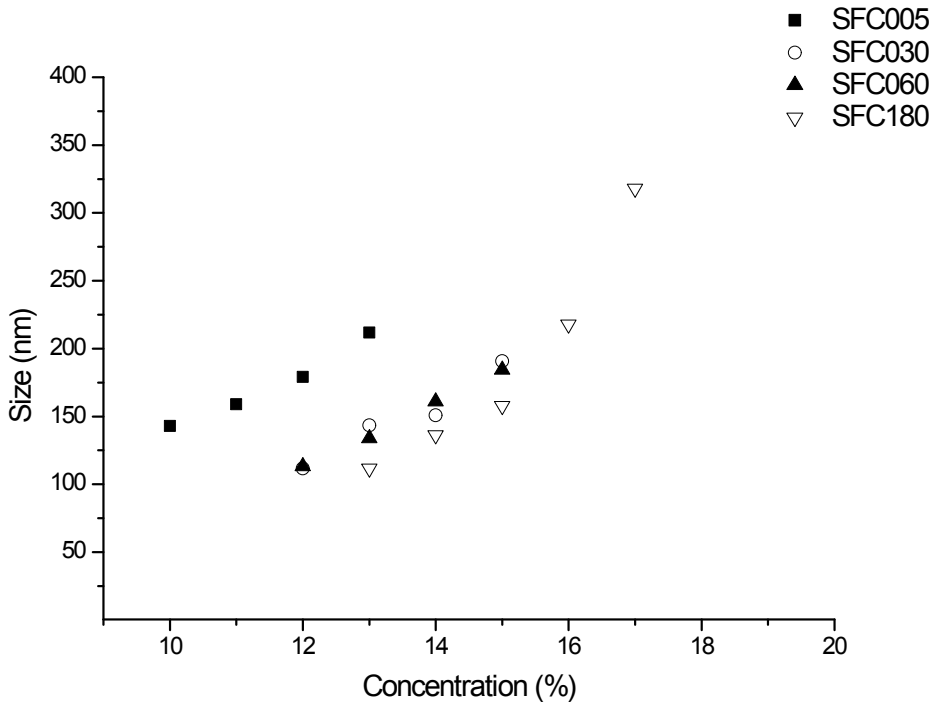

Figure 21. Fiber sizes of EHD fabricated SFCs dissolved in formic acid by SFC concentration.

study, the zero viscosity or solution plateau moduli are used for the size prediction of EHD fabricated SF products.

In Figure 22, the particle size variation of SFCs is plotted against $(G_N^0)_{soln}$. As in Figure 20, SFC005, SFC030, and SFC060 had a common linear fit (R^2 = 0.96) but if the SFC180 results are included, the linear accuracy decreases rapidly to R^2 = 0.73.

In the bead dominant region, the SF molecules are moderately entangled. In this region, particle formation is less affected by chain entanglement than in the semi-dilute, highly entangled region (intermediate form) or in the concentrated region (fine fiber form).

Actually, unlike electrospinning, the particle size variation in electrospraying is seriously affected by the droplet size formed at the end of the tip. From the Rayleigh limit, the droplet size (d) emitted from the tip in electrospraying can be determined from the following equation [112]:

$$= \left(\frac{^{2}}{64\pi\, \epsilon_0 \gamma} \right)^{\frac{1}{3}} \qquad (13)$$

where Q is the charge (electrical shear force), ε_0 is the permittivity of free space and ɣ is the surface tension of the droplet.

In this equation, the droplet size is greatly affected by the charge (i.e. applied voltage). This electrical force acts as a shear force at the surface of the droplet. Therefore, the shear viscosity of the liquid is critical. For this reason, the zero shear viscosities of SF-FA solutions were fitted with the size of particles. Figure 23 shows the relationship between the zero shear viscosity and size distribution.

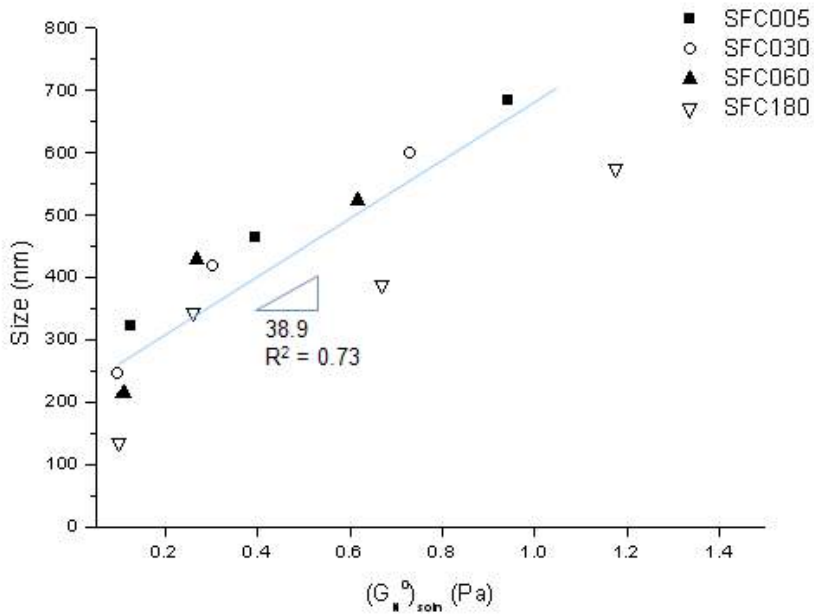

Figure 22. Particle sizes of EHD fabricated SFCs dissolved in formic acid by SFC solution plateau modulus.

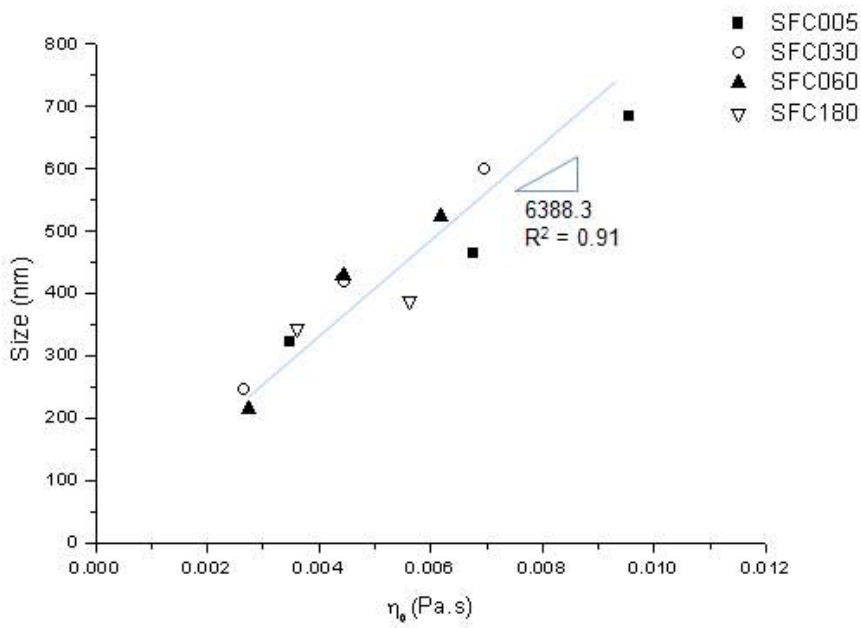

Figure 23. Particle sizes of EHD fabricated SFCs dissovled in formic acid by zero shear viscosity of SFC solution.

Surprisingly, it fit well with a determination coefficient of R^2 = 0.91. Therefore, in terms of particle formation, the zero shear viscosity has a more dominant and accurate relationship than the chain entanglement parameter, $(G_N^0)_{soln}$.

In the case of fiber formation, the SFC solution is in the semi-dilute, highly entangled region or the concentrated region. Here, chain entanglement plays an important role. When the size distribution was plotted against the $(G_N^0)_{soln}$ (Figure 24), the coefficient of determination for the linear fit was higher (R^2 = 0.86) than when the zero shear viscosity was used (R^2 = 0.24) (Figure 25). During electrospinning, solvent evaporation occurs, and liquid polymer jets are subdivided into thinner fibers. In this fabrication, chain entanglement has a crucial role because it inhibits fiber subdivision: The more chain entanglement that arises, the greater the thickness of the resulting fibers. Therefore, $(G_N^0)_{soln}$ provided a more accurate relationship with fiber size than the zero shear viscosity.

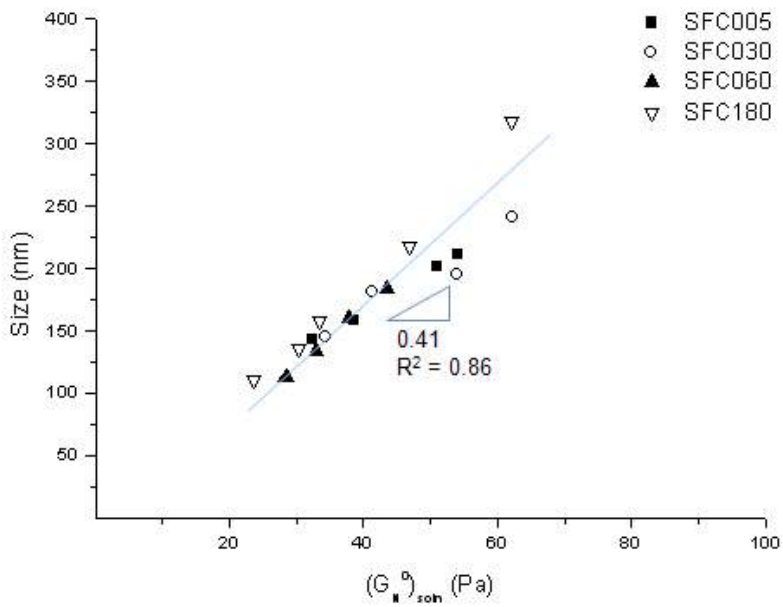

Figure 24. Fiber sizes of EHD fabricated SFCs dissolved in formic acid by SFC solution plateau modulus.

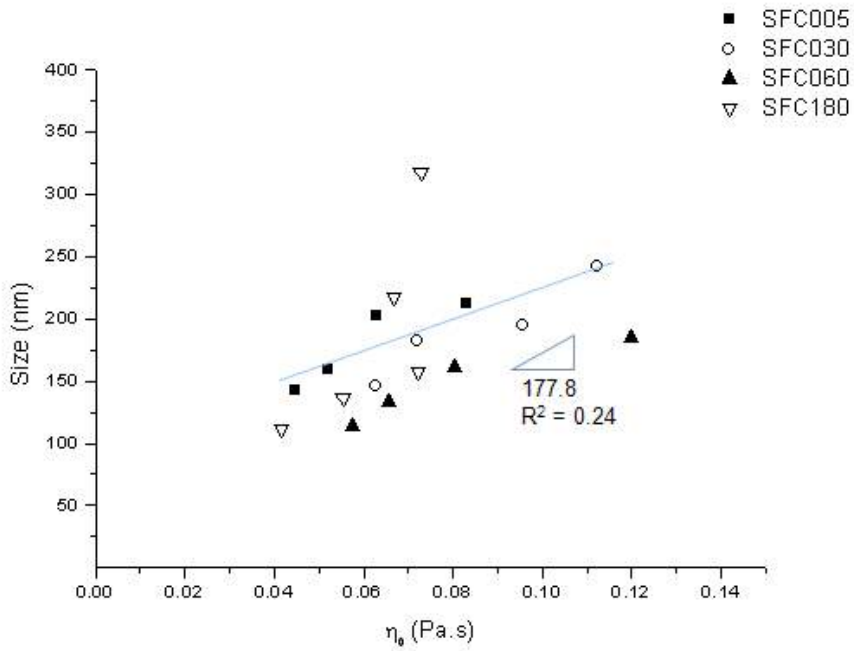

Figure 25. Fiber sizes of EHD fabricated SFCs dissolved in formic acid by zero shear viscosity of SFC solution.

4.3.2. EHD fabrication of HFIP

HFIP is widely used for the EHD fabrication of proteins [113] and other polymers, such as poly(vinyl alcohol) (PVA)/poly(ethylene terephthalate) (PET) [114], nylon [115], and chitosan [116], because of its excellent solvation power. Indeed, many researchers have fabricated SF nanofibers using HFIP as a solvent

4.3.2.1. Effect of concentration and molecular weight of SF

Figure 26 shows SEM images of SFCs fibers prepared from EHD fabrications with HFIP. Both the dissolution time and concentration of the SFCs affected the shape and size of products. As in the case of EHD fabrication of SFCs using FA as a solvent, we attempted to categorize the morphology of products: bead dominant forms, intermediate forms, fine fiber forms, and flat fiber forms.

The bead dominant forms were only observed with 1 wt% of SFC030, SFC060, and SFC180. For SFC005, bead dominant forms were not observed and intermediate forms only occurred at 1-3 wt%; above 5 wt%, fine fiber forms were obtained and above 11 wt%, flat fiber forms were obtained. With SFC030, intermediate forms were observed only at 3 wt% and fine fiber forms were observed between 5 and 9 wt%. When the concentration exceeded 11 wt%, flat fiber forms were observed. With SFC060 and SFC180, the concentration of fine fiber forms was 7-12 wt% and that of flat fiber forms was above 13 wt%.

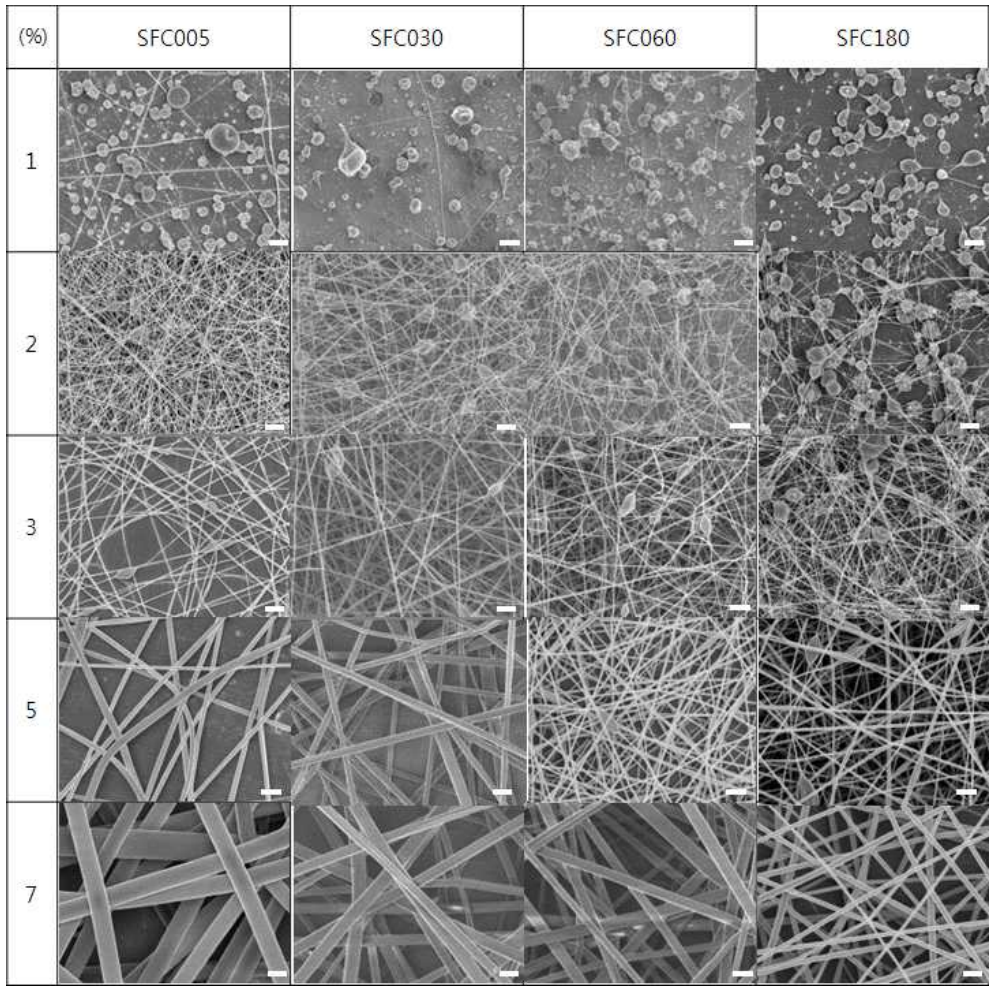

Figure 26. SEM images of EHD fabricated SFCs dissolved in HFIP. Scale bar : 1 μm. Applied voltage is 13 kV, flow rate is 0.3 ml/hr, distance from tip to collector is 10 cm.

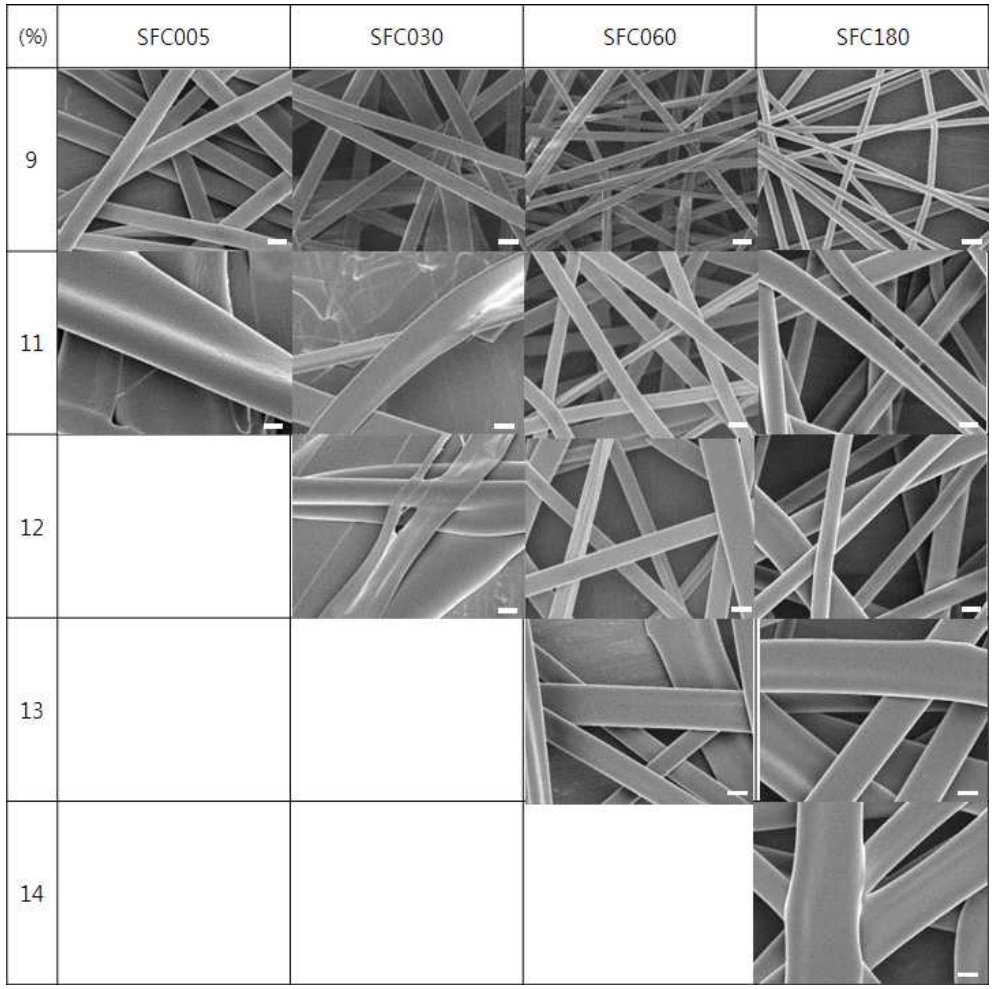

Figure 26. (Continued)

The size distribution of products was also affected by concentration and molecular weight (Figure 27). The sizes of fibers with SFC005 increased from 300 nm to 1.14 μm as concentration increased from 5 wt% to 9 wt%. In SFC030, when concentration increased from 5 wt% to 10 wt%, average fiber size increased from 275 nm to 1.07 μm. Other SFC fibers also showed the similar trend: SFC060 fibers increased from 203 nm to 1.15 μm with concentration increasing from 6 wt% to 12 wt%, and SFC180 fibers grew from 215 nm to 1.21 μm when the concentration was increased from 7 wt% to 12 wt%. When comparing the size of fibers at equal SFC concentrations (8 wt%), fiber sizes were 1.04 μm and 664, 480, and 320 nm for SFC005, SFC030, SFC060, and SFC180, respectively.

This trend can be elucidated by the size measurements using DLS (Figure 28). Sizes of the SF macromolecules in HFIP were 14.5 and 11.9 nm for SFC005 and SFC030, respectively. Both SFC060 and SFC180 were measured to be 10.0 nm. These macromolecule sizes were smaller than in formic acid or aqueous solution because of the favorable solvation capability of HFIP. Since HFIP has six fluorines and one hydroxyl group per molecule, it forms strong hydrogen bonds with the solutes. Thus, HFIP is capable of dissolving various substances having functional groups such as amides or ethers. For these reasons, more smaller sized SF macromolecules are formed in HFIP than other solvents. One exception was the size of SFC180 in HFIP. In the case of SFC180, the size of SF molecule was 10 nm, which is larger than that observed with formic acid (2.53 nm). It is thought that although the HFIP has a strong solvation power, it is limited from penetrating more deeply into SF macromolecules because

of

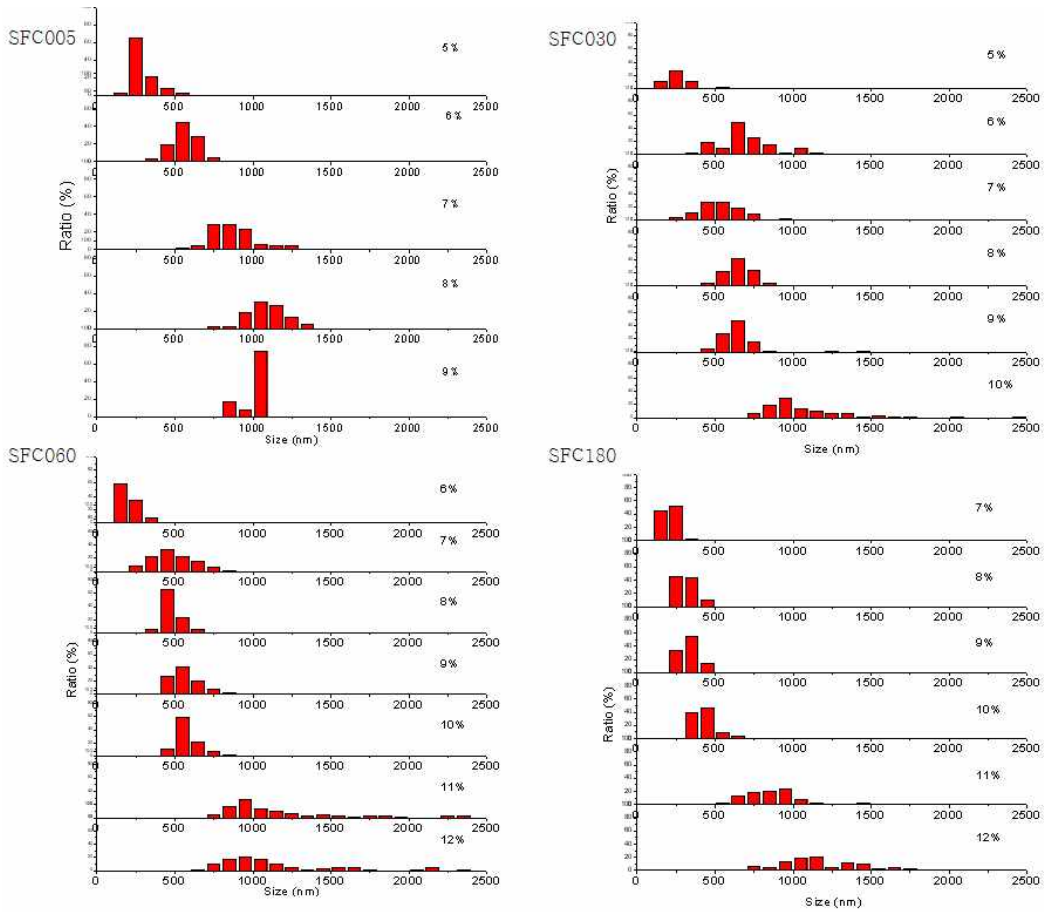

Figure 27. Fiber size distributions of EHD fabricated SFCs dissolved in HFIP.

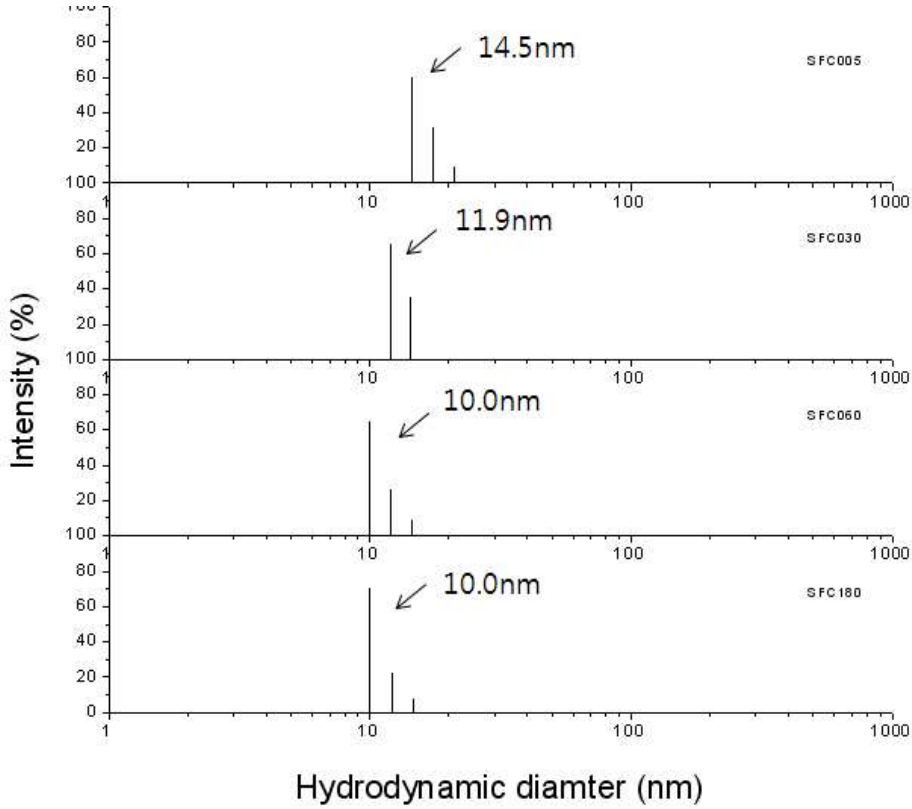

Figure 28. Hydrodynamic diameter of SFCs molecules in HFIP.

steric hindrance. It has been reported that formic acid molecules can penetrate SF macromolecules because it has the smallest side group (hydrogen) among carboxyl acids [92]. On the other hand, HFIP is larger than formic acid, which induces steric hindrance, preventing its penetration into SF macromolecules.

Nevertheless, with increasing dissolution time of SF in $CaCl_2$/EtOH/H_2O solution, more smaller sized SF molecules were formed, and this difference results in a size reduction of EHD products.

It can be clearly seen that both the concentration and molecular weight of SFCs significantly affects the morphology and size of EHD fabricated products. At the same concentration, the products' shapes were converted from intermediate form to fine fiber form and their sizes increased with increasing molecular weight. These conversions of a products' morphology and size in HFIP solvent systems are similar to EHD fabrications involving formic acid, but more drastic conversions of morphology and product sized appeared compared with formic acid systems

The reason of this drastic conversion may be attributable to solvent volatility. HFIP is a highly volatile solvent. While the vapor pressure at 20℃ of formic acid is 6.0 kPa, HFIP's is 16 kPa (for reference, water's is 2.3 kPa and that of EtOH is 5.3 kPa). Therefore, during EHD fabrication, solvent evaporation occurs very quickly. This leads to thin and mechanically distinct polymer skins around the polymer jet, and residual solvent remaining inside this region will evaporate later [115, 117, 118]. This phenomena disrupts the subdivision of the

polymer liquid jet into thinner fibers, and induces hollow-tube formation. In this state, atmospheric pressure and electrostatic force collapse the hollow tubes, causing thicker and flatter fibers to be formed. Similar cases were reported in the polymer chaining of nylon [115], poly(ether imide) [117], and wheat protein [118] using HFIP as a solvent.

However, apart from the high volatility of HFIP, the increase of viscosity results from chain entanglement might be responsible for the drastic changes. As mentioned earlier, both the concentration and molecular weight of SFC play a critical role in the EHD fabrication. These two factors affect chain entanglement and determine the viscosity of the polymer solution. In order to understand the effects of SFC viscosity in HFIP, the rheological properties of SF-HFIP solution were measured by ARES.

4.3.2.2. Relationship between shear viscosity of SF-HFIP solution and the EHD fabrication

Figure 29 shows the shear viscosities of SF-HFIP solutions. Instrument errors occurred at low SFC concentrations and the corresponding data have been omitted. Except at very high concentrations, most SFCs exhibited Newtonian behavior thanks to the strong solvation power of HFIP, which makes SF-HFIP solutions stable. However, above 10 wt% for SFC005, 11 wt% for SFC030, and 13 wt% for SFC060 and SFC180, shear thinning was observed. In those regions, too many chain entanglements were formed and chains

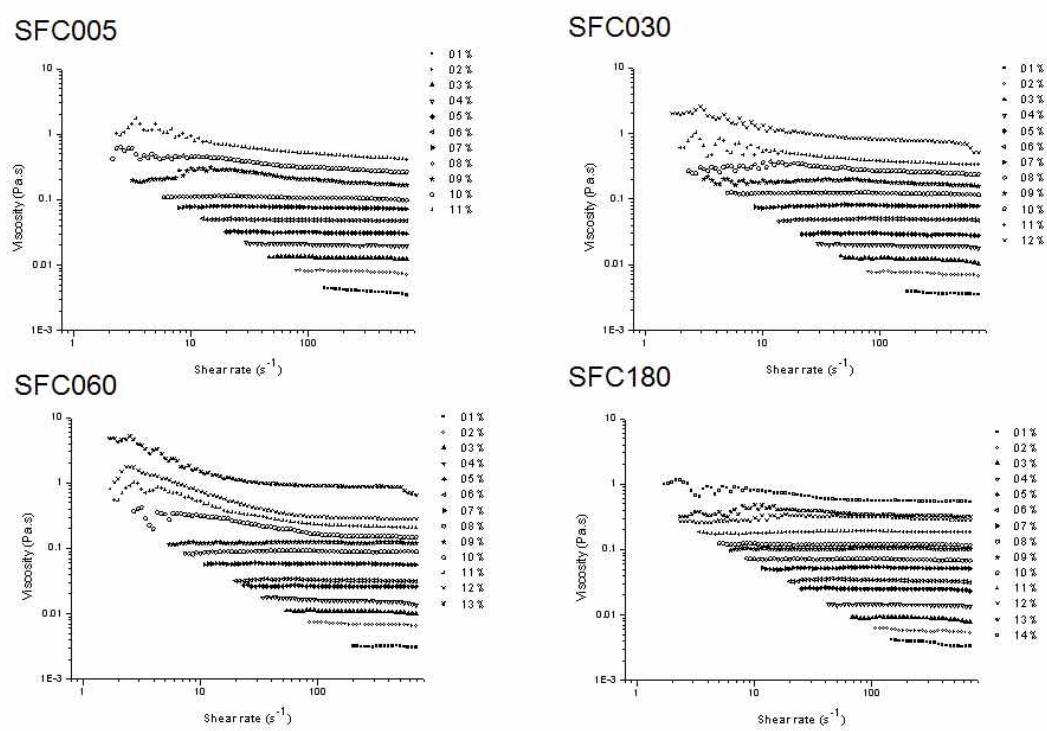

Figure 29. Shear viscosity of SF-HFIP solutions prepared by various dissolution times in $CaCl_2$/EtOH/H_2O solution and concentration.

were disentangled by the shear force. Due to the high viscosity, when other researchers fabricate SF nanofibers with HFIP, very high flow rates are applied to the dope solution and micro-sized fibers are formed [119-121].

By linear fitting, the zero shear viscosity was estimated and plotted against the concentration of SFCs (figure 30). Based on the morphology of EHD fabricated products, the zero shear viscosity increased depending on the exponent of concentration. The intermediate-form region corresponded to slopes of 1.05-1.53 ($\eta \propto c^{1.05-1.53}$), the fine fiber region had slopes ranging from 2.93 to 4.38 ($\eta \propto c^{2.93-4.38}$). For slopes exceeding 5.93, a flat fiber region was observed ($\eta \propto c^{5.93-13.63}$). These changes of slope are due to chain entanglement in terms of SF molecular weight and concentration. As mentioned in the literature survey, the concentration and slope of zero shear viscosity versus concentration can be divided into several regions according to chain entanglement. The intermediate region can be classified as a semi-dilute, highly entangled region, but its slope range is 1.05-1.53, which differs strongly from other research on linear synthetic polymers (4.25-4.5) [31]. This difference is due to micelle formation of SFCs in HFIP. In our DLS measurements (Figure 28), SF molecules form micelles ranging from 14.2 nm to 10.0 nm in size, which is unlike other linear polymers that exist as single chains and form random coils with each other. Additionally, SF micelles entangle each other on a much larger scale than linear polymers. Therefore, modeling chain entanglement of SF with conventional methods is inappropriate.

Additionally, the properties of HFIP affect the chain entanglement

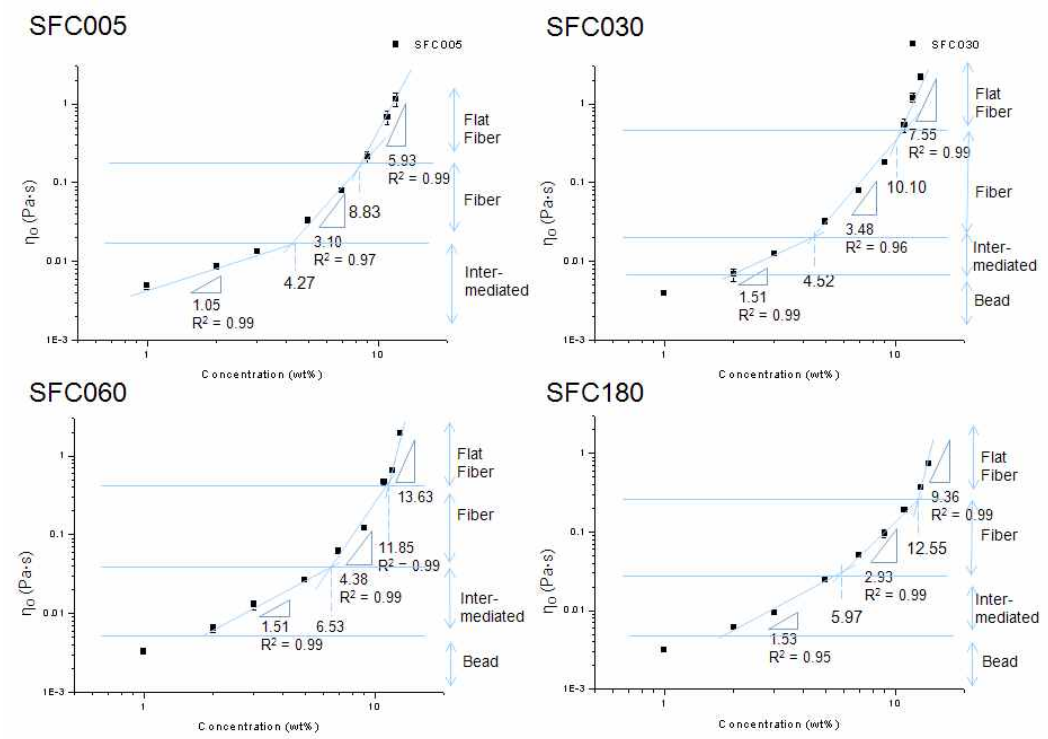

Figure 30. Effect of molecular weight and concentration of SFCs on zero shear viscosity of SFC solutions dissolved in HFIP.

of SF. Despite equal concentrations and molecular weights, zero viscosities were higher in HFIP than formic acid.

These phenomena are due to chain entanglements in HFIP. As mentioned earlier, HFIP has strong solvation due to hydrogen bond formation of fluorine and hydroxyl groups (in other words, due to its strong affinity for hydrogen bonding, HFIP is very sticky). At the same time, HFIP forms hydrogen bonds with several SF molecules, not with only one chain. Hydrogen bonds with monomolecules or low molecular weight polymers are very weak such as those in water, but those forming with high molecular weight polymer result in very strong forces. For this reason, HFIP forms hydrogen bonds with several SF molecules, and thus restricts their mobility. Then, more chain entanglements arise and beaded fibers or fibers can be formed at low concentrations or low molecular weights.

4.3.2.3. Relationship between dynamic viscosity of SF-HFIP solution and EHD fabrication

The dynamic viscosity, an additional rheological property of SF-HFIP solutions, can be used to determine the rheological properties of SF-HFIP solutions (Figure 31). Here, the storage modulus and loss modulus increased with increasing of concentration and molecular weight because of increased chain entanglement and crosslinking [100-102].

Similarly, SF in formic acid, at low frequency G'' is higher than G' and then reverses at the crosspoint, meaning that the dope solution

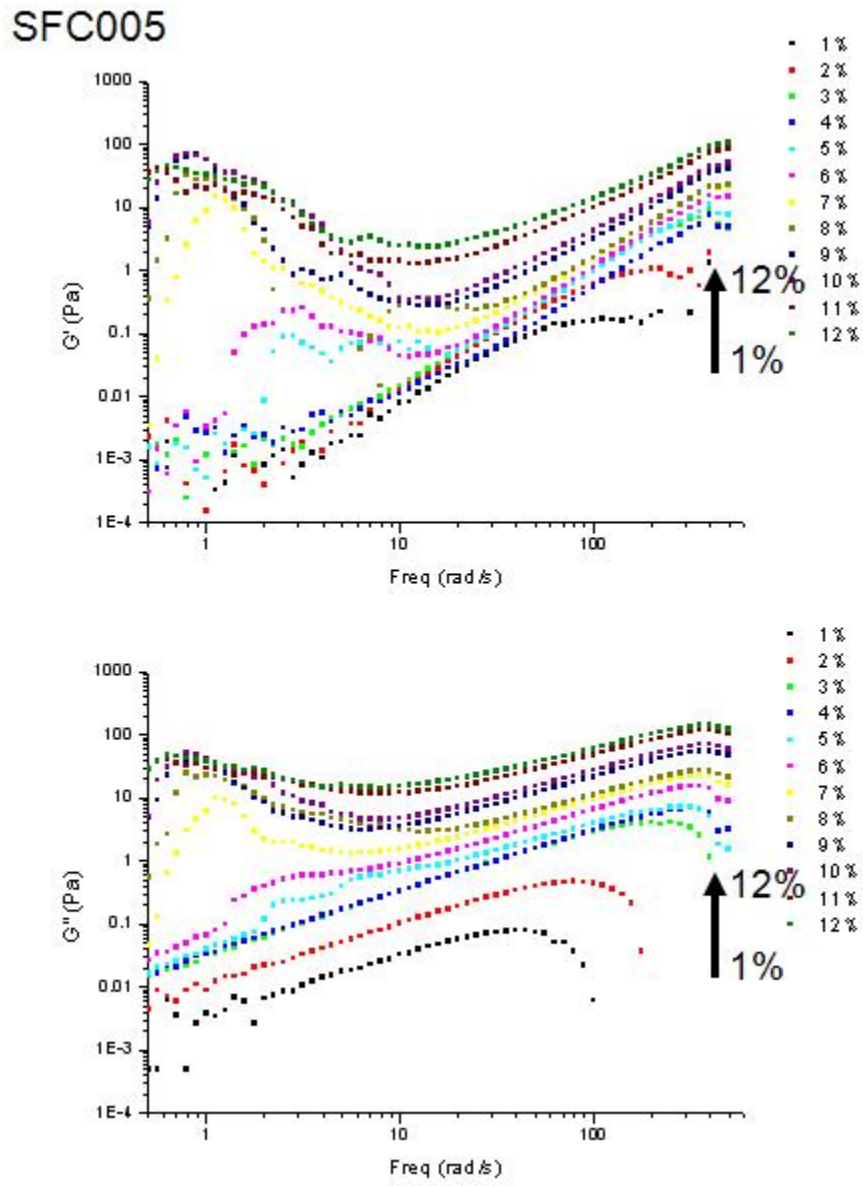

Figure 31. Dynamic viscosity of SF-HFIP solutions prepared by various dissolution times in $CaCl_2$/EtOH/H_2O solution and concentration.

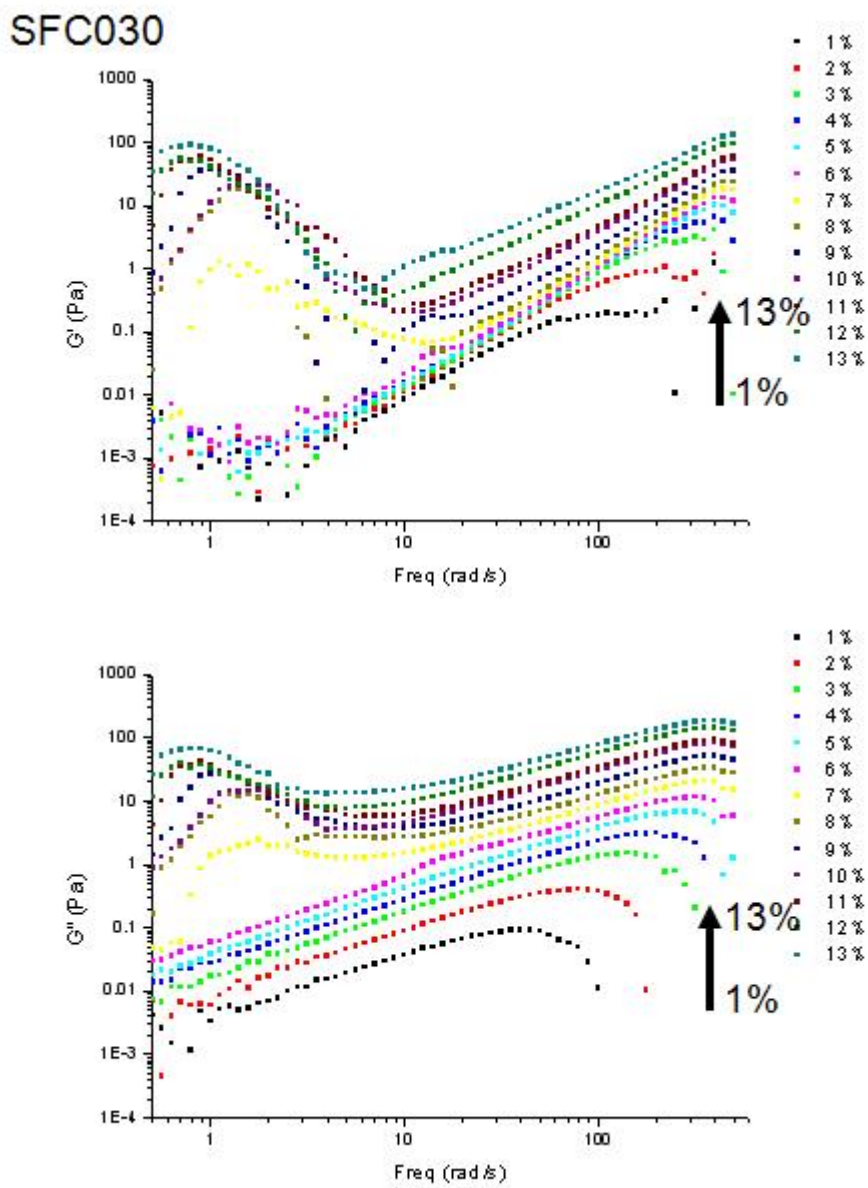

Figure. 31. (Continued)

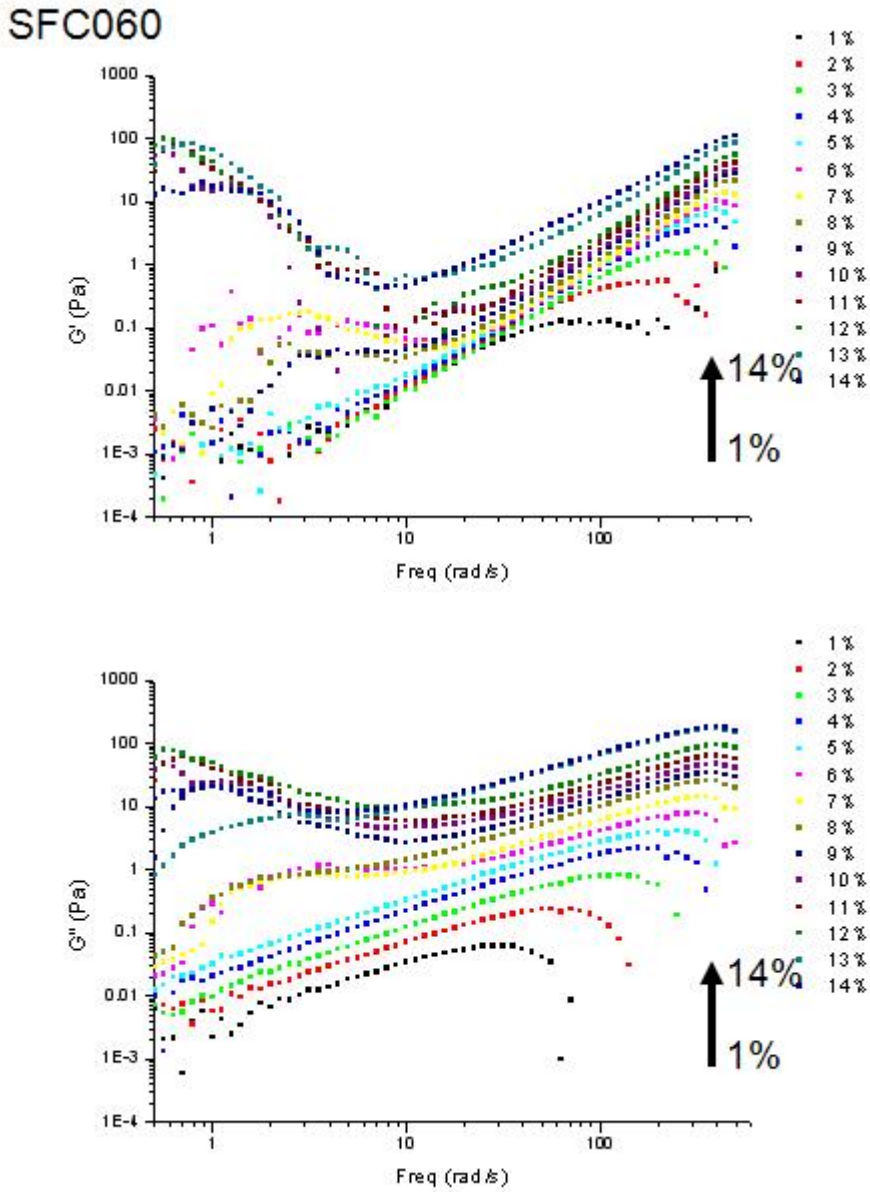

Figure. 31. (Continued)

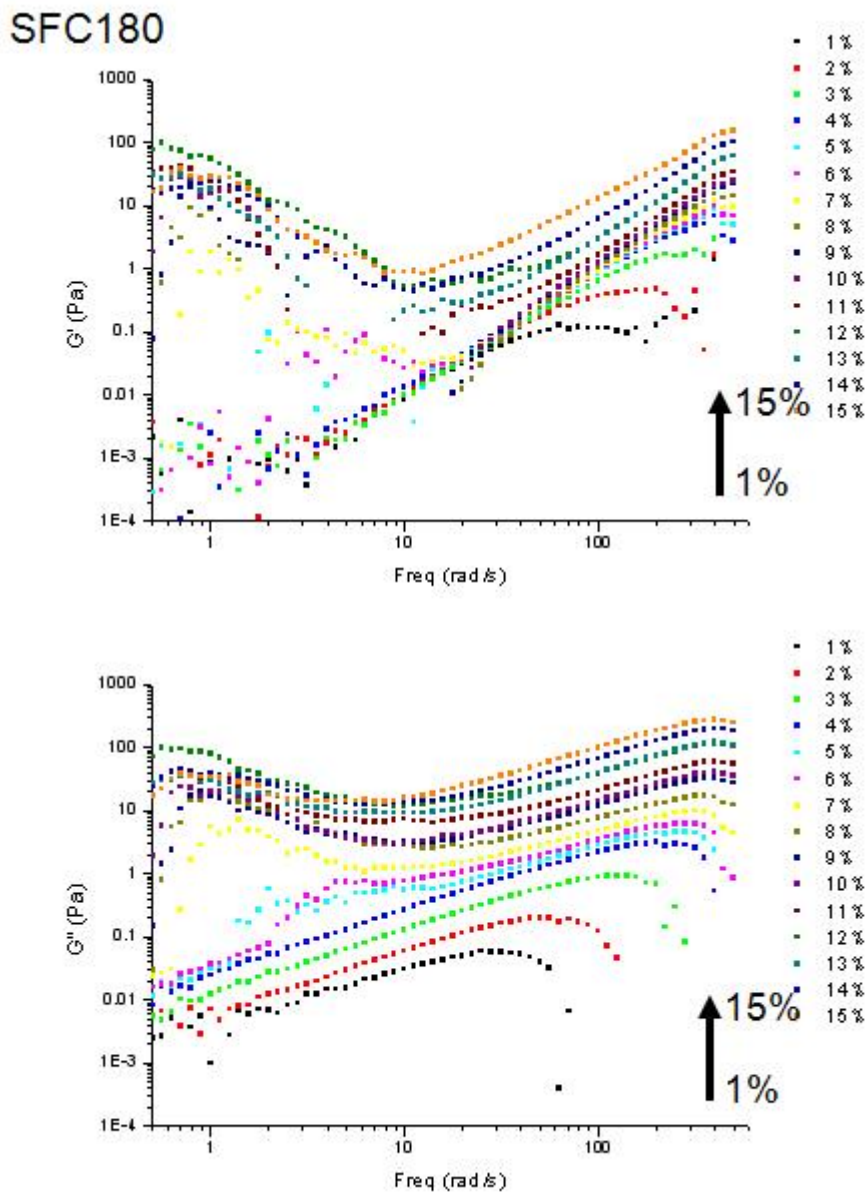

Figure. 31. (Continued)

converted from liquid state to gel state. Due to the conversion of solution state, G′ plateaus and G″ decreases above the crosspoint. Additionally, in Figure 32, the frequency at the crossover point of G′ and G″ can be seen to increase with increasing concentration and molecular weight.

However, while the moduli of the SF-FA solutions ranged from 0.001 Pa to 10 Pa, the moduli of SF-HFIP solutions increased from 0.001 Pa to 100 Pa. That is, SF molecules formed more chain entanglements in HFIP than in FA; therefore, more strain and energy are needed to disrupt chain entanglement.

4.3.2.4. Application of solution plateau modulus to EHD fabrication of SF-HFIP solution

Because the dynamic viscosity of SF-HFIP solutions was similar to that of SF FA solutions, $(G_N^0)_{soln}$ was also applicable to SF-HFIP solutions (calculated by the INT method).

Figure 33 shows that $(G_N^0)_{soln}$ increased exponentially with concentration, and the resulting slopes were similar: $(G_N^0)_{soln} \propto c^{2.98-3.12}$.

Regardless of the fact that the slope is slightly higher than SF-FA, its variation width is much larger. The bead predominant form occurred under 0.15 Pa and the intermediate form occurred from 0.15 Pa to 10 Pa. Fine fibers were formed above 10 Pa and flat fibers were formed above 300 Pa. These values are about 10 times higher than SF-FA solution at equal SF concentrations and molecular weights;

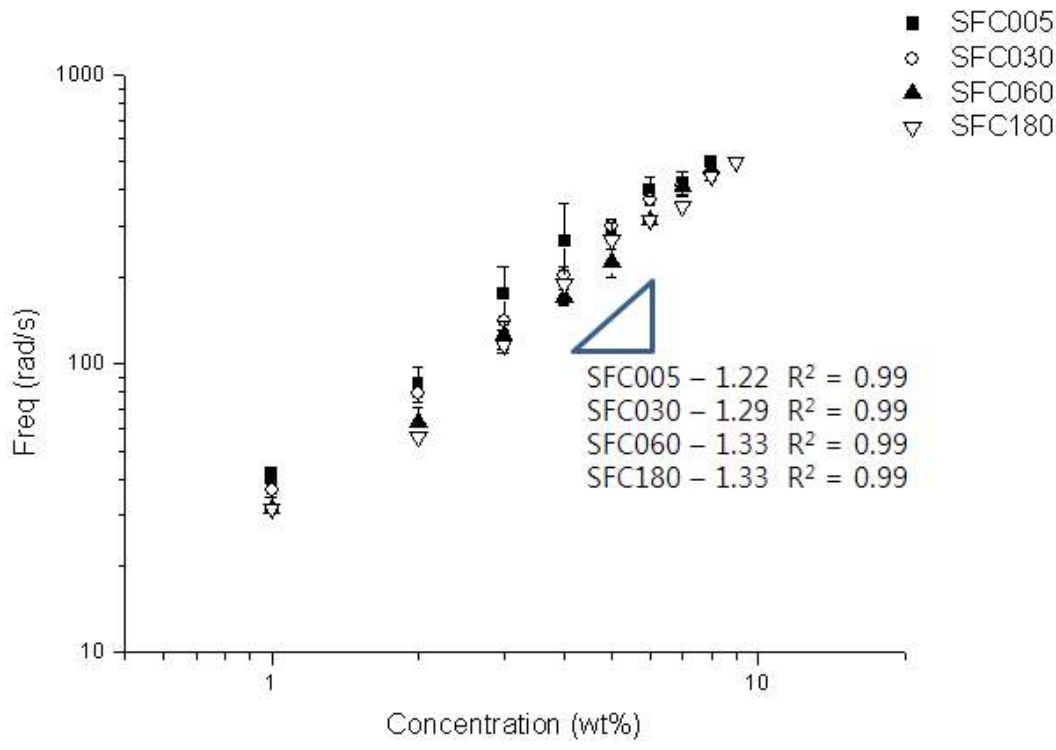

Figure 32. Crossover frequency where G' = G" (tanδ = 1) of SFC solutions dissolved in HFIP. Crossover frequencies over 8 wt% for SFC005, 9 wt% for SFC030, 8 wt% for SFC060 and 9 wt% for SFC180 were not measured due to instrumental limit.

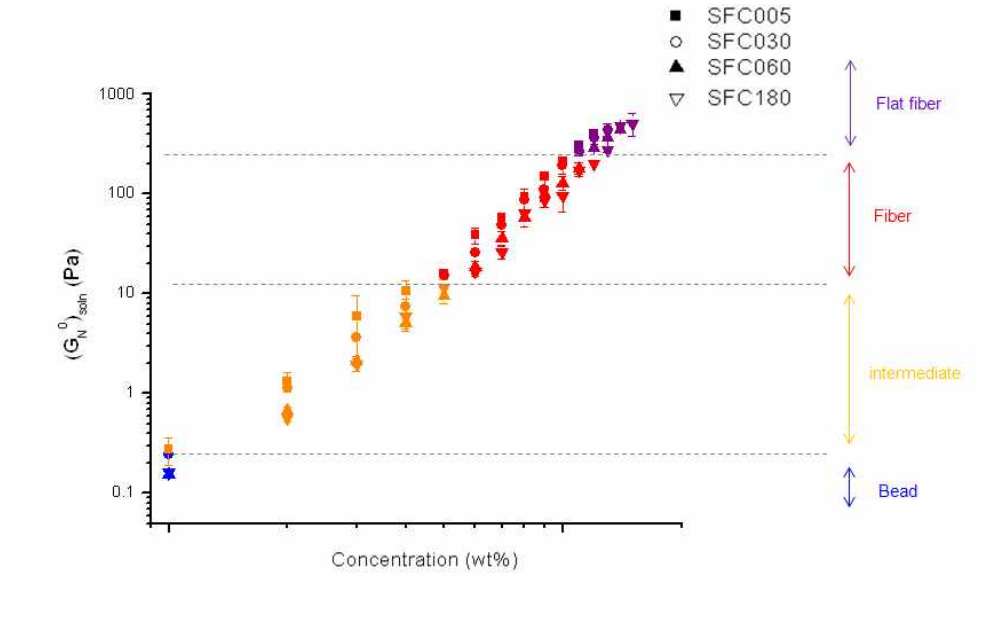

Figure 33. Effect of molecular weight and concentration of SFCs on SFC solution plateau modulus ($(G_N^0)_{soln}$) dissolved in HFIP.

this is owing to the favorability of HFIP toward hydrogen bonding and that chains become more entangled when captured by HFIP.

By these results, $(G_N^0)_{soln}$ can also be used as a parameter of SF-HFIP solutions in determining the degree of chain entanglement. In addition, $(G_N^0)_{soln}$ can be applied to size variation analysis of fibers fabricated by the EHD fabrication.

Size variations were estimated as a function of concentration, which is a parameterization used by most researchers (Figure 34). Sizes of SFCs were plotted against concentration, and the slopes of each SFC have different molecular weights increasing from 0.15 to 0.2 (R^2 = 0.8 -0.91). However, when the results for all SFCs were merged, accuracy decreased to 0.45.

Another substituted parameter, $(G_N^0)_{soln}$ was plotted against size variation (Figure 35). Before estimation, the sizes at 7 wt% and 8 wt% of SFC005 were conspicuously high (58.4 Pa for 920 nm and 94.7 Pa for 1040 nm). These two points were treated as experimental error and omitted from calculation. However, their slopes did not greatly differ (an increase from 3.83 to 3.98) and accuracy greatly increased from 0.67 to 0.81. When compared with SF-FA solution, accuracy was slightly reduced and it is thought that because of rapid solvent evaporation, nearly flat fibers were formed and their sizes drastically increased.

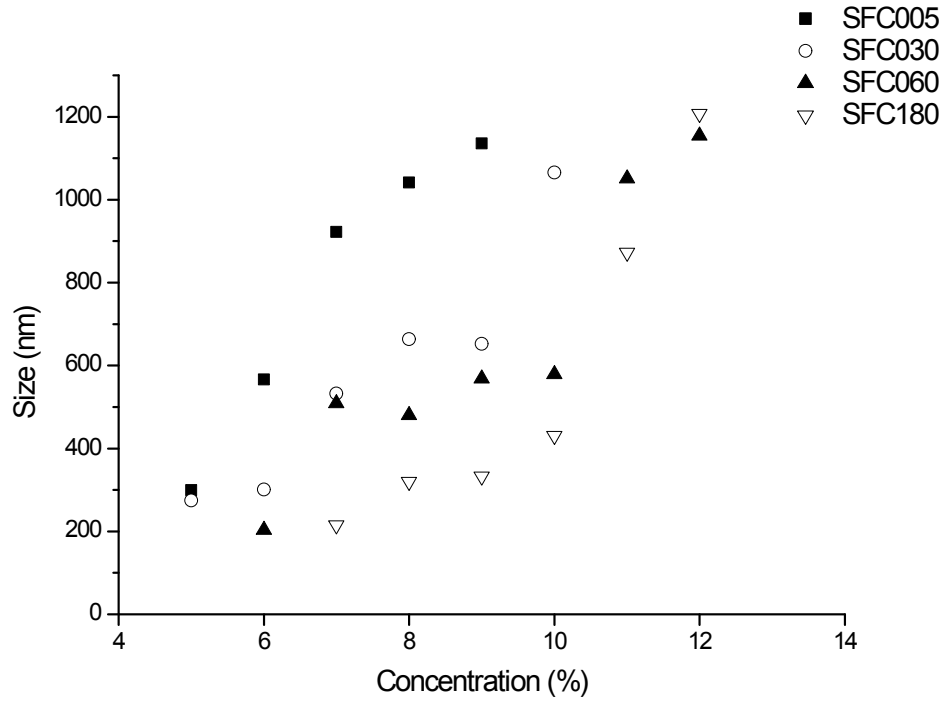

Figure 34. Fiber sizes of EHD fabricated SFCs dissolved in HFIP by SFC concentration.

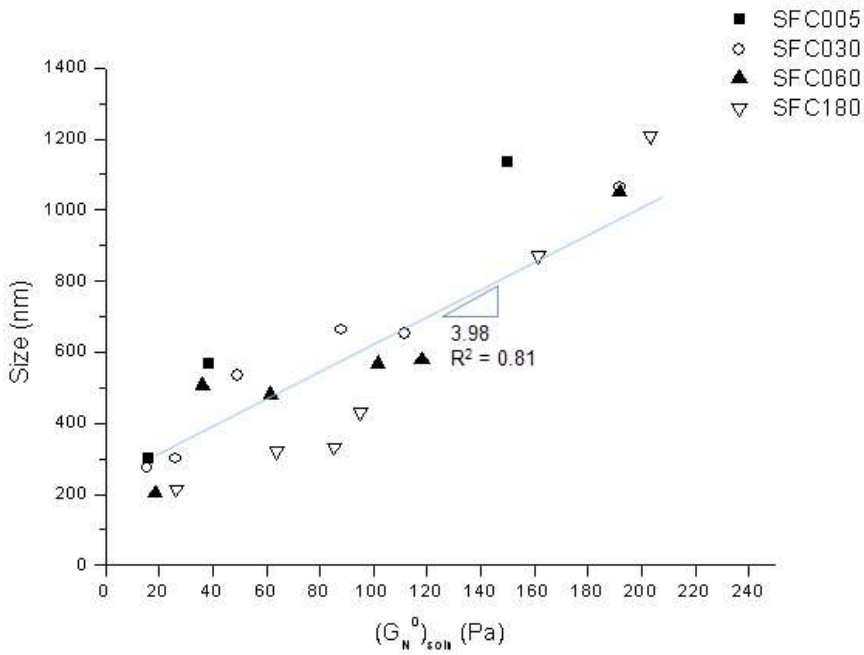

Figure 35. Fiber sizes of EHD fabricated SFCs dissolved in HFIP by SFC solution plateau modulus.

4.4. Prediction of shape and size of SF particles or fibers using solution plateau modulus

In the EHD fabrication of SF with formic acid or HFIP, it was found that $(G_N^0)_{soln}$ is closely related to chain entanglement and fiber size variation.

Therefore, SFC solutions were prepared with random molecular weight and concentration. With dissolving times in $CaCl_2/EtOH/H_2O$ of 15, 120 and 360 min, SFC015, SFC120, and SFC360 were prepared. Their concentrations were also randomly selected.

For formic acid, 12 wt% of SFC015 and 17 wt% of SFC360 were selected. Their calculated $(G_N^0)_{soln}$ were 60.73 Pa and 77.27 Pa (Table 3). These values fall within the fine fiber region (Figure 19) and, actually, all of their shapes corresponded (Figure 36).

When substituting the $(G_N^0)_{soln}$ of each SFC to graph $(G_N^0)_{soln}$ against size (Figure 35), their approximate sizes were 255 nm and 323 nm. Their actual sizes were 199 ± 52 nm and 259 ± 83 nm. When comparing these values, the approximate sizes were within the error range of the actual values.

For HFIP, 8 wt% of SFC015, 12 wt% of SFC120, and 15 wt% of SFC360 were selected. Their $(G_N^0)_{soln}$ values were 199.89 Pa, 500.71 Pa, and 333.39 Pa (Table 4). The values of 199.89 Pa and 333.39 Pa belong to the fine fiber region while 500.71 Pa falls within the flat

Table 3. Size prediction of EHD fabricated SFCs dissolved in formic acid by solution plateau modulus

Sample	Conc. (wt%)	$(G_N^0)_{soln}$ (Pa)	$Size_{Prediction}$ (nm)	$Size_{Measurement}$ (nm)
SFC015	12	60.73	255.39	199 ± 52
SFC360	17	77.27	323.01	259 ± 83

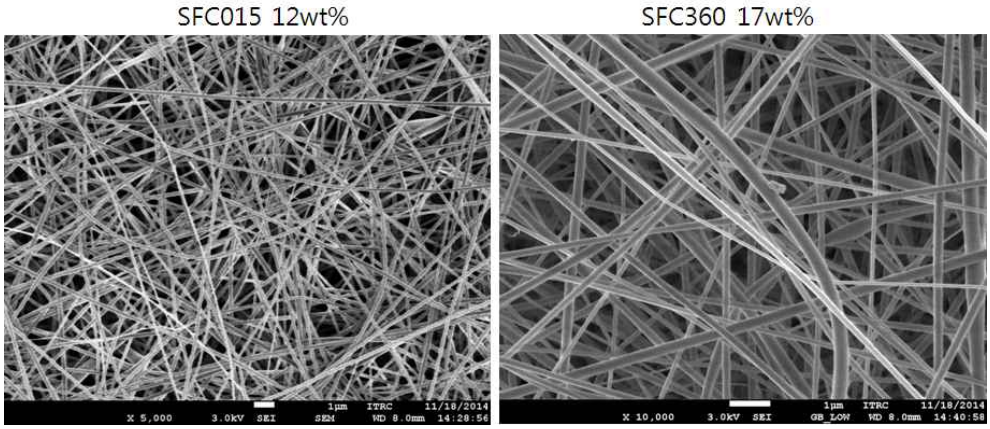

Figure 36. SEM images of EHD fabricated SFC015 for 12 wt% and SFC360 for 17 wt% dissolved in formic acid. Scale bar : 1 μm. Applied voltage is 13 kV, flow rate is 0.3 ml/hr, distance from tip to collector is 10 cm.

Table 4. Size prediction of EHD fabricated SFCs dissolved in HFIP by solution plateau modulus

Sample	Conc. (wt%)	$(G_N^0)_{soln}$ (Pa)	$Size_{Prediction}$ (nm)	$Size_{Measurement}$ (nm)
SFC015	8	199.89	1015.56	964 ± 452
SFC120	12	500.71	×	×
SFC360	15	333.39	1546.89	1742 ± 485

fiber region (Figure 33). Additionally, from the SEM images (Figure 37), the actual product shape for EHD fabricated 12 wt% of SFC120 in HFIP was flat fibers. With 8 wt% of SFC015 and 15 wt% of SFC360, fibers were formed.

As with formic acid, the $(G_N^0)_{soln}$ of each sample was substituted to $(G_N^0)_{soln}$ then graphed; their calculated sizes were 818 nm and 1.35 μm, respectively. Their actual sizes were 964 ± 452 nm and 1.74 ± 0.49 μm. Thus, their calculated sizes were within the error range of the actual size.

From several comparisons of the $(G_N^0)_{soln}$ values of SF-FA solution and SF-HFIP solution, solutions matching the shapes and sizes of EHD fabricated product can be predicted. Although it is difficult to exactly determine a correct size, it appears that $(G_N^0)_{soln}$ may constitute a particularly useful parameter in predicting approximate size and product shape (bead-predominant, intermediate, fine fiber, and flat fiber form).

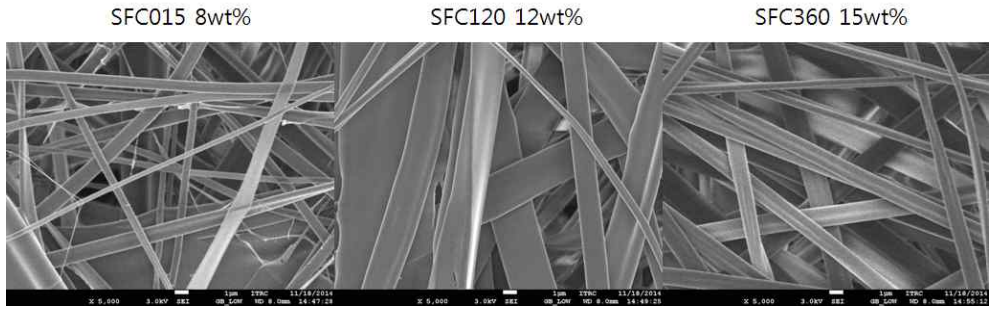

Figure 37. SEM images of EHD fabricated SFC015 for 8 wt%, SFC120 for 12 wt% and SFC360 for 15 wt% dissolved in HFIP. Scale bar : 1 μm. Applied voltage is 13 kV, flow rate is 0.3 ml/hr, distance from tip to collector is 10 cm.

V. Conclusion

In this study, SF was EHD fabricated using 1 M LiCl/DMSO, formic acid and HFIP were used as solvent, and the effects of chain entanglement on EHD fabrications were investigated.

Firstly, SF microspheres were successfully fabricated with 1 M LiCl/DMSO as a newly tested solvent.

The shear viscosity of SF dope solution (by chain overlap or entanglement) may be the primary parameter in determining the final morphology of SF microparticles

Secondly, SF nanoparticles or fibers were fabricated by EHD fabrications using formic acid and HFIP.

SEM images and rheological properties of SF dope solutions show that the chain entanglement of SF molecules in solution significantly affects the morphology and size of products fabricated by EHD fabrications.

Conventional parameters using shear viscosity or solution entanglement number are inappropriate for determining the chain entanglement of SF molecules because of the micelle formation of SF, which is not a common trait among linear polymers.

The solution plateau modulus can be a substitutive parameter for determining the degree of chain entanglement of SF molecules in solution. Additionally, it can be used to predict the morphology and

size of products fabricated by EHD fabrications.

These results show that SF molecules have unique entanglement behaviors due to their unusual micelle formation, and that these are important to in the EHD fabrication of SF. In other words, an understanding of SF chain entanglement will lead to successful EHD fabrication of SF.

VI. References

[1] Y. Wu and R. L. Clark, Electrohydrodynamic Processing of Micro- and Nanometer Biological Materials, *Biomaterials Fabrication and Processing Handbook.* CRC Press, Boca Raton, ch. 11. 275 - 333 (2008).

[2] S. Chakraborty, I. -C. Liao, A. Adler and K. W. Leong, Electrohydrodynamics: A facile technique to fabricate drug delivery systems, *Advanced Drug Delivery Reviews.* **61**, 1043-1054 (2009).

[3] Z. -M. Huang, Y. -Z. Zhang, M. Kotaki and S. Ramakrishna, A review on polymer nanofibers by electospinning and their applications in nanocomposites, *Composites Science and Technology.* **63**, 2223-2253 (2003).

[4] C. H. Park and J. Lee, Electrosprayed polymer particles: Effect of the solvent properties. *Journal of Applied Polymer Science,* **114**, 430-437 (2009).

[5] Formhals, Anton, Process and apparatus for preparing artificial threads, *U.S. Patent.* 1,975,504 (1934).

[6] Formhals, Anton, Method and apparatus for spinning, *U.S. Patent,* 2,349,950 (1944).

[7] S. Zhao, Q. Zhou, Y. Long, G. Sun and Y. Zhang, Nanofibrous patterns by direct electrospinning of nanofibers onto topographically structured non-conductive substrates, *Nanoscale*, **5**(11), 4993-5000 (2013).

[8] J. -W. Kim, Y. Yamagata, B. J. Kim and T. Higuchi, Direct and dry micro-patterning of nano-particles by electrospray deposition through a micro-stencil mask, *Journal of Micromechanics and Microengineering*. **19**(2), 025021 (2019).

[9] D. Li, Y. Wang and Y. Xia, Electrospinning nanofibers as uniaxially aligned arrays and layer-by-layer stacked films, Advanced Materials, **16**(4), 361-366 (2004).

[10] V. A. Ganesh, A. S. Nair, H. K. Raut, T. M. Walsh and S. Ramakrishna, Photocatalytic superhydrophilic TiO2 coating on glass by electrospinning, *RSC Advances*. **2**(5), 2067-2072 (2012).

[11] H. Q. Liu and Y. L. Hsieh, Ultrafine fibrous cellulose membranes from electrospinning of cellulose acetate, *Journal of Polymer Science Part B: Polymer Physics*. **40**(18), 2119-2129 (2002)

[12] E. D. Boland, G. E. Wnek, D. G. Simpson, K. J. Pawlowski and G. L. Bowlin, Tailoring tissue engineering scaffolds using electrostatic processing techniques: A study of poly(glycolic acid) electrospinning, *Journal of Macromolecular Science Part A-Pure and Applied Chemistry*. **38**(12), 1231-1243 (2001).

[13] M. A. T. Cardoso, M. Talebi, P. A. M. H. Soares, C. U. Yurteri and J. R. van Ommen, *Functionalization of lactose as a biological carrier for bovine serum albumin by electrospraying, International Journal of Pharmaceutics*. **414**(1-2), 1-5 (2011).

[14] D. Zhang and J. Chang, Electrospinning of Three-Dimensional Nanofibrous Tubes with Controllable Architectures, *Nano letters*. **8**(10), 3283-3287 (2008).

[15] T. J. Sill and H. A. von Recum, Electrospinning: Applications in drug delivery and tissue engineering, *Biomatierials*. **29**, 1989-2006 (2008).

[16] J. Doshi and D. H. Reneker, Electrospinning process and applications of electrospun fibers, *Journal of Electrostatics*. **35**(2-3), 151-160 (1995).

[17] S. L. Shenoy, W. D. Bates, H. L. Frisch and G. E. Wnek, Role of chain entanglements on fiber formation during electrospinning of polymer solutions: good solvent, non-specific polymer-polymer interaction limit, *Polymer*. **46**(10), 3372-3384 (2005).

[18] G. H. Altman, F. Diaz, C. Jakuba, T. Calabro, R. L. Horan, J. S. Chen, H. Lu, J. Richmond and D. L. Kaplan, Silk-based biomaterials, *Biomaterials*. **24**(3), 401-416 (2003).

[19] S. W. Ha, A. E. Tonelli and S. M. Hudson, Structural studies of Bombyx mori silk fibroin during regeneration from solutions and wet fiber spinning, *Biomacromolecules*. **6**(3), 1722-1731 (2005).

[20] J. H. Kim, C. H. Park, O. -J. Lee, J. -M. Lee, J. W. Kim, Y. H. Park and C. S. Ki, Preparation and in vivo degradation of controlled biodegradability of electrospun silk fibroin nanofiber mats, *Journal of Biomedical Materials Research Part A.* **100A**(12), 3287-3295 (2012).

[21] C. S. Ki, J. W. Kim, J. H. Hyun, K .H. Lee, M. Hattori, D. K. Rah and Y. H. Park, Electrospun three-dimensional silk fibroin nanofibrous scaffold, *Journal of Applied Polymer Science*, **106**(6), 3922-3928 (2007).

[22] I. C. Um, T. H. Kim, H. Y. Kweon, C. S. Ki and Y. H. Park, A Comparative Study on the Dielectric and Dynamic Mechanical Relaxation Behavior of the Regenerated Silk Fibroin Films, *Macromolecular Research*. **17**(10), 785-790 (2009).

[23] M. Fini, A. Motta, P. Torricelli, G. Glavaresi, N. N. Aldini, M. Tschon, R. Giardino and C. Migliaresi, The healing of confined critical size cancellous defects in the presence of silk fibroin hydrogel, *Biomaterials*. **26**(17), 3257-3536 (2005).

[24] A. Lammel, X. Hu, S. -H. Park, D. L. Kaplan, and T. R. Scheibel, Controlling silk fibroin particle features for drug delivery. *Biomaterials*. **31**, 4583 - 4591 (2010).

[25] T. T. Cao, Z. Z. Zhou and Y. Q. Zhang, Processing of beta-Glucosidase-Silk fibroin nanoparticle bioconjugates and their characteristics, *Applied Biochemistry and Biotechnology,* **173**(2), 544-551 (2014) .

[26] U. J. Kim, J. Park, H. J. Kim, M. Wada and D. L. Kaplan, Three-dimensional aqueous-derived biomaterial scaffolds from silk fibroin, *Biomaterials*, **26**(15), 2775-2785 (2005).

[27] S. Sukigara, M. Gandhi, J. Ayutsede, M. Micklus and F. Ko, Regeneration of Bombyx mori silk by electrospinning - part 1: processing parameters and geometric properties, *Polymer*, **44**(19), 5721-5727 (2003).

[28] B. -M. Min, G. Lee, S. H. Kim, Y. S. Nam, T. S. Lee and W. H. Park, Electrospinning of silk fibroin nanofibers and its effect on the adhesion and spreading of normal human keratinocytes and

fibroblasts in vitro, *Biomaterials.* **25**, 1289 - 1297 (2004).

[29] H. Wang, H. Shao and X. Hu, Structure of silk fibroin fibers made by an electrospinning process from a silk fibroin aqueous solution, *Journal of applied polymer science*. **101**, 961 - 968 (2006).

[30] A. Gholami, H. Tavanai and A. R. Moradi, Production of fibroin nanopowder through electrospraying, *Journal of Nanoparticle Research*. **13**(5), 2089-2098 (2010).

[31] M. G. McKee, G. L. Wilkes, R. H. Colby and T. E. Long, Correlations of Solution Rheology with Electrospun Fiber Formation of Linear and Branched Polyesters. *Macromolecules.* **37**, 1760 - 1767 (2004).

[32] P. Gupta, C. Elkins, T. E. Long and G. L. Wilkes, Electrospinning of linear homopolymers of poly(methyl methacrylate): exploring relationships between fiber formation, viscosity, molecular weight and concentration in a good solvent. *Polymer.* **46**, 4799 - 4810 (2005).

[33] Z. Jun, H. Q. Hou, a. Schaper, J. H. Wendorff and A. Greiner, Poly-L-lactide nanofibers by electrospinning - Influence of solution viscosity and electrical conductivity on fiber diameter and fiber morphology, *E-Polymers*. 009 (2003).

[34] N. Bock, T. R. Dargaville and M.A. Woodruff, Electrospraying of polymers with therapeutic molecules: State of the art, *Progress in Polymer Science*, **37**(11), 1510-1551 (2012).

[35] H. L. Frisch and R. Simha, Monolayers of linear macromolecules,

Journal of Chemical Physics. **24**(4), 652-655 (1956).

[36] A. Koski, K. Yim ans S. Shivkumar, Effect of molecular weight on fibrous PVA produced by electrospinning, *Materials Letters*. **58**(3-4), 493-497 (2004).

[37] Y. Yamashita, F. Ko, A Tanaka and H Miyake, Characteristics of Elastomeric Nanofiber Membranes Produced by Electrospinning, *Journal of Textile Engineering*. **53**(4), 137-142 (2007).

[38] R. G. Larson, T. Sridha, L. G. Leal, G. H. McKinley, A. E. Likhtman and T. C. B. McLeish, Definitions of entanglement spacing and time constants in the tube model, *Journal of Rheology*. **47**(3), 809-818 (2003).

[39] L. J. Fetters, D. J. Lohse, D. Richter, T. A. Witten and A. Zirkel, Connection between polymer molecular weight, density, chain dimensions, and melt viscoelastic properties, *Macromolecules*. **27**(17), 4639-4647 (1994).

[40] S. Megelski, J. S. Stephens, D. B. Chase and J. F. Rabolt, Micro- and nanostructured surface morphology on electrospun polymer fibers, *Macromolecules*. **35**(22), 8456-8466 (2002).

[41] J. M. Deitzel, J. D. Kleinmeyer, J. K. Hirvonen and N. C. B. Tan, Controlled deposition of electrospun poly(ethylene oxide) fibers, *Polymer*. **42**(19), 8163-8170 (2001).

[42] X. H. Zong, K. Kim, D. F. Fang, S. F. Ran, B. S. Hsiao and B. Chu, Structure and process relationship of electrospun bioabsorbable nanofiber membranes, *Polymer,* **43**(16), 4403-4412 (2002).

[43] K. Tanaka, N. Kajiyama, K. Ishikura, S. Waga, A. Kikuchi, K. Ohtomo, T. Takagi and S. Mizuno, Determination of the site of disulfide linkage between heavy and light chains of silk fibroin produced by *Bombyx mori*, *Biochimica et Biophysica Acta (BBA) - Protein Structure and Molecular Enzymology*, **1432**(1), 92-103 (1999).

[44] C. -Z. Zhou, F. Confalonieri, N. Medina, Y. Zivanovic, C. Esnault, T. Yang, M. Jacquet, J. Janin, M. Duguet, R. Perasso and Z. -G. Li, Fine organization of Bombyx mori fibroin heavy chain gene, *Nucleic Acids Research*, **28**(12), 2413-2419 (2000).

[45] H. -J. Jin and D. L. Kaplan, Mechanism of silk processing in insects and spiders. *Nature*. **424**, 1057-1061 (2003).

[46] Q. Lu, H. Zhu, C. Zhang, F. Zhang, B. Zhang and D. L. Kaplan, Silk self-assembly mechanisms and control from thermodynamics to kinetics. *Biomacromolecules.* **13**, 826 - 832 (2012).

[47] F. Zhang, B. Zuo, Z. Fan, Z. Xie, Q. Lu, X. Zhang and D. L. Kaplan, Mechanisms and Control of Silk-Based Electrospinning. *Biomacromolecules.* **13**, 798 - 804 (2012).

[48] I. C. Um, H. Y. Kweon, Y. H. Park and S. Hudson, Structural characteristics and properties of the regenerated silk fibroin prepared from formic acid. *Int. J. Biol. Macromol.* **29**, 91 - 97 (2001).

[49] H. J. Cho, C. S. Ki, K. H. Lee and I. C. Um, Molecular weight distribution and solution properties of silk fibroins with different dissolution conditions. *Int. J. Biol. Macromol.* **51**, 336 - 341 (2012).

[50] K. Yoon, H. N. Lee, C. S. Ki, D. Fang, B. S. Hsiao, B. Chu and

I. C. Um, Effects of degumming conditions on electro-spinning rate of regenerated silk, *International Journal of Biological Macromolecules*. **61**, 50-57 (2013).

[51] H. J. Kim, I. C. Um, Effect of degumming ratio on wet spinning and post drawing performance of regenerated silk. *Int. J. Biol. Macromol*. **67**, 387 - 393 (2014).

[52] A. Matsumoto, A. Lindsay, B. Abedian and D. L. Kaplan, Silk fibroin solution properties related to assembly and structure. *Macromolecular Bioscience.* **8**, 1006 - 1018 (2008).

[53] E. Iizuka, Silk thread - mechanism of spinning and its mechanical-properties, *Applied polymer symposia.* **41**, 173-185 (1985).

[54] J. Magoshi, Y. Magoshi and S. Nakamura, Crystallization, liquid crystal, and fiber formation of silk fibroin, *Applied polymer symposia.* **41**, 187-204 (1985).

[55] X. Chen, D. P. Knight and F. Vollrath, Rheological characterization of Nephila spidroin solution. *Biomacromolecules.* **3**, 644-648 (2002).

[56] A. E. Terry, D. P. Knight, D. Porter and F. Vollath, PH induced changes in the rheology of silk fibroin solution from the middle division of Bombyx mori silkworm, *Biomacromolecules.* **5**(3), 768-772 (2004).

[57] Q. Wang, Y. Yang, X. Chen and Z. Shao, Investigation of Rheological Properties and Conformation of Silk Fibroin in the Solution of AmimCl. *Biomacromolecules.* **13**, 1875 - 1881 (2012).

[58] A. Nisal, C. Kalelkar, J. Bellare and A. Lele, Rheology and microstructural studies of regenerated silk fibroin solutions. *Rheologica Acta.* 52, 833 - 840 (2013).

[59] J. S. Ko, K. Yoon, C. S. Ki, H. J. Kim, D. G. Bae, K. H. Lee, Y. H. Park and I. C. Um, Effect of degumming condition on the solution properties and electrospinnablity of regenerated silk solution, *International Journal of Biological Macromolecules.* **55**, 161-168 (2013).

[60] H. J. Kim and I. C. Um, Relationship between rheology and electro-spinning performance of regenerated silk fibroin prepared using different degumming methods, *Korea-Australia Rheology Journal.* **26**(2), 119-125 (2014).

[61] H. J. Cho, Y. J. Yoo, J. W. Kim, Y. H. Park, D. G. Bae and I. C. Um, Effect of molecular weight and storage time on the wet- and electro-spinning of regenerated silk fibroin, *Polymer Degradation and Stability.* **97**(6), 1060-1066 (2012).

[62] A. Alessandrino, B. Marelli, C. Arosio, S. Fare, M. C. Tanzi and G. Freddi, Electrospun silk dibroin mats for tissue engineering, *Engineering in Life Sciences.* **8**(3), 219-228 (2008).

[63] H. Liu, X. Li, G. Zhou, H. Fan and Y. Fan, Electrospun sulfated silk fibroin nanofibrous scaffolds for vascular tissue engineering, *Biomaterials.* **32**(15) 3784-3793 (2011).

[64] H. Wang, H. Shao and X. Hu, Structure of silk fibroin fibers made by an electrospinning process from a silk fibroin aqueous solution, *Journal of Applied Polymer Science.* **101**(2), 961-968 (2006).

[65] J. -P. Chen, S. -H. Chen and G. -J. Lai, Preparation and characterization of biomimetic silk fibroin/chitosan composite nanofibers by electrospinning for osteoblasts culture, *Nanoscale Research Letters*. **7**, 1-11 (2012).

[66] K. Ohgo, C. Zhao, M. Kobayashi and T. Asakura, Preparation of non-woven nanofibers of Bombyx mori silk, Samia cynthia ricini silk and recombinant hybrid silk with electrospinning method, *Polymer*. **44**(3), 841-846 (2003).

[67] A. Muthumanickkam, S. Subramanian, M. Goweri, W. S. Beaula and V. Ganesh, Comparative study on eri silk and mulberry silk fibroin scaffolds for biomedical applications, *Iranian Polymer Journal*. **22**(3), 143-154 (2013).

[68] B. Dhandayuthapani, Y. Yoshida, T. Maekawa and D. S. Kumar, Fabrication and Characterization of Nanofibrous Scaffold Developed by Electrospinning, *Materials Research-Ibero-American Journal of Materials*. **14**(3), 317-325 (2011).

[69] S. Sukigara, M. Gandhi, J. Ayutesede, M. Micklus and F. Ko, Regeneration of Bombyx mori silk by electrospinning. Part 2. Process optimization and empirical modeling using response surface methodology, *Polymer*. **45**(11), 3701-3708 (2004).

[70] B. -M. Min, L. Jeong, K. Y. Lee and W. H. Park, Regenerated Silk Fibroin Nanofibers: Water Vapor-Induced Structural Changes and Their Effects on the Behavior of Normal Human Cells, *Macromolecular Bioscience*. **6**(4), 285-292 (2006).

[71] F. Zhang, B. Q. Zuo, and L. Bai, Study on the structure of SF

fiber mats electrospun with HFIP and FA and cells behavior. *Journal of materials science.* **44**(20), 5682 – 5687 (2009)

[72] C. Chen, C. Chuanbao, M. Xilan, T. Yin and Z. Hesun, Preparation of non-woven mats from all-aqueous silk fibroin solution with electrospinning method, Polymer. **47**(18), 6322-6327 (2006).

[73] T. Hodgkinson, Y. Chen, A. Bayat and X. -F. Yuan, Rheology and Electrospinning of Regenerated Bombyx mori Silk Fibroin Aqueous Solutions. *Biomacromolecules* **15**, 1288 – 1298 (2014).

[74] J. Zhu, H. Shao and X. Hu, Morphology and structure of electrospun mats from regenerated silk fibroin aqueous solutions with adjusting pH. *International Journal of Biological Macromolecules.* **41**(4), 469 – 474 (2007).

[75] J. Zhu, Y. Zhang, H. Shao and X. Hu, Electrospinning and rheology of regenerated Bombyx mori silk fibroin aqueous solutions: The effects of pH and concentration. *Polymer.* **49**(12), 2880 – 2885 (2008).

[76] S. D. Aznar-Cervantes, D, Vicente-Cervantes, L. Meseguer-Olmo, J. L. Cenis and A. A. Lozano-Pérez, Influence of the protocol used for fibroin extraction on the mechanical properties and fiber sizes of electrospun silk mats, *Materials Science and Engineering: C.* **33**(4), 1945-1950 (2013).

[77] Y. Baimark, P. Srihanam, Y. Srisuwan and P. Phinyocheep, Preparation of porous silk fibroin microparticles by a Water-in-Oil emulsification-diffusion method, *Journal of Applied Polymer Science.* **118**(2), 1127-1133 (2010).

[78] X. Wang, T. Yucel, Q. Lu, X. Hu and D. L. Kaplan, Silk nanospheres and microspheres from silk/pva blend films for drug delivery, *Biomaterials*. **31**(6), 1025-1035 (2010).

[79] Y. Zhang, W. -D. Shen, R. -L. Xiang, L. -J Zhuge, W. -J. Ga and W. -B. Wang, Formation of silk fibroin nanoparticles in water-miscible organic solvent and their characterization, *Journal of Nanoparticle Research*. **9**(5), 885-900.

[80] Z. Cao, X. Chen, J. Yao, L. Huang and Z. Shao, The preparation of regenerated silk fibroin microspheres, *Soft Matter*. **3**(7), 910-915.

[81] J. Kundu, Y. -I. Chung, Y. H. Kim, G. Taeb and S. C. Kundu, Silk fibroin nanoparticles for cellular uptake and control release, *International Journal of Pharmaceutics*. **388**(1-2), 242-250 (2010).

[82] T. Hino, M. Tanimoto and S. Shimabayashi, Change in secondary structure of silk fibroin during preparation of its microspheres by spray-drying and exposure to humid atmosphere, *Journal of Colloid and Interface Science*. **266**(1), 68-73 (2003).

[83] Z. Zhao, A. Chen, Y. Li, J. Hu, X. Liu, J. Li, Y. Zhang, G. Li and Z. Zheng, Fabrication of silk fibroin nanoparticles for controlled drug delivery, *Journal of Nanoparticle Research*. **14**(4), 1-10 (2012).

[84] X. Wang and D. L. Kaplan, Functionalization of silk fibroin with neutravidin and biotin, *Macromolecular Bioscience*. **11**(1), 100-110 (2011).

[85] A. S. Lammel, X. Hu, S. -H. Park, D. L. Kaplan and T. R. Scheibel, Controlling silk fibroin particle features for drug delivery,

Biomaterials, **31**(16), 4583-4591 (2010).

[86] V. Gupta, A. Aseh, C. N. Rios, B. B. Aggarwal and A. B. Mathur, Fabrication and characterization of silk fibroin-derived curcumin nanoparticles for cancer therapy, *International Journal of Nanomedicine*. **4**(1), 115-122 (2009).

[87] R. Rajkhowa, L. Wang and X. Wang, Ultra-fine silk powder preparation through rotary and ball milling, *Powder Technology*. **185**(1), 87-95 (2008).

[88] E. Wenk, A. J. Wandrey, H. P. Merkle and L. Meinel, Silk fibroin spheres as a platform for controlled drug delivery, *Journal of Controlled Release*. **132**(1), 26-34 (2008).

[89] Z. Ekemen, Z. Ahmad, E. Stride, D. Kaplan and M. Edirisinghe, Electrohydrodynamic bubbling: An alternative route to fabricate porous structures of silk fibroin based materials, *Biomacromolecules*. **14**(5), 1412-1422 (2013).

[90] M. Enayati, M. -W. Chang, F. Bragman, M. Edirisinghe and E. Stride, Electrohydrodynamic preparation of particles, capsules and bubbles for biomedical engineering applications, *Colloids and Surfaces A: Physicochemical and Engineering Aspects*. **382**(1-3), 154-164 (2011).

[91] R. Rajkhowa, V. B. Gupta and V. K. Kothari, Tensile stress-strain and recovery behavior of Indian silk fibers and their structural dependence, *Journal of Applied Polymer Science*, **77**(11), 2418-2428 (2000).

[92] H. Oh, M. K. Kim and K. H. Lee, Preparation of sericin microparticles by electrohydrodynamic spraying and their application in drug delivery, *Macromolecular Research*. **19**(3), 266-272 (2011).

[93] A. -L. Dupont, Cellulose in lithium chloride/N,N-dimethyl acetamide, optimisation of a dissolution method using paper substrates and stability of the solutions, *Polymer*. **44**(15), 4117-4126 (2003).

[94] H. Teramoto, K. Nakajima and C. Takabayashi, Chemical modification of silk sericin in lithium chloride/dimethyl sulfoxide solvent with 4-cyanophenyl lsocyanate, *Biomacromolecules*. **5**(4), 1392-1398 (2004).

[95] I. C. Um, H. Y. Kweon, K. G. Leeand W. H. Park, The role of formic acid in solution stability and crystallization of silk protein polymer, *International Journal of Biological Macromolecules*. **33**, 203 - 213 (2003).

[96] Q. Ying and B. Chu, Overlap concentration of macromolecules in soution, *Macromolecules*. **20**, 362-366 (1987).

[97] E. D. von Meerwall, E. J. Amis and J. D. Ferry, Self-diffusion in solutions of polystyrene in tetrahydrofuran: comparison of concentration dependences of the diffusion coefficients of polymer, solvent, and a ternary probe component, *Macromolecules*. **18**(2), 260-266.

[98] C. Holland, A.E. Terry, D. Porter and F. Vollrath, Comparing the rheology of native spider and silkworm spinning dope. *Letters*. **5**, 870-874 (2006).

[99] A. Raghu and S. Ananthamurthy, Nanorheology of regenerated silk fibroin solution. *Bulletin of materials science*. **31**(3), 359-365 (2008).

[100] S. Rammensee, D. Huemmerich, K.D. Hermanson, T. Scheibel and A.R. Bausch, Rheological characterization of hydrogels formed by recombinantly produced spider silk, *Apllied Physics A*. **82**, 261-264 (2006).

[101] B. Ozbas, K. Rajagopal, J. P. Schneibor and D. J. Pochan, Semiflexible Chain Networks Formed via Self-Assembly of β-Hairpin Molecules, *Physical review letters*. **93**, 268106 (2004).

[102] B. Hinner, M. Tempel, E. Sackmann, K. Kroy and E. Frey, Enatnaglement, elasticity, and viscosous relaxation of actin solutions, *Physical review letters*. **81**(12), 2614-2617 (1998).

[103] A. E. Terry, D. P. Knight, D. Porter and F. Vollrath, pH induced changes in the rheology of silk fibroin solution from the middle division of *Bombyx mori* silkworm, *Biomacromolecules.* **5**, 768-772 (2004).

[104] J. D. Ferry, Viscoelastic Properties of Polymers, *John Wiley & Sons*. New york, 1980.

[105] A. Ochi, K. S. Hossain, J. Magoshi and N. Nemoto, Rheology and Dynamic Light Scattering of Silk Fibroin Solution Extracted from the Middle Division of *Bombyx mori* Silkworm. *Biomacromolecules.* **3**, 1187 - 1196 (2002).

[106] C. Mo, C. Holland, D. Porter, Z. Shao and F. Vollarth,

Concentration state dependence of the rheological can structural properties of reconstituted silk, *Biomacromolecules.* **10**, 2724-2728 (2009)

[107] A. Kozina, P. Diaz-Leyva, C. Friedrich and E. Bartsch, Structural and dynamical evolution of colloid-polymer mixtures on crossing glass and gel transition as seen by optical microrheology and mechanical bulk rheology, *Soft matter*. **8**, 1033-1046 (2012).

[108] X. Yan, D. Xu, J. Chen, M. Zhang, B. Hu, Y. Yuc and F. Huang, A self-healing supramolecular polymer gel with stimuli-responsiveness constructed by crown ether based molecular recognition. *Polymer chemistry*. **4**, 3312-3322 (2013).

[109] C. Liu, J. He, E. van. Ruymbeke, R. Keunings and C. Bailly, Evaluation of different methods for the determination of the plateau modulus and the entanglement molecular weight, *Polymer*. **47**, 4461 - 4479 (2006).

[110] A. Eckstein, J. Suhm, c. Friedrich, R. -D. Maier, J. Sassmannshausen, M. Bochmann and R. Mulhaupt, Determination of Plateau Moduli and Entanglement Molecular Weights of Isotactic, Syndiotactic, and Atactic Polypropylenes Synthesized with Metallocene Catalysts, *Macromolecules.* **31**, 1335 - 1340 (1998).

[111] C. M. Roland, J. K. Kallitsis and K. G. Gravalos, Plateau modulus of epoxidized polybutadiene, *Macromolecules*. **26**, 6474 - 6476 (1993).

[112] D. C. Taflin, T. L. Ward and E. J. Davis, Electrofied droplet fission and the Rayleigh limit, *Langmuir.* **5**, 376-384 (1989).

[113] J. A. Matthews, G. E. Wnek, D. G. Simpson and G. L. Bowlin, Electrospinning of collagen nanofibers, *Biomacromolecules.* **3**, 232-238 (2002).

[114] G. H. Li, Y. Zhao, M. Lv, Y. Shi and D. Cao, Super hydrophilic poly(ethylene terephthalate) (PET)/poly(vinyl alcohol) (PVA) composite fibrous mats with improved mechanical properties prepared via electrospinning process, *Colloids and Surfaces A: Physicochemical and Engineering Aspects.* **436**, 417-424 (2013).

[115] H. Fong, W. Liu, C. -S. Wang and R. A. Vaia, Generation of electrospun fibers of nylon 6 and nulon 9-montomorillonite nanocomposite, *Polymer.* **43**, 775-780 (2002).

[116] B. -M. Min, S. W. Lee, J. N. Lim, Y. You, T. S. Lee, P. H. Kang and W H. Park, Chitin and chitosan nanofibers: electrospinning of chitin and deacetylation of chitin nanofibers, *Polymer.* **45**, 7137-7142 (2004).

[117] S. Koombhongse, W Liu and D. H. Reneker, Flat polymer ribbons and other shapes by electrospinnin,. *Journal of Polymer Science Part B: Polymer Physics.* **39**(21), 2598-2606 (2001).

[118] D. L. Woerdeman, P. Ye, S. Shenoy, R. S. Parnas, G. E. Wnek and O. Trofimova, Electrospun fibers from wheat protein: investigation of the interplay between molecular structure and the fluid dynamics of the electrospinning process, *Biomacromolecules.* **6**, 707-712 (2005).

[119] S. Aznar-Cervante, M. I. Roca, J. G. Martinez, L. Meseguer -Olmo, J. L. Cenis, J. M. Moraleda and T. F. Otero, Fabrication of

conductive electrospun silk fibroin scaffolds by coating with polypyrrole for biomedical applications, *Bioelectrochemistry.* **85**, 36-43 (2012).

[120] L. Jeong, I. -S. Yeo, H. N. Kim, Y. I. Yoon, D. H. Jang, S. Y. Jung, B. -M. Min and W. H. Park, Plasma-treated silk fibroin nanofibers for skin regeneration, *International Journal of Biological Macromolecules*, **44**(3), 222-228 (2009).

[121] T. Ni, P. Senthil-Kumar, K. Dubbin, S. D. Aznar-Cervantes, N. Datta, M. A. Randolph, J. L. Cenis, G. C. Rutledge, G. C. Rutledge, I. E. Kochevar and R. W. Redmond, A photoactivated nanofiber graft material for augmented Achilles tendon repair, *Lasers in Surgery and Medicine*. **44**(8), 645-652 (2012).

초 록

실크 피브로인은 전기수력학적 공정에 의해 나노섬유로 제조되어 다양한 분야에서 많은 가능성을 인정받고 있다. 그럼에도 불구하고 대부분의 연구에서는 오직 전기수력학적 공정에 의해 섬유를 제조하는 것에만 초점을 맞추고 있으며 실크 피브로인의 전기수력학적 제조가 진행되는 과정은 아직까지 완전히 해석하지 못하고 있다. 본 연구에서는 실크 피브로인의 전기수력학적 제조 공정에 실크 피브로인 방사원액의 유변학적인 특성들이 미치는 영향을 살펴보았다. 그리고 전기수력학적 공정에 의해 제조된 결과물의 형태와 크기를 예측하기 위해 새로운 유변학적인 척도를 제시하였다. $CaCl_2$/EtOH/H_2O 용액에 용해한 시간을 5, 30, 60, 180분으로 조절하여 분자량이 다른 SFC005, SFC030, SFC060, SFC180을 제조하여 실험을 진행하였다.

먼저 1 M LiCl/DMSO 용매를 이용하여 200 마이크로 크기의 실크 피브로인 미세입자를 제조하였으며 실크 피브로인의 농도와 분자량에 상관없이 점단점도에 의하여 미세입자의 형태를 예측하는 것이 가능함을 확인하였다.

그리고 가장 흔히 쓰이는 용매인 포름산과 HFIP를 이용하여 전기수력학적 제조를 진행하여 전단응력과 유동점도와의 상관성을 살펴보고 방사원액의 평탄 탄성계수를 이용하여 전기수력학적 공정의 진행 양상을 살펴보았다. 제조된 입자 및 섬유의 크기와 유변학적 척도들의 상관관계를 살펴보았으며 입자의 크기 예측에는 전단점도를, 섬유의 크기 예측에는 평탄 탄성계수를 적용하는 것이 더 적절함을 확인하였다. 결과적으로 실크 피브로인의 유변학적 척도들이 전기수력학적 공정을 조절함에 있어서 중요한 역할을 할 수 있을 것으로 판단된다.

색인어 : 실크 피브로인, 전기수력학적 제조, 점도, 미세입자, 사슬얽힘, 평탄 탄성계수

학번 : 2010-30307